Instituting Retarders for Geopolymers Developed for Downhole Applications

by

Fawzi Chamssine

Thesis submitted in fulfilment of
the requirements for the degree of
PHILOSOPHIAE DOCTOR
(PhD)

U S

University
of Stavanger

Faculty of Science and Technology
Institute of Energy and Petroleum Engineering
2023

Acknowledgements

Preface

Geopolymers are a cementitious material that has been under study for many years. The material is noticed as a potential full replacement for traditional cementitious material both in construction and petroleum industry. The applicability of geopolymer material in the oil & gas industry, for well cementing and zonal isolation applications, is dependent on the development of chemical admixtures that can enhance performance and prepare the material for downhole conditions. Many admixtures are available in literature, however no inclusive study has been presented for their efficiency and applicability yet under a variety of temperatures from low to elevated. The results are highly dependable on the source of solid precursor, which in this case is granite-based geopolymer.

In this study, chemical admixtures of different roles have been examined on granite-based geopolymer material for oil & gas applications. The solid precursor mix design was previously developed inhouse at the University of Stavanger. The study focuses on the applicability of chemical admixtures using cement testing equipment following on available standards of cement testing to create a realistic comparison with traditional cement. The study touches up on both, applicability in the field under downhole conditions and scientific analysis of chemical reactions triggered by chemical admixtures. This thesis is part of the SafeRock Project which is in collaboration between UiS and operator and service companies. Thus, the need to present efficient admixtures and focus on their behavior in downhole conditions was a necessity to progress through the project.

This work is composed of a review section describing the work in this research study and published articles that dive in-depth into the scientific findings. The papers are attached in the appendix and labeled using

roman numbers. The outcome of this research can be summarized by the following papers:

Paper I: A variety of chemical admixtures were tested with the objective of finding a suitable retarder for granite-based geopolymer system at an operational temperature of 50°C. Rheological and short-term mechanical properties were examined for curing periods up to 7 days. Findings included the combination of different admixtures together where it was concluded that zinc and potassium species have a great impact on the setting time and that more in-depth analysis must be done specially the effect of temperature on slurry behavior and mechanical properties.

Paper II: The effect of temperature and admixture concentrations was examined on workability, viscosity, fluid loss, compressive strength, sonic strength development, and crystallography. Results highlighted the effect of chemical admixture and the link between mix design and operational temperature.

Paper III: Analysis of microstructure and crystallography was conducted in-depth to find the reason behind poisoning phenomenon of retarders and the properties of the outcome product. Results did not highlight any accurate visualization of the retarders' effect, which suggests the focus must be on a reaction level. In addition, results indicated that the retarders had an active window up to 14 days, and then they were incorporated into the bulk matrix as observed in mechanical strength measurements.

Paper IV: Analysis of reaction mechanism was done using computational modeling (density functional theory calculations) and Raman spectroscopy at 50°C. An in-house lab-controlled sample was developed to avoid the complexity of minerals involved in the reaction.

Paper V: Investigation of possible role of calcium and sodium species as strength development agents, in addition to zinc and potassium species as retarders, was conducted at operational temperature of 60°C BHCT &

80°C BHST. Findings indicated that strength development agents can assist in countering the poisoning phenomenon imposed on mechanical properties by retarders. However, tuning of concentrations must be studied to have a mix design with superior properties.

Paper VI: Development of three mix designs and tuning using calcium species, as accelerators, incorporated into the dry solid precursors. Rheological and mechanical properties were tested to assess the applicability of these neat mix designs at a range of temperature between 5 to 60°C. It is concluded that operational temperature and composition of mix designs highly affect the kinetics of the reaction, or in other words the degree of completion of the reaction.

List of Publications

I. Chamssine, Fawzi, Gargari, Pedram, and Mahmoud Khalifeh. "Impact of Admixtures on Pumpability and Short-Term Mechanical Properties of Rock-Based Geopolymer Designed for Zonal Isolation and Well Abandonment." Paper presented at the Offshore Technology Conference, Houston, Texas, USA, May 2022. doi: https://doi.org/10.4043/31880-MS

II. Chamssine, F, Khalifeh, M, Eid, E, Minde, MW, & Saasen, A. "Effects of Temperature and Chemical Admixtures on the Properties of Rock-Based Geopolymers Designed for Zonal Isolation and Well Abandonment." Proceedings of the ASME 2021 40th International Conference on Ocean, Offshore and Arctic Engineering. Volume 10: Petroleum Technology. Virtual, Online. June 21–30, 2021. V010T11A031.ASME. https://doi.org/10.1115/OMAE2021-60808

III. Chamssine, F., Khalifeh, M., and Saasen, A. "Effect of Zn2+ and K+ as Retarding Agents on Rock-Based Geopolymers for Downhole Cementing Operations." ASME. J. Energy Resour. Technol. May 2022; 144(5): 053002. https://doi.org/10.1115/1.4053710

IV. Chamssine, F., Gasparotto, L.H.S., Souza, M.A.F., Khalifeh, M., Freitas, J.C.O. "Retarding mechanism of Zn2+ species in geopolymer material using Raman spectroscopy and DFT calculations."Sci Rep 12, 21036 (2022). https://doi.org/10.1038/s41598-022-25552-0

V. Chamssine, F, Khalifeh, M, & Saasen, A. "Rheological and Mechanical Properties of Rock-Based Geopolymers Developed for Well Abandonment: Effect of Chemical Admixtures at Elevated Temperatures." Proceedings of the ASME 2022 41st International Conference on Ocean, Offshore and Arctic Engineering. Volume 10: Petroleum Technology. Hamburg, Germany. June 5–10, 2022. V010T11A037.ASME. https://doi.org/10.1115/OMAE2022-78376

VI. Chamssine, F., Agista, M., & Khalifeh, M. (2023). Temperature-Dependent Classification of Geopolymers Derived from Granite Designed for Well Cementing Applications (submitted to a scientific journal 2023)

Table of Contents

Table of Figures

xv

List of Tables

1   Introduction

Cementitious material formulate one of the most successful material in the world where around 1 m^3 per person is produced yearly worldwide [1]. The production of such material is on the rise due to an expected increase in urbanization levels following the global population growth [2]. It is forecasted that the global annual cement use by 2050 will increase from currently around 4.13 Gt/year to 4.68 Gt/year [3]. Cement has been widely used in multiple industries from construction to zonal isolation applications in petroleum and geothermal wells, due to its sustained properties, abundance of raw material, and relatively low cost of process and production [4]. However, the consequences of producing such material, specifically in the form of concrete and Ordinary Portland Cement (OPC), carry a huge burden on the global climate. The latest data sets on carbon dioxide (CO_2) emissions until 2018 estimated that between ±6% and ±8% of global CO_2 emissions account for cement production [5].

Environmental challenges with CO_2 emissions, connected mainly to raw materials' mining and processing, have encouraged researchers and the scientific society to investigate the potential of utilizing alternative material, with significantly lower carbon footprint, as a partial or full replacement to currently used OPC [6-8]. One of many materials under study has been Geopolymers, an aluminosilicate material exhibiting quite feasible performance specifically under aggressive conditions [9, 10]. However, to make this material applicable in the field, specifically oil and gas, many alternations and tuning must be done through the addition of chemical admixtures, to get the material up to adequate performance standards. Chemical admixtures divide into multiple categories and roles such as retarders, accelerators, strength developing agents, superplasticizers, anti-foam…etc. The scope of this work is to explore potential chemical admixtures, such as retarders and accelerators, and investigate their effect on the material's performance,

considering different parameters such as temperature and pressure, all tested under operational conditions.

1.1   *The Nature of Geopolymers*

Geopolymer material is a subclass of alkali activated material, which composes of a low calcium (Ca) and aluminosilicate-rich cementitious systems synthesized by the utilization of natural or processed raw material such as granite & kaolin, or industrial waste such blast furnace slag and fly ash [11-14]. Geopolymers were introduced in 1975 by Joseph Davidovits; these materials have long repeating chains of tetrahedral Al_2SiO_5 minerals which form polymer-like structure [15]. Multiple types of alkali-activators are used to activate the raw material such as potassium hydroxide (KOH), sodium hydroxide (NaOH), potassium silicate $((K_2O)_x \cdot SiO_2)$, and sodium silicate $((Na_2O)_x \cdot SiO_2)$. These alkali solutions initiate dissolution of complex minerals leading to the formation of 3-D aluminosilicate structures through transportation, nucleation, and polycondensation of aluminum (Al) and silicon (Si) containing molecules [16].

Geopolymers are considered as a prospective alternative for OPC especially in the oil and gas industry, due to various reasons regarding several current shortcomings associated with OPC and the high CO_2 footprint involved in OPC production [15, 17-19]. According to the work of Khalifeh *et al.* [17] and Duxon *et al.*[12], geopolymers poses properties that make it superior to OPC such as low chemical shrinkage, low permeability, high durability in corrosive mediums, and the ability of not being affected significantly by oil-based drilling fluids contaminants [20]. Geopolymers' formation mainly consists of Si and Al reacting with an alkali silicate activator such as potassium silicate (K_2SiO_3), sodium hydroxide (NaOH), potassium hydroxide (KOH)…etc. Polymerization occurs when aluminosilicate react and dissolve in a highly alkaline medium, where free tetrahedral SiO^-_4 and AlO^-_4 are released in the slurry; afterwards these tetrahedral units bond

2

through oxygen atoms (O_2) to form a repetitive chain structure of -Si-O-Al-O- [21]. The polymeric structure is also very dependent on the Si:Al ratio as shown in Figure 1 [22]. In addition, the reactions occurring during polymerization were described by Komnitsas [23] as the following:

$$(Si_2O_5.Al_2O_2)_n + H_2O + OH^- \rightarrow Si(OH)_4 + Al(OH)^{4-} \tag{1}$$

$$Si(OH)_4 + Al(OH)^{4-} \rightarrow \left(\begin{array}{c} | \quad\quad | \\ -Si-0-Al-0- \\ | \quad\quad | \\ 0 \quad\quad 0 \end{array} \right) n + 4\ H_2O \tag{2}$$
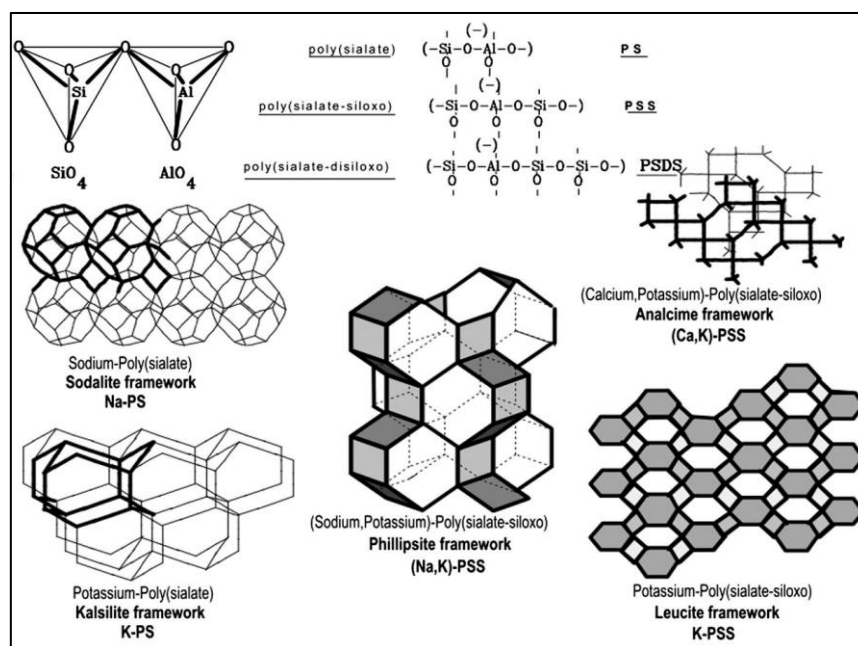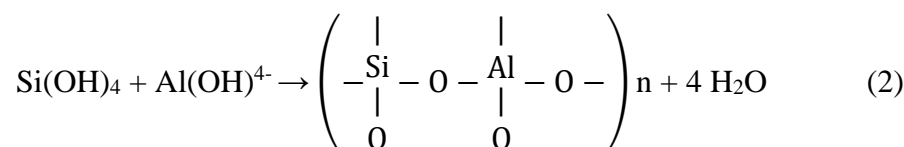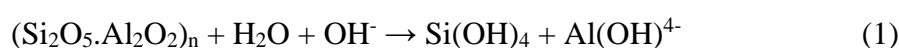
Figure 1. Structure of sialates with different Si:Al ratios. Retrieved from [22].

1.1.1 Mechanism of Reactions

Geopolymeric structure develops over polycondensation reaction of the alumino-silicate oxides with the alkali-polysilicates, which in turn results in a Si-O-Al bond with a tetrahedral structure forming the main geopolymeric structure [24, 25]. Polycondensation reaction's degree and alkaline element form can be described by $M_n[-(Si-O_2)_z-Al-O]_n.wH_2O$ where M is the alkaline element, z is either 1, 2, or 3, and n is the degree of polycondensation [26]. The reaction mechanism involved in the dissolution of Al and Si rich material in the alkali activator phase can generally be described by the three stages as proposed by Glukhvosky (Figure 2) [27].

| (1) Destruction-Coagulation | (2) Coagulation-Condensation | (3) Condensation-Crystallisation |

Figure 2. General mechanism stages of geopolymer, as described by Glukhvosky [27]

The first stage of mechanism of reactions can be initiated with hydroxide ions (OH^-), from high pH mediums, which will break the Si-O-Si and Al-O-Si bonds by disrupting and restructuring their ionic structure. The products from this electronic distribution will yield -Si-OH (silanol), -Si-O$^-$ (sialate), and complex Al species mainly $Al(OH)^{-4}$. Negative charged molecules will be neutralized by the presence of alkaline cations such as sodium (Na^+) or potassium (K^+) ions, depending on the type of alkali activator used, which will slow down any reverse reaction leading to the reformation of Si-O-Si or Al-O-Si. During the second stage, coagulated structures initiate in the presence of accrued ionic species which pushes the system to begin with polycondensation. Si monomers initiate reaction series, fastened by the presence of OH^- ions, with other monomers to start building polymeric structures. In the third stage,

precipitation starts to form due to the presence of solid particles in the initial stage which moves on along with the reaction order.

Mechanism of reactions can vary significantly depending on the initial composition of the solid precursors and the nature of the alkali activator, in addition to the mixing/curing conditions. Other mechanistic models have risen to tackle the variation in initial solid phase composition and provide a more extensive description of reaction stages and products. Palomo *et al.* [28] suggested a mechanism based on the formation of zeolites during alkali activated fly ash reactions. The mechanism involved two main phases; (1) initial nucleation alongside to the dissolution of Al particles followed by polymerization reactions which forms complex ionic species, (2) growth of species and crystallization. It was concluded that the final products will be an aluminosilicate gel also labeled as N-A-S-H (Figure 3), which is considered as a pre-zeolite precursor. This model was later modified to give a clearer description of the synthesis of N-A-S-H gel where the formation starts by the dissolution of Al and Si sourced material to form monomers; interactions between monomers will occur to form dimer, trimers, tetramers, and so on. N-A-S-H gel starts to form (via precipitation) after the reaction reaches saturation [28, 29].
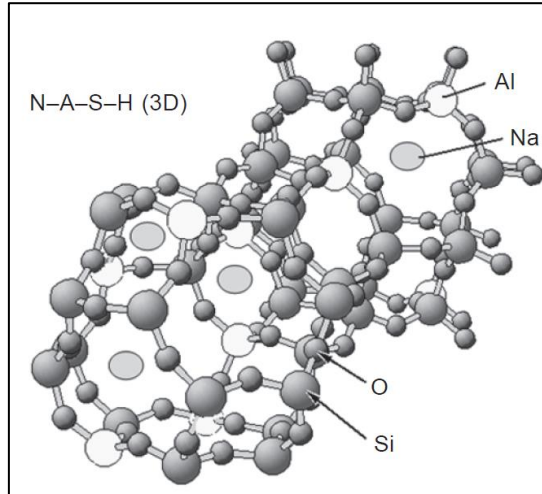
Figure 3. Proposed structure N-A-S-H gel. Retrieved from [30]

Main reaction products of the Si and Al alkali activation is an amorphous aluminosilicate hydrate phase, which is an inorganic polymer known as N-A-S-H gel. It is composed of Si and Al in a tetrahedral structure forming a 3-D structure as presented in Figure 3. In addition, secondary products are of a zeolite nature such as zeolite Y, zeolite P, and hydroxysodalite [31, 32].

In addition, the dissolution of Si-O-Al bonds and incorporation of soluble species in the system is highly dependent on pH of the system [33]. A study by Hajimohammadi *et al.* [34], concluded that the increase of pH using OH solutions can increase the rate of dissolution of Si in the system. This availability of Si monomers will aid in the hydrolysis reactions, thus having a more complete reaction. The understanding of the system at hand, from pH to the type of precursor used, could aid in the tuning of geopolymer precursor selection and create a medium with the most efficient kinetic behavior.

1.2   Geopolymers Vs. Ordinary Portland Cement

These two binding materials are different on all levels: composition, mechanism, reaction phases, early properties, etc. However, it is worthwhile to mention some aspects of differentiation for the sake of comparison and critical analysis. As mentioned in section 1.1.1, the mechanism of geopolymer materials divides into 3 main phases of which dissolution of minerals is a must to start coagulating molecules in the effort to form repeatable chains of Si-O-Al. Similarly in OPC, the first stage of mechanism is the dissolution where molecular units get in contact with water on the molecule's surface [35].   Yet, since OPC is rich in Ca, because of having clinkers (Ca_3Si and Ca_2Si), quite different reactions paths should occur [36]. According to a recent observation of reaction mechanics by Bullard *et al.* [37], the reaction phases can be divided into 4 stages; (i) initial reaction, (ii) period of slow reaction, (iii) acceleration period, and finally (iv) deceleration period. This was presented by measuring the rate of reaction of alite ($C_3SiO_5 = C_3S$), a component that measures about 50%-70% of OPC by mass, as presented below in Figure 4.
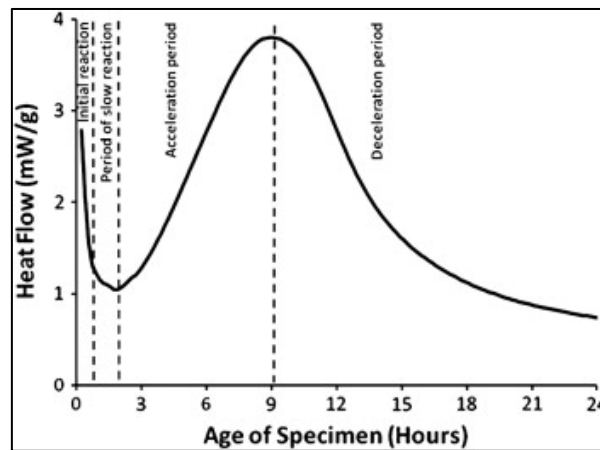
Figure 4. Reaction rate of alite as a function of time measured by isothermal calorimetry. Retrieved from [37].

7

The following overview can show how these phases behave:

(i)   Initial reaction involves the wetting of C_3S surface, where an exothermic reaction occurs involving the rapid dissolution of these species [38]. The following reaction takes place:

$$C_3S + 3H_2O \rightarrow 3Ca^{2+} + H_2SiO_4^{2-} + 4OH^- \qquad (1)$$
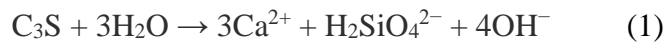
(ii)   Slow dissolution, another term for deceleration of the reaction, can be attributed to the formation of metastable layers of calcium silicate hydrates (C-S-H) [39]. These layers prevent the C_3S molecule access to water and hence diffusion.

(iii)   Acceleration through colliding silica (Si) phases with existing C-S-H nucleating on C_3Ss' surface [40].

(iv)   Deceleration of reaction due to depletion of small particles, lack of space to grow, or shortage of water [37].

The purpose of presenting this overview is to highlight the immense differences in composition, particle nature, and eventually reaction phases. This not only controls the properties, but also controls the behavior of chemical of admixtures which in turn must adapt to the system's mechanism.

1.3   *Role of Chemical Admixtures*

Every well cement job has a set of objectives and milestones to achieve under harsh conditions of elevated pressure and temperature, usually in a short time window. To be able to engineer a compatible cementitious material, various factors must be considered such as well depth, wellbore environment, and pressure & temperature regimes [41]. For geopolymers to be applicable in a wide range of underground temperatures and pressures, chemical admixtures are a must to tune the slurry's behaviour to match with wellbore conditions. Admixtures can highly alter the slurry's properties allowing to displace smoothly between casing and formation, accelerate strength development, and maintain sustainable

long-term properties serving as a zonal isolation or P&A material [41]. Although multiple admixtures have been developed for OPC, with different disciplinary functions, their chemistry is not of a match to efficiently function in geopolymer material due to the different mechanisms governing the reactions as mentioned in section 1.2. Furthermore, chemical admixtures work mainly on different properties of the slurry such as particle size, reactivity of different phases, chemical nature, etc. Thus, it is worth to mention that many chemical admixtures are available for different geopolymer systems, however, there is lack of data regarding their behaviour and effects on geopolymerization reactions has been a hurdle in their applicability in the field and thus the applicability of geopolymers in general.

Various types of chemical admixtures can be utilized considering the main mechanism of geopolymer material into account. Chemical admixtures such as accelerators and retarders. In the next section we will discuss these two admixtures.

1.3.1 Accelerators

Accelerators are mainly added to cementitious material to decrease setting time and accelerate the hardening process. In principle, these can be used as an antidote for other chemical admixtures which delay the setting time [42]. Accelerators such as chloride (Cl) containing species, Ca species, and Na species have been under study previously. Rattanasak *et al.*[43] examined $CaCl_2$ as an accelerator on fly ash based geopolymer of which it significantly accelerated initial and final setting time, up to a 100 Bearden units of consistency (BC). Moreover, nano-SiO_2 has been used by Ngernkham *et al.* [44] of which showed a decrease in setting time of fly ash based geopolymer. To its advantage, higher early strength development can be a side effect of using accelerators in the field as perceived by Bhavsar *et al.* [45] when coarse aggregates and Si fumes were used in efforts to upgrade fly ash based geopolymers. Moreover, sodium carbonate (Na_2CO_3) was also utilized as a strength

development agent by Jeon *et al.* [46] in fly ash-based geopolymers. The results highlighted a noticeable improvement in matrix strength and reduced setting time of slurry. A summary of the most common accelerators is mentioned in Table 1, considering the geopolymer system examined in each study.

Table 1. List of some accelerators described in literature

Accelerator	Year	Geopolymer System	Reference
$CaCl_2$	2011	Fly Ash	[43]
Nano SiO_2	2014	Fly Ash	[44]
NaOH	2021	Metakaolin	[47]
Al_2O_3	2007	Metakaolin	[16]
Na_2CO_3	2015	Fly Ash	[46]

1.3.2   Retarders

In OPC, retarders' main role is to delay the setting time of cementitious material by delaying the mechanism of setting by complicating its formation mechanism through different approaches of adsorption, precipitation, nucleation, and complexation [41]. However, geopolymers are under the impression that they behave differently from OPC where a poisoning effect can take place on the Si-O-Al matrix causing an elongation in oligomerization period or delay in polycondensation phase, or both.

Retarders can behave in different manners with one affecting the pumping time while the other can impact the hardening time. The first compensates the effect of temperature on slurries and increases the time allocated for the displacement phase [48]. While the later, targets early strength development and reduces the heat evolution rate of the mix design [49]. In previous studies, two types of retarders were mainly presented: inorganic and organic retarders. Starting with inorganic, their main function works by coating the binder particles and hinder the dissolution phase by hydroxides within the slurry. They are of many

forms such as phosphates, oxides (ZnO and PdO), and borax. However, organic retarders are mainly formed of lignosulphonates, carbohydrates of hydroxyl nature (sugars), and hydroxycarboxylic acids and salts. In addition, magnesium chloride ($MgCl_2$) was examined on phosphate cement-based materials by Du *et al.* [50] where $MgCl_2$ acted as a retarder. Furthermore, tartaric acid ($C_4H_6O_6$) has also been pointed to as a retarder specifically for one-part geopolymers as described Van Deventer *et al.* [51]. Another retarder used is ethylene glycol ($C_2H_6O_2$) where it was studied by Coppola *et al.* [52] on slag-based system where it demonstrated a significant effect of slowing setting time. Most used retarders of both natures are summarized in Table 2 below.

Table 2. List of some retarders described in literature

Retarder	Year	Geopolymer System	Reference
Na_2SO_4	2011	Fly Ash	[43]
Sucrose	2011	Fly Ash	[43]
Plastocrete RT6 Plus (Synthetic)	2017	Fly Ash	[53]
Lignosulfonate	2022	Fly Ash	[54]
ZnO	2020	Metakaolin	[55]
Red Mud	2020	Manganese Phosphate	[56]
$MgCl_2$	2022	Phosphate	[50]
$C_4H_6O_6$	2010	Glassy aluminosilicate	[51]
$C_2H_6O_2$	2020	Slag	[52]

1.4   Combination Between Chemical Admixtures

The tuning of chemical admixtures has always been a challenge for geopolymer material due to the intermolecular relations governing the reaction mechanism of different chemicals in a complex system. The incorporation of different chemical admixtures at once, serves the aim to accommodate different properties of the slurry such as retardation, early strength development, lower density, etc. of which all must be balanced to deliver the perceived outcome (Paper V). The incorporation of different chemical admixtures must be able to address the contradicting

properties of the elements such as having retarders for retarding setting time and accelerators/strength development agents for rapid strength development, after gelation, in the same mix design. These admixtures might overtake each other and result in opposite outcomes. Thus, the correlation between chemical admixtures must consider the active element in every admixture, the concentrations introduced to each mix design, and most importantly the targeted slurry behaviour at every stage of the reaction.

In the following, different chemical admixtures were examined for the granite-based geopolymer. Many analytical and characterization techniques, from slurry to mechanical properties and chemical reaction analysis techniques, were implemented to observe the effect of chemical admixtures on the properties before and after setting. The study was done at a range of operational temperatures from 5 to 60°C of BHCT. The approach was highly dependent on analysing the effect of chemical admixtures and in-depth examination of the reaction mechanism of successful candidates. The study carried on examining strength development agents and develop geopolymers not by only using chemical admixtures but by also altering the neat recipe to fit to a range of temperatures with the efforts to reduce the dependency on chemical admixtures.

2. Scope and Objectives

The main objective of this Ph.D dissertation is to present retarders and accelerators to control the pumpability of geopolymers for downhole applications in petroleum and geothermal wells, while trying to maintain the early strength development in an acceptable range. Moreover, the purpose evolves around observing the effect of chemical admixtures on other prior/post setting properties of geopolymer materials. The sub-objectives are listed as following:

• Present the mechanisms of geopolymerization and retardation.

• Describe accelerators and retarders to expedite the pumping time for downhole conditions and at a range of BHCT (5-60°C).

• Examine the effect of chemical admixtures on the inner structure and morphology of geopolymers.

• Present the effects of the additives on early and final strength development.

Throughout the project four steps were adapted to develop the outcome presented in this thesis, the steps can be identified as the following:

Step I: Different accelerators and retarders were tested to find their potential in a granite-based geopolymer system. The identification of potential candidates was done briefly using short term rheological and mechanical properties analysis.

Step II: After unravelling potential chemical admixtures, the focus was set on Zn^{2+} species and K^+ species as strong candidates for developing granite-based geopolymers for downhole conditions. Thorough analysis was conducted to examine the effect of temperature on retarder systems of similar nature and their effect on crystallography and morphology in

geopolymer systems was examined for short- and long-term curing periods under downhole conditions.

Step III: The behaviour of Zn^{2+} species in granite-based geopolymer systems could not be easily identified on a mechanism level in the previous step, thus further investigation into the chemical mechanism of Zn^{2+} species was conducted. Analytical equipment and computational modelling were used to identify probable step by step mechanism of Zn^{2+} species into geopolymer systems.

Step IV: After identifying the mechanism of Zn^{2+} species, efforts were conducted to integrate strength development agents into high temperature applications in combination with Zn species as a retarder. However, due to system's complexity and requirement of fine tuning of the chemical admixture system a new path was decided on to be discovered. The new path aimed to develop different classes of granite-based geopolymer system, depending on the operating temperature, to minimize the usage of chemical admixtures into the system and reduced complexity factors in the system at hand.

I	Identify potential retarders and accelerators for granite-based geopolymer system
	Paper I & Paper II
II	• Examine effect of chemical admixtures on strength development and post setting properties • Examine effect of chemical admixtures on crystallography and morphology of geopolymers
	Paper II & Paper III
III	Identify mechanism of geopolymerization and retardation
	Paper IV
IV	Describe accelerators and retarders to expedite the pumping time for downhole conditions and at a range of BHCT (5-60℃)
	Paper V & Paper VI

Figure 5. Steps of the research plan

3. Materials

3.1 Rock-Based Mineral: Granite

Granite is a natural existing rock mainly composed of various groups of quartz, feldspar, mica or hornblende, which forms a large part of the bedrock of Finland and Scandinavia [57]. Granite is used as the base for producing the described geopolymer material.

Multiple techniques were used to analyse the chemical composition of mineral material. Inductively Coupled Plasma Mass Spectrometry (ICP-MS) and X-ray fluorescence (XRF) can be potential techniques to explore the composition of granite and other solid precursor material under use. The ICP-MS and XRF analysis of granite samples is presented in Table 3 and Table 4, respectively. It is noticed that both techniques highly present differences in chemical composition, however it must be noted that each technique is of a uniqueness of its own. The first is based on dissolving the mineral in a highly acidic solution, then running the solution in an ICP-MS. One of the main differences is that ICP-MS analysis considers elements in the form of oxides, which according to Richter *et al.* [58] and Croudace *et al.* [59] has more advantages then considering single elements since these readings will not be highly affected by variations in concentrations, giving a much clearer image of the chemical composition. The process of comparison is linked to ''Log-Ratio Calibrations'', in XRF, which on its own is a comparison of calibration models for elements and involves an intense differentiation between calibration models that can present different readings depending on the correlation at hand [60]. In this study, ICP-MS of geochemistry data has been utilized as a benchmark for chemical analysis and comparison due to the clearer readability of results, ease in analysis, and composition calculations for mix designs. It must be noted that all chemical composition calculations for mix designs presented in this

study were based on ICP-MS analysis of different solid precursors according to their weight percentage introduced to the dry blend.

Table 3. Chemical composition of the granite rock analyzed with ICP-MS Analysis

Element	SiO_2	Al_2O_3	Fe_2O_3	CaO	MgO	Na_2O	K_2O	TiO_2	MnO	P_2O_5	LOI
Result (wt%)	73.44	13.33	2.06	1.12	0.44	3.12	5.11	0.23	0.04	0.06	0.9

Table 4. Chemical composition of the granite rock using XRF

Elements in Solid	Result (wt%)
Aluminum, Al	7.3
Barium, Ba	0.1
Calcium, Ca	1.4
Chromium, Cr	<0.1
Copper, Cu	<0.1
Iron, Fe	2.5
Potassium, K	5.1
Magnesium, Mg	0.6
Manganese, Mn	<0.1
Sodium, Na	2.2
Nickel, Ni	<0.1
Phosphorus, P	0.1
Lead, Pb	<0.1
Silicon, Si	32
Strontium, Sr	<0.1
Titanium, Ti	0.3
Zinc, Zn	<0.1
Sulphur, S	<0.1
Chlorine, Cl	<0.1
Zirconium, Zr	<0.1

From the results presented above, it can be observed that granite is highly rich in Si and Al based on the oxide readings presented in Table 3. While

rich in the latter elements but the granite utilized in this work has poor Ca and Mg content which raised some challenges in the development of geopolymer material if this material is to be used alone without any modification to the chemical composition using other solid precursors or chemical admixtures.

Examining the X-ray diffraction (XRD) measurements of the granite and the different peak fitting analysis (Figure 6), it can be observed that different phases of quartz, albite, and microcline are available and easily detected. However, biotite, muscovite, clinochlore, and chamosite were concluded from different resources such as the Norges Geologiske Undersøkelse (NGU) [61]. Further in-depth refinements helped in identifying each element into their mineral group. The refinement has all mineral phases mentioned in the Feldspar diagram (Figure 7), from K rich to Na rich and Ca rich. The final representation and qualitative representation of phases is presented in Table 5 after excluding mineral groups with less than 2% concentration. In Figure 6, main phases of quartz, albite, microcline, biotite, and chamosite are presented at their major peaks. Minor phases such clinochlore and oligoclase phases are minorly distributed throughout the spectrum that it is not easily detected visually.
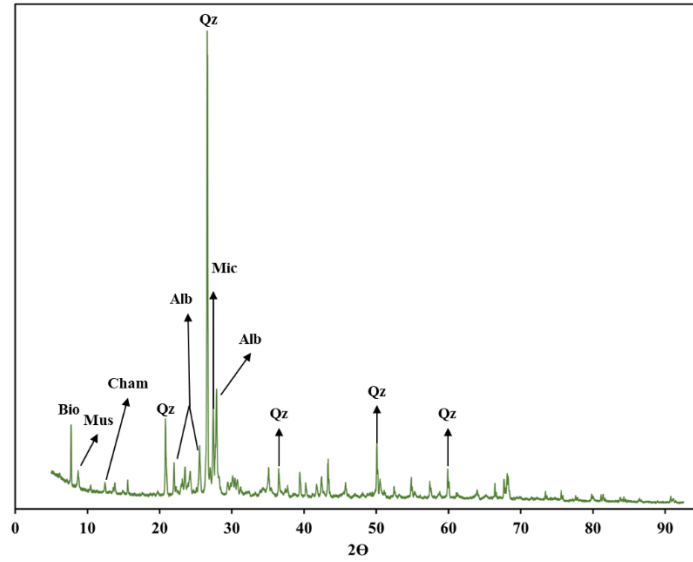
Figure 6. Crystallography of granite; Qz=Quartz, Alb=Albite, Mic=Microcline, Cham=Chamotite, Bio=Biotite, Mus=Muscovite
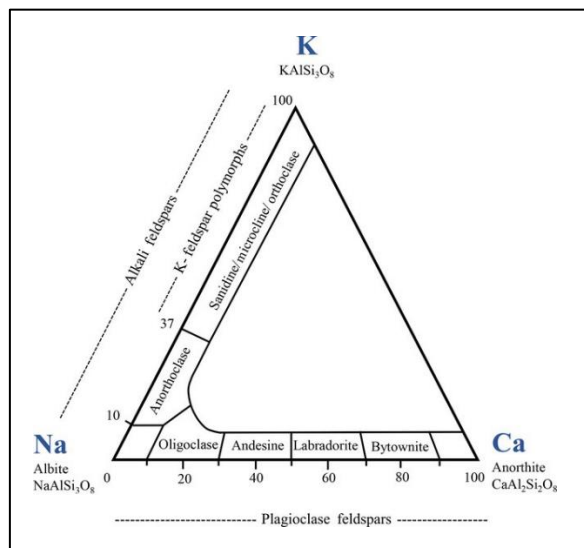
Figure 7. Feldspar classification diagram. Retrieved from [62]

Table 5. Quantitative representation of phases using XRD refinements

Phase	Wt%	Group
Quartz	30.383	Quartz
Microcline	26.961	Feldspar
Albite	17.284	Feldspar
Clinochlore	7.737	Chlorite
Oligoclase	5.125	Plagioclase
Muscovite	4.899	Muscovite
Chamosite	4.072	Chlorite
Biotite	3.539	Biotite

The microstructure of granite was examined using scanning electron microscopy (SEM) and is presented in Figure 8. A heterogeneous structure can be observed with many cavities. Inside these cavities, a series of hexagonal-like shaped crystals which in turn come in a variety of dimensions are present.
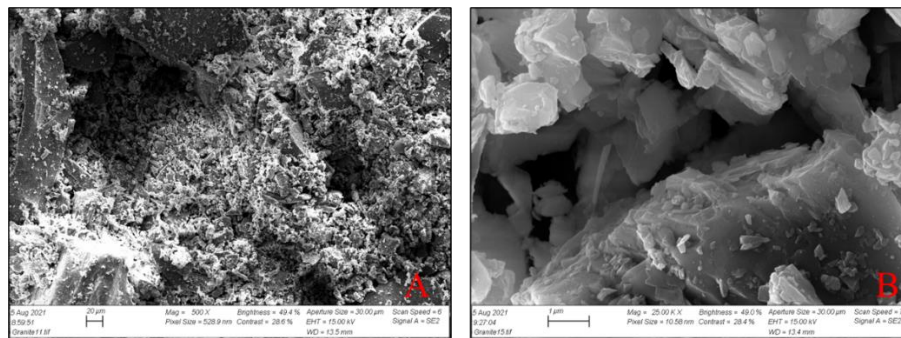
Figure 8. SEM imaging of granite; (A) at magnitude 500X, (B) at magnitude 25,000 X

3.2 *Blast Furnace Slag*

Blast Furnace Slag (BFS) is widely available as an industrial by-product from pig-iron production, heavily rich with silicates, alumina, alumina silicates, Mg, and Ca which develops simultaneously with Fe in molten

conditions in a blast furnace [63]. BFS was introduced in different weight percentages to support the strength development of granite-based geopolymers. Due to its amorphous nature and Ca containing elements, BFS can act as a strength development agent and create interconnected phases of hydrates which support the geopolymer matrix [64].

The chemical composition of the utilized BFS in this study is presented in Table 6. The results are presented using ICP-MPS readings which in turn are present in oxide form. High concentrations of Ca and Mg are present in the composition which motivate the inclusion of BFS in solid dry blends for geopolymer material. Previous studies indicated the benefit of utilizing BFS in achieving superior mechanical properties in geopolymer blends [65-68]. In summary, these benefits are in the form of a faster early reaction phase due to presence of Ca and Mg which enhances hydration and promotes the production of C-S-H and hydrotalcite like phases. However, it must be noted that usually C-S-H phases do not highly show in XRD reflections of the end-product, although BFS has relatively high Ca concentrations.

Table 6. Chemical composition of BFS using geochemistry indicates.

Element	SiO_2	Al_2O_3	Fe_2O_3	CaO	MgO	Na_2O	K_2O	TiO_2	MnO	Cr_2O_3	LOI
Result (wt%)	35.78	12.72	0.18	33.74	12.77	0.55	0.82	2.23	0.58	0.06	0.3

In addition, since the utilized BFS is highly amorphous no clear composition readings can be concluded from XRD patterns. Moreover, elemental analysis and the morphology nature of BFS samples are presented in Figure 9.

Element	Wt%	At%
O K	49.22	66.23
MgK	5.82	5.16
AlK	4.79	3.82
SiK	13.98	10.72
K K	0.15	0.08
CaK	26.03	13.98
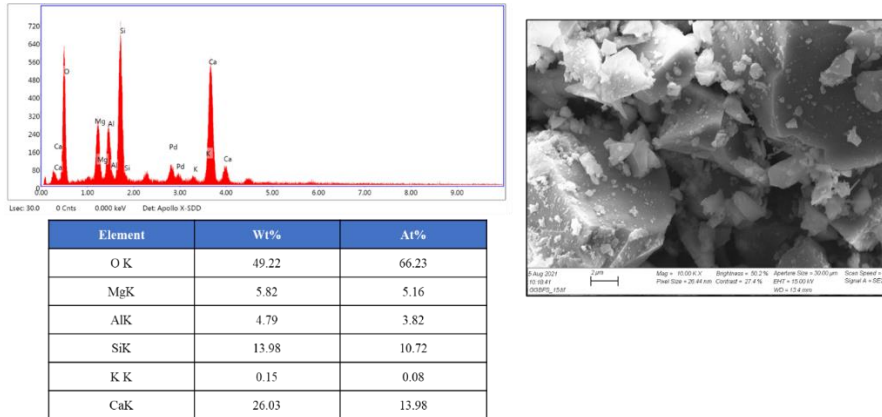
Figure 9. SEM and EDS analysis of presented area of BFS

It must be noted that the BFS used in Paper II was not from the same batch used in the other Papers (I, III, IV, V, VI).

3.3   Microsilica

Highly reactive microsilica, 95.5 wt% purity, was used to balance Si/Al content in geopolymer mix design development. The excess free silica can enhance geopolymer matrices and support strength development and decrease permeability in the matrix. The chemical composition using, XRF technique, is presented in Table 7.

Table 7. XRF elemental analysis of microsilica

Elements in Solid	Result (wt%)
Aluminum, Al	<0.1
Barium, Ba	<0.1
Calcium, Ca	0.1
Chromium, Cr	<0.1
Copper, Cu	<0.1
Iron, Fe	2.5
Potassium, K	0.5
Magnesium, Mg	0.1
Manganese, Mn	<0.1
Sodium, Na	<0.1
Nickel, Ni	<0.1
Phosphorus, P	<0.1
Lead, Pb	<0.1
Silicon, Si	46
Strontium, Sr	<0.1
Titanium, Ti	<0.1
Zinc, Zn	<0.1
Sulphur, S	0.1
Chlorine, Cl	<0.1

3.4   Mix Design Nature and Reference Samples

The mix designs utilized in this study were a combination of granite, BFS, and microsilica. The solid precursors were introduced together under different wt% which in turn resulted in different chemical compositions presented forward ahead. The nature of mix designs was developed to be a suitable starting point for the addition of chemical admixtures. One thing to note that the BFS used in Paper II was different from the ones used in the other papers and that was due to a new batch from the source provider. However, the mix designs were engineered to have relatively consistent results. In addition, in some studies, neat class G cement was used as a benchmark sample to compare with the geopolymer samples at the conditions understudy.

3.5 Activator/Hardener Phase

A mixture of Potassium silicate solution (K_2SiO_3) with a molar ratio between 2.3 to 2.5 was used as the main hardener phase to produce geopolymer slurries.

Potassium hydroxide (KOH) pellets were used in preparing alkali solutions of mainly a molarity of 4 M. The pellets were with a purity of 99%.

3.6 Chemical Admixtures

A variety of chemical admixtures was used with each having its own role and effects on the geopolymer slurries under study. A summary of the chemical admixtures is provided in Table 8 below. These admixtures are soluble in water and were introduced via water to the hardener phase prior mixing with the solid phase or directly to the dry blend.

Table 8. List of chemical admixtures used in this study

Material	Chemical Formula	Purity	Function
Zinc Nitrate Hexahydrate	$Zn(NO_3)_2 \cdot 6H_2O$	≥99	Retarder
Potassium Nitrate	KNO_3	≥99	Accelerator
Sodium Hydroxide	$NaOH$	≥99	Accelerator
Aluminum Oxide	Al_2O_3	≥99	Accelerator
Sucrose	$C_{12}H_{22}O_{11}$	≥99	Retarder
Calcium Carbonate	$CaCO_3$	≥90	Accelerator
Calcium Oxide	CaO	>90	Accelerator

4. Slurry Preparation

Geopolymer slurries were prepared by using granite, BFS, and microsilica as the main solid precursor with chemical admixtures introduced to the slurry mixture via excess water. The slurries were mixed following API 10B-2 recommendations using a high shear commercial lab blender [69]. After preparing the alkali solution, it was mixed in the blender for 10 seconds at 4000 RPM, afterwards chemical admixtures, pre-mixed with distilled water, were added to the alkali solution and mixed again for 10 seconds at 4000 RPM. Next the solid precursor was added at 400 RPM for 15 seconds, then was mixed for 35 seconds at 12000 RPM following API 10-B2 recommendations.

5. Methods

The testing methodology followed throughout this project is presented in Figure 10. The approach considers that first a neat recipe must be prepared, afterwards chemical admixture(s) was introduced to the neat mix design. Then a series of properties were tested as described below where finally the hydraulic sealability of the mix design was tested under elevated pressure and temperature conditions to verify the usage of such mix design as a zonal isolation material. If the mix design fails in achieving any hydraulic sealability the process was ran again with tuned and engineered chemical admixtures to qualify the material as a barrier material with isolation capabilities. It is worthwhile that sealability of the neat mix design has been measured; the sealability test was utilized as a quality assurance on the impact of the chemical admixture on the sealing capability of the geopolymer.
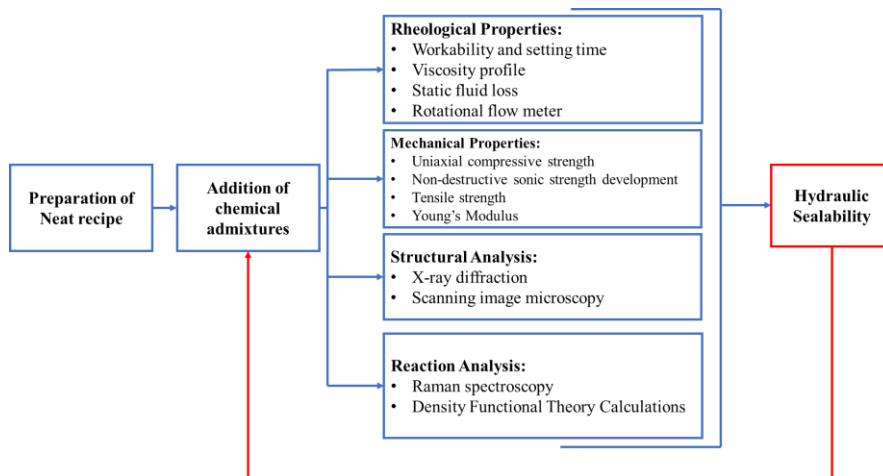
Figure 10. Testing strategy for slurry design

The standards and recommendations used as a guideline for experimental setup and handling were imported from the standard testing procedures of cement. Mainly two standards were utilized in this project; API 10-

B2 recommendations [69] and API 10TR-7 [70]. The use of cement standards set a benchmark for experimental procedure which acted as a guideline to insure credibility and realistic comparison in cases between geopolymer and OPC products. In addition, these recommendations are well known by the oil & gas industry which minimizes the knowledge gap to other readers from petroleum background. However, for analytical testing methods, the procedures were inspired and developed from pre-existing research done on material of similar nature.

It must be noted that conditioning of samples was done following recommended practices prior to some experiments. Samples were conditioned using an atmospheric consistometer with a temperature ramp up rate as 1°C/min. Many properties were examined and are divided categorically according to the following:

5.1   Slurry Properties

Slurry properties were examined for every slurry to ensure the proper qualification of mix designs for downhole conditions. It was to make sure that the mix design will have sufficient time to reach the desired depth, with the right rheology and fluid properties to ensure a successful operation. The following slurry properties were examined as part of the qualification of mix designs:

Workability and setting time – Atmospheric and pressurized consistometer were used following API RP 10-B2 recommendations [69]. The standard for workability was set from the starting point until 40 Bearden unites of consistency (Bc), while setting time was set from 40 Bc to 100 Bc. This standard was followed upon to ensure equipment safety and create a higher benchmark for the slurry.

Viscosity - Mix designed were tested using a rotational viscometer, known as V-G meter viscometer. Measurements were done at rotational speeds of 3, 6, 30, 60, 100, 200, and 300 RPM both in ascending and

descending order, where the average was then calculated and plotted versus shear rate. Slurries were conditioned prior to testing.

Density – Density was measured using a pressurized mud balance following API RP 10B-2 recommendations [69]. Slurries were conditioned prior to testing.

Static fluid-loss – API HPHT test cell was used to measure the fluid loss at 1000 psi at room temperature. The slurries were conditioned prior to testing. A sieve of 250 μm having a hardened filter paper of 45 μm was used with a pressure applied by a CO_2 flow line. The measurement was done for 30 minutes (mins). Slurries were conditioned prior to testing.

Rotational Flow Meter – Rotational tests were performed using a scientific rheometer to evaluate the rheological behaviour of mix designs. Shear rates were measured through different intervals where pre-shear, ramp up, and ramp down tests were performed. The test starts with the pre-shearing at 100 1/s for 60 seconds afterwards ramp up (0.01-511 1/s) and ramp down (511-0.01 1/s). Slurries were conditioned prior to testing.

Zeta Potential - The electrical potential of chemical admixtures was measured using dynamic light scattering with a laser source of wavelength 633 nm at a scattered angel of 13°. The samples were diluted in distilled water to reach 0.1 wt.% at room temperature (25°C). Sample holders DTS 1070 were used as the experimental apparatus. Following the start of the experiment 300 seconds were allowed for equilibration. An average of three measurements was considered to ensure the right qualification of results. These measurements have been conducted to observe the effect of electrokinetic potential of the admixtures on viscosity.

5.2   Mechanical Properties and Microstructure

Uniaxial Compressive Strength (UCS) – Measurements were performed using a mechanical tester having a variety of loading rates ranging from 30 kN/min to 7 kN/min depending on the sensitivity of slurries prepared. The recommended practises following these measurement was API 10TR-7 [70]. Slurries were conditioned prior to curing and were poured into plastic molds of diameter of 5 cm and height 10 cm. Mix designs were cured for 1,3,7,14, and 28 days. The uniaxial stress was calculated using the equation (1) where σ is the force in (MPa), F is the max force prior to cracking in Newton (N), and A is the contact area between the sample and the loading frame in mm^2.

$$\sigma = \frac{F}{A} \qquad\qquad (1)$$

Young's Modulus – The modulus of elasticity is concluded by the following equation (2):

$$YM = \frac{F/A}{\Delta L/L} \qquad\qquad (2)$$

where YM is the elasticity modul in GPa, F is the max force prior to cracking in N, and A is the area of contact between the sample and the loading frame in mm^2, L refers to the highest sample and changes occurring on it in mm.

Non-destructive Sonic Strength Development - An ultrasonic cement analyser was used to measure sonic strength development at confined downhole conditions. The equipment operates by constantly measuring the sonic strength emitted throughout the sample where a transducer was positioned at both ends of the cell. Afterwards, compressive strength was calculated by implementing transit time values into a default algorithm (mainly algorithms related to OPC). However, since in most cases

28

geopolymer samples were measured, these samples have unique algorithms dependent on the chemistry of the mix design, new algorithms were developed using compressive strength data at different time intervals in correlation to the testing time on the sonic strength development equipment. This resulted with a polynomial equation developed from plotting the compressive strength results vs. transit time. These correlations can be found in Appendix 2.

Tensile Strength – Samples were cured similarly to the compressive strength tests, however, they were shaped to have a disk shape having a ratio of thickness to diameter of 0.6 following ASTM D3967-16 recommendations [71]. The disk-shaped samples were tested using a curved jaw setup with a load of 50 N/s applied over the sample where the force was calculated using equation (3) where σ_t is tensile strength in MPa, F is the maximum force prior to cracking of disk in N, T is thickness of the specimen in mm, and D is the diameter of the specimen in mm. The setup used is presented in Figure 11.
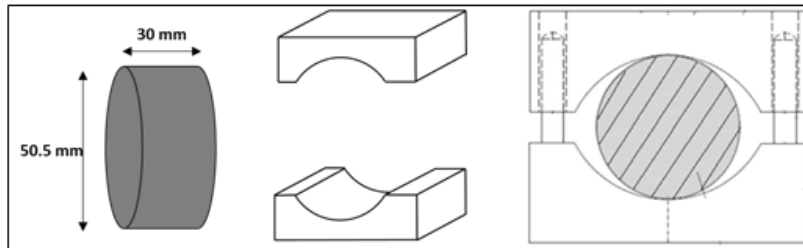
Figure 11. Tensile test setup with a schematic of sample shape and testing jaws used.

$$\sigma_t = 1.2 \; \frac{F}{\pi DT} \qquad\qquad (3)$$

Hydraulic Sealability Measurements – To measure hydraulic sealability of mix designs after setting at downhole conditions, slurries were cured in a cylindrical steel tube (KF HUP S355J2H) having a diameter of 82 mm, thickness of 3 mm, and height of 150 mm with a roughness of 1 μm of Ra. The cylinder was constructed with a two-sided caps to be tightened using metal bolts. The setup is presented in Figure 12.
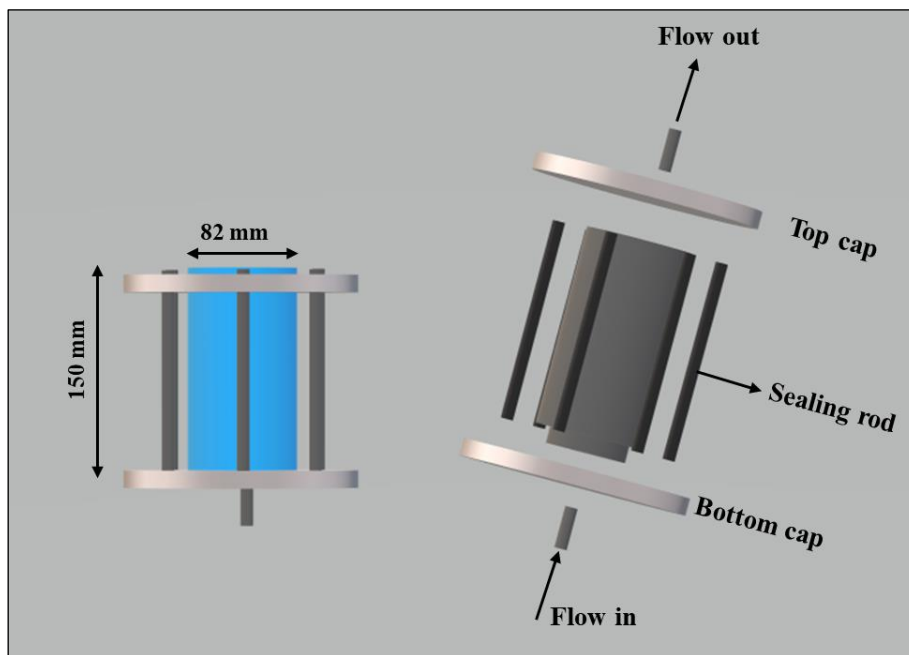
Figure 12. Hydraulic Sealability Setup (Paper III)

X-Ray Diffraction (XRD) – This method was used to give insights regarding the crystallography of the material and the manner of change in solid composition post-curing. The process was performed by directing X-ray to atoms at the surface of the sample which then a reflection of different waves was collected. Bragg's law (equation (4)) was used to interpret the relation between the wavelength λ, the angle of

reflection θ, and spacing between lattice planes of crystal atoms *d* [72]. The Scherrer equation (5) can be used to calculate *d* [73].

$$\lambda = 2 \ x \ d \ x \ sin\theta \qquad (4)$$

$$d = \frac{k\lambda}{B \cos\theta} \qquad (5)$$

In this study, a Bruker-AXS Micro-diffractometer D8 Advance was used having a 2Θ range of 5-92° with a 1°/min step and 0.010^{o} increment. The tested samples were manually grinded into fine powder and dried overnight at 40°C prior to analysis.

Scanning Electron Microscopy (SEM) – Morphology of cured solidified samples was examined using an SEM machine. The samples were cut into small pieces of ~2 mm thickness and dried in a vacuum oven overnight. Afterwards the samples were coated with Pd plasma layer of 10 nm to inhibit electron charging. Element mapping was carried alongside morphology analysis using an energy dispersive X-ray spectroscopy (EDS).

5.3   Chemical Reaction Analysis

Raman Spectroscopy – Slurry paste was analysed using a 532 nm diode laser operating at 25 mW. The spectra were measured from 400 to 4000 cm^{-1} offering a wide overview of composition analysis and a tool to track reaction evolution, specifically Si-Q^{n} sites. In principle, spectra were collected with a 30 mins time interval.

5.4   Computational Modelling

Calculations of density functional theory (DFT) were executed to investigate reaction development while having a retarder in the mix design, refer to Paper IV. The computational modeling work was conducted as a part of bi-lateral collaboration between the University of Stavanger (UiS) and the Federal University of Rio Grande do Norte (UFRN)

where the researcher from UiS conducted the experimental part (e.g., Raman Spectroscopy) and researchers from UFRN performed the DFT calculations and modeling. Dehydration reactions where considered between $Si(OH)_4$ and $[Al(OH)_4]^-$ in addition to the retarder (Zn^{2+} species) considered for the study. These reactions were used to model the formation of Al-O-Si and X-O-Si bonds, where X represents a retarder molecule. The Gaussian 16 software was used for modeling molecular structures through the utilization of different laws of quantum chemistry and mechanics to model structures and energies [74]. The Gaussian 16 software used utilizes different laws of quantum chemistry and mechanics to model structures and energies.

6. Results and Discussions

6.1 Performance of Chemical Admixtures – Focus on Retardation (Paper I)

Identification of chemical admixtures with a retarding role is a starting point for the development of geopolymer material for any field application. The applicability of geopolymer in field applications is dependent on whether adequate pumping time can be achieved [75]. However, the effect of chemical admixtures was not exclusive to pumping time, there were also significant effects on rheological and mechanical properties that must be considered (Paper I). Various admixtures were tested as a starting point while looking into their direct short-term effect on mechanical properties. The strategy was to consider previous literature findings and find a chemical admixture of interest for further investigation.

A variety of chemical admixtures were tested starting with sucrose which had demonstrated retarding effects both on OPC and geopolymer material [76, 77]. Moreover, it was noticed that the use of Al_2O_3 was implemented with efforts to manipulate the silica to alumina ratio (Si/Al) which in turn creates a retardation effect through decreasing the Si/Al ratio as described by De Silva *et al.* [16]. However, the use of Al_2O_3 was highly dependent on the mix design's composition, mainly the Ca content since the focus was mainly on high Ca systems. Thus, the effect of this admixture on a low Ca system would be presented in this section. In addition to the previously mentioned admixtures, zinc (Zn^{2+}) species were an element of focus due to its ability in creating a retardation phenomenon in geopolymer systems [78]. Nevertheless, the use of Zn^{2+} species, in the form of $Zn(NO_3)_2 \cdot 6H_2O$ (alternatively named $Zn(NO_3)_2$), can delay the final setting time, which justified the use of K^+ species in the form of KNO_3 to assist in early strength development and gel hardening as recognized from previous studies [79]. However, it must be

noted that nitrate ions (NO_3^-) can influence the system's kinetics through increasing the ionic strength in the systems and changing the cations' structure size as elaborated by Desbats *et al.* [80] and Kinrade *et al.* [81].

The strategy here was to examine the effect of chemical admixtures, at variant wt% of the total weight (solid & liquid phase combined), in a granite-based mix design, using K_2SiO_3 as a hardening phase. Chemical composition of mix design is highlighted in Appendix 1. The mix designs of studied samples are presented in Table 9*.

Table 9. Mix designs under study with different chemical admixtures (Paper I)

Mix Design (wt. %)						
Mix Design	Solid	Liquid	$K(NO_3)^-$	$Zn(NO_3)_2$	Sucrose	Al_2O_3
Geo-Neat	66.23	33.77	-	-	-	-
Geo-Sp-1	66.23	33.77	-	-	1	-
Geo-Sp-2	66.23	33.77	-	-	2	-
Geo-Sp-3	66.23	33.77	-	-	3	-
Geo-AP-1	66.23	33.77	-	-	-	1
Geo-AP-3	66.23	33.77	-	-	-	3
Geo-ZK	66.23	33.77	0.14	0.57	-	-
Geo-ZKS	66.23	33.77	0.14	0.57	3	-

6.1.1 Pumpability and Setting Time

Workability experiments were conducted at a BHCT of 50°C and atmospheric pressure using an atmospheric consistometer. Starting with sucrose, different concentrations have demonstrated a varying effect on geopolymer mix design as presented in Figure 13. The slurry's workability progressed with the increase in wt% of sucrose in comparison to the neat recipe. The best was attributed to Geo-SP-3 of 3 wt% of sucrose.

* A typo mistake exists in the mix design table in Paper (I,II,III,IV,& V). The correct liquid wt% is 33.77 %. A correction has been made throughout the thesis.

The retardation effect of sucrose has been previously examined by Assi *et al.* [76] where they concluded that sucrose can significantly affect the incorporation between hardener and precursor by affecting the slurry's viscosity which enhances contact time between components and delays setting time.
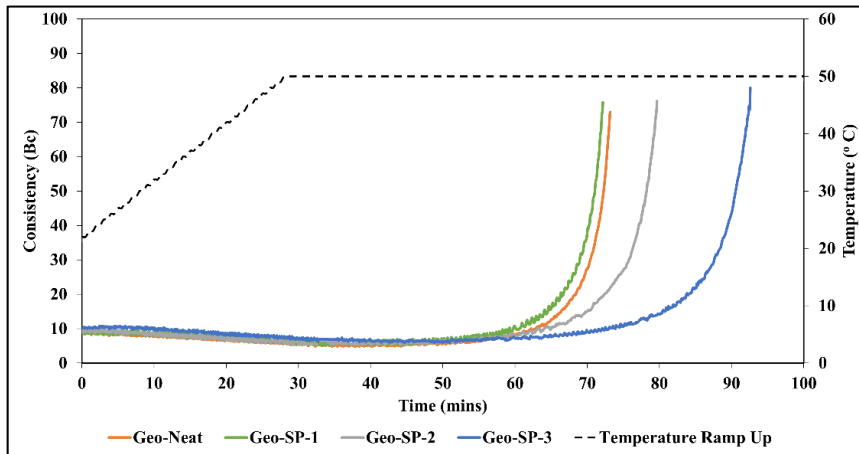
Figure 13. Effect of sucrose on workability of mix designs (Paper I)

Moving on to the effect of Al_2O_3, two concentrations were examined 1wt% and 3wt%, respectively. The effect of Al_2O_3 on workability is presented in Figure 14. It can be observed that Al_2O_3 acted as an accelerator due to a decrease in Si/Al ratio, which demonstrated an accelerating phase leading to almost no significant difference between 1wt% and 3wt%.

Furthermore, it was noticed that $Zn(NO_3)_2$ and $K(NO_3)$ mixture gave the highest retardation effect in comparison to the neat mix design and to other tested chemical admixtures as presented in Figure 15. However, the addition of sucrose was conducted to study its synergistic effect to reach even higher workability and to have an overview of how such admixtures will behave together. Geo-ZK had around 170 mins of workability while Geo-ZKS, the combination with sucrose, had around

220 mins. Nevertheless, this combination may interrupt the formation of gels to harden properly seeing the deviation in the setting time curve towards the end of the test.
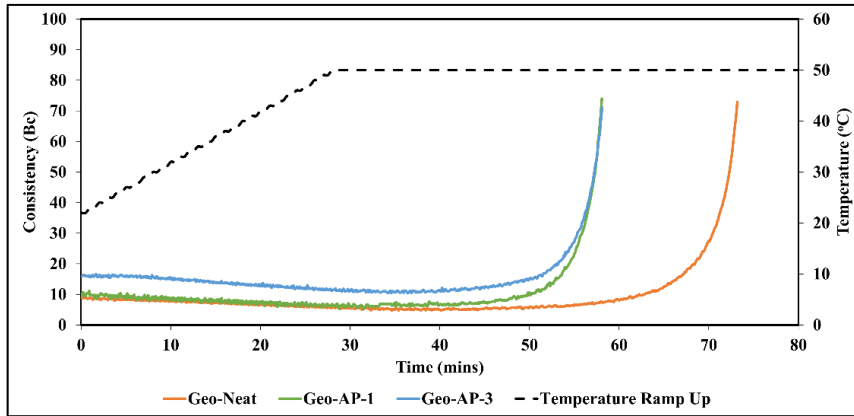
Figure 14. Effect of Al_2O_3 on workability profile of mix designs (Paper I)
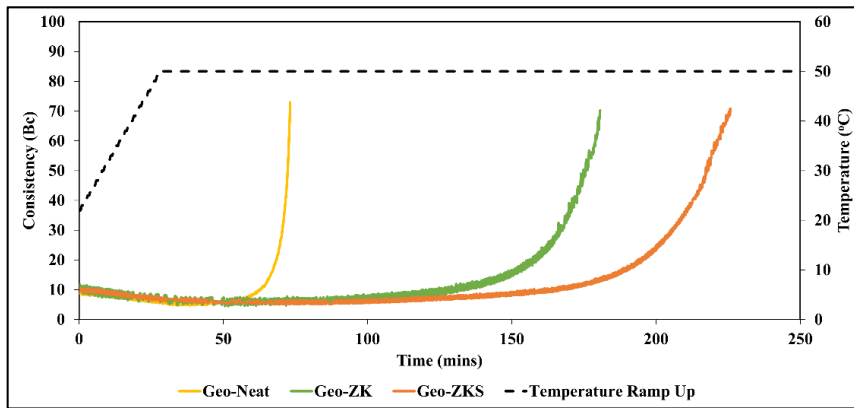
Figure 15. Effect of $Zn(NO_3)_2$, $K(NO_3)$, and sucrose combination on workability of mix designs (Paper I)

6.1.2   *Fluid Loss and Viscosity*

Fluid loss tests were conducted to all mix designs with the various chemical admixtures; however, it was observed that for all samples they had less than 1 ml of fluid loss in 30 mins, which indicated no significant compromise by chemical admixtures to fluid-loss properties.

On the other hand, viscosity measurements had some variations in measurements based on the data acquired in Figure 16. Geopolymer slurries demonstrated a Bingham plastic behavior [82], where no clear observation of changes with behavior was noticed as a result of adding chemical admixtures. It was noticed that a reduction in viscosity was observed in samples containing sucrose at higher shear rates between 200 and 500 1/s. Although ramp-up and ramp-down readings were recorded, only the average values are presented in Figure 16 due to data abundancy.
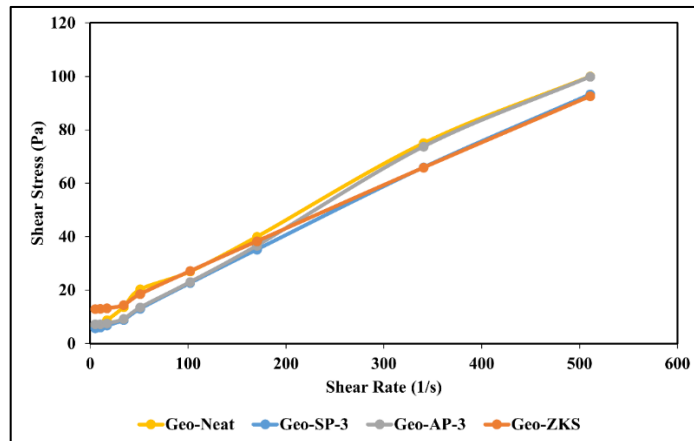
Figure 16. Effect of chemical admixtures on viscosity profiles (Paper I)

6.1.3   *Short-Term Mechanical Properties*

Samples achieving the highest workability in every admixture category were cured and their compressive strengths were measured after 1 and 7 days as presented in Figure 17. It can be observed that samples with

Al_2O_3 (Geo-AP-3) achieved the highest compressive strength in comparison to other mix designs. In connection to previous studies [16, 83], the reduction in Si/Al ratio and availability of a K^+ source in the alkali solution developed the Young's moduli of the matrix, hence achieving better compressive strength measurements in comparison to the neat sample (geo-Neat). On the other hand, the samples' compressive strength was reduced having sucrose (Geo-SP-3) and the combination of sucrose, $Zn(NO_3)_2$, and $K(NO_3)$ (Geo-ZKS) in comparison to the neat sample (Geo-Neat). The reduction in compressive strength can be associated to a poisoning mechanism triggered by the presence of $Zn(NO_3)_2$ species [77, 78].
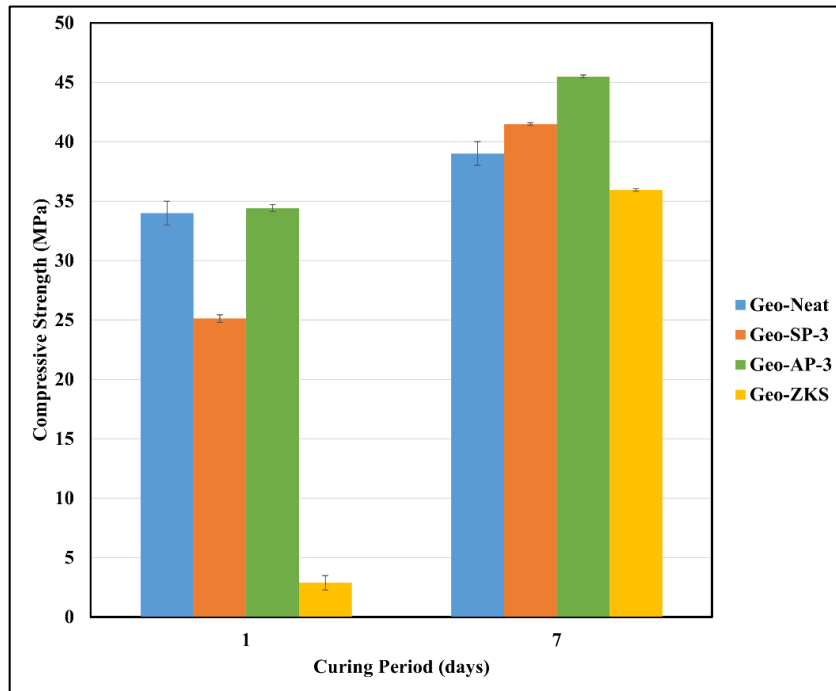
Figure 17. Compressive strength measurements after 1 and 7 days of curing (Paper I)

Since the focus was on finding retarders with the adequate workability time, the combination between sucrose, $Zn(NO_3)_2$, and $K(NO_3)$ (Geo-ZKS) requires more investigation specifically the effect of temperature and some tuning into concentrations introduced into the geopolymer mix design. However, since low compressive strength was measured, it seems that sucrose, although assisting in extending workability, induces high poisoning mechanisms into the geopolymer system. Thus, effect of temperature and concentration tuning would be investigated without the addition of sucrose into the $Zn(NO_3)_2$ and $K(NO_3)$ mixture.

6.2 *Performance of $Zn(NO_3)_2$ and $K(NO_3)$ – Focus on Temperature Effect and Admixture Concentrations (Paper II)*

After having examined the combination of sucrose, $Zn(NO_3)_2$, and $K(NO_3)$ (Paper I) and concluding that sucrose can have a detrimental effect by adding to the already existing poisoning phenomenon exerted by Zn^{2+} species, it was decided to proceed with $Zn(NO_3)_2$ and $K(NO_3)$ alone to examine their effects separately on the mix design system. Some adjustments have been made to the dry solid precursor blend to follow up on the poisoning phenomenon noticed previously. The chemical composition of the dry solid precursor blend is presented in Appendix 1. Adjustments in the concentration of chemical admixtures where two K/Zn ratios were tested and the effect of temperature was observed on pumping time/workability, viscosity measurements, sonic strength development, and compressive strength. Two temperatures were decided upon to be the basis of comparison 50°C and 60°C BHCT. Samples were cured for 1,3, and 7 days at BHST of 70°C and 80°C at a pressure of 14 MPa. Mix designs under study are presented below in Table 10. It must be noted that Neat Class G cement was used as a benchmark reference, only to observe the differences between geopolymer and already existing OPC class. It must be noted that a different type of BFS was used in this

study, due to challenges to acquire an identical batch of BFS from the provider.

Table 10. Mix designs implemented in studying concentration and temperature effect (Paper II)

	Sample Composition (wt. %)				
Mix design	Solid	Liquid	$K(NO_3)$	$Zn(NO_3)_2$	K/Zn Ratio
Neat Class-G	66	44	-	-	-
GEO-Neat	66.23	33.77	-	-	-
GEO-K	66.23	33.77	0.3	-	-
GEO-Zn	66.23	33.77	-	0.3	-
GEO-K/Zn -1	66.23	33.77	0.045	0.3	0.15
GEO-K/Zn - 2	66.23	33.77	0.075	0.3	0.25
GEO-K/Zn - 3	66.23	33.77	0.143	0.571	0.25

6.2.1 Slurry Properties: Workability and Viscosity Measurements

The workability of different geopolymer mix designs can be observed in Figure 18. The chemical admixture $Zn(NO_3)_2$ acted as retarders at both operating BHCTs in comparison to the neat geopolymer slurry (Geo-Neat) as what can be concluded from Table 11 where workability and setting time measurements were recorded in mins for each mix design at both operating BHCTs. Geo-Zn had a good performance in terms of workability, but still setting time was a challenge. Thus, the implementation of both $Zn(NO_3)_2$ and $K(NO_3)$ was done in the efforts to achieve longest workability with a relatively shorter setting time. The start was with a K/Zn ratio of 0.15 and 0.25 (Geo-K/Zn-1 & Geo-K/Zn-2) based on concentrations introduced to the mix design. Geo-K/Zn-1 had a higher workability in comparison to Geo-K/Zn-2, however a longer setting time as well which can be attributed to the effect of $Zn(NO_3)_2$ in poisoning the polycondensation phase. Thus, in efforts to increase

workability to match with Geo-Zn, the concentrations of $Zn(NO_3)_2$ and $K(NO_3)$ was doubled while maintaining a K/Zn ratio of 0.25 which in principle created a balance between $Zn(NO_3)_2$ effect and $K(NO_3)$. It can be argued that the addition of K^+ species created the effect of shortening setting time due to the availability of access K^+ ions which in turn assisted in the polycondensation phase of reaction where hardening and gelation of slurry initiates [79, 84]. In addition the presence of NO_3^- ions can affect the polycondensation step of the Geopolymeric gel formation through affecting reaction kinetics and cation size formed [80]. Noticeably the Geo-Zn and Geo-K/Zn-3 had similar workability measurements at BHCT of 50°C, however Geo-K/Zn-3 had a much better setting time of 13 mins.

Increasing the temperature have demonstrated an acceleration effect on all mix designs. Siyal *et al.* [85] examined the effect of temperature on setting time of fly ash based geopolymer using the Taguchi method. They concluded that the solubility of solid precursor decreases at low temperatures which in turn decelerates the dissolution and polycondensation phases of the reaction. However, higher temperatures ranging between 60-80°C lower workability since higher amount of Si and Al molecules are released into the reaction which explains the short setting time detected in mix designs at BHCT of 60°C.
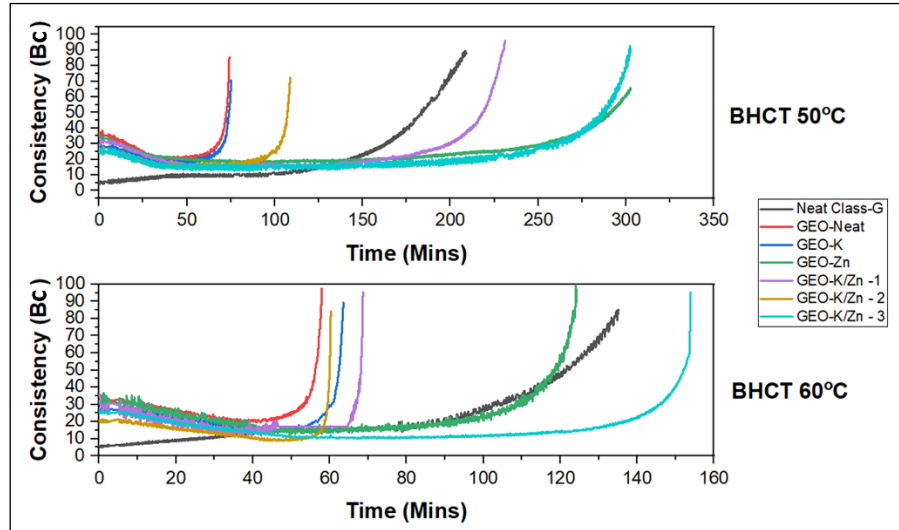
Figure 18. Consistency profiles of mix designs measured at BHCT of 50 and 60°C and ambient pressure (Paper II).

Table 11. Workability and setting time measurements at 50 and 60°C (in mins) (Paper II)

Mix Design	BHCT 50°C		BHCT 60°C	
	Workability	Setting Time	Workability	Setting Time
Neat Class-G	175	33	112	31
GEO-Neat	70	1	53	2
GEO-K	70	2	60	2
GEO-Zn	277	52	113	8
GEO-K/Zn -1	210	18	65	2
GEO-K/Zn -2	103	3	57	1
GEO-K/Zn -3	277	13	147	4

The best performing mix design, in terms of workability and setting time, in this case Geo-K/Zn-3, was picked for further analysis in comparison with Neat Class-G OPC and neat geopolymer slurries (Geo-Neat).

Viscosity measurements presented in Figure 19 show a non-Newtonian fluid behavior exhibiting a Bingham plastic fluid behavior while Neat Class-G presented a Herschel-Bulkley type shear thinning behavior [82]. However, noticeably no significant changes were observed on geopolymer sample Geo-K/Zn-3 although changes in temperature and addition of admixtures were implemented in comparison to its counterpart (Geo-Neat).
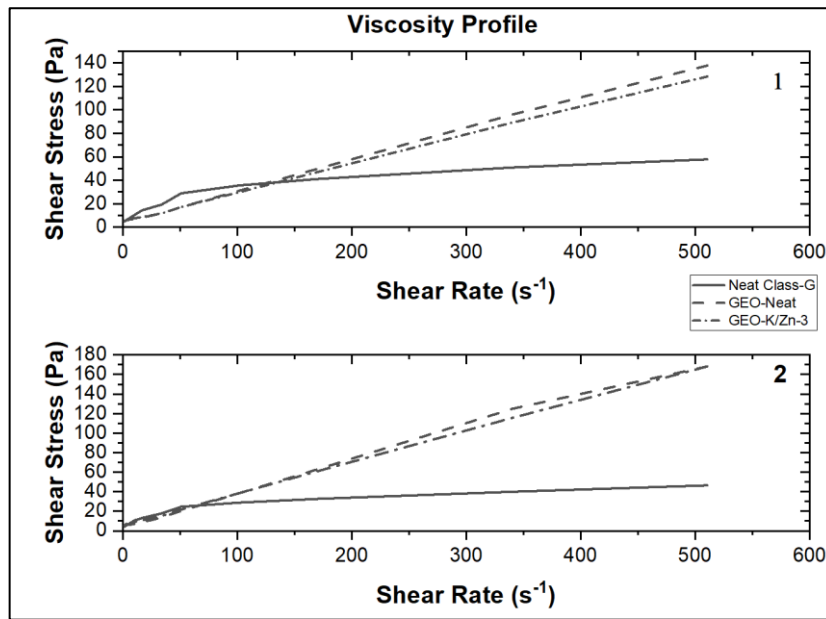
Figure 19. Viscosity measurements of Neat Class-G, Geo-Neat, & Geo-K/Zn-3 (1) at 50°C BHCT;(2) at 60°C BHCT (Paper II)

To more elaborate on the viscosity measurements, zeta potential for chemical admixtures was conducted and presented in Table 12. The measurements were performed and evaluated in accordance to a pervious study conducted by Varenne *et al.* [86]. It has been observed that both $Zn(NO_3)_2$ and $K(NO_3)$ zeta potential measurements were below ±25 mV which indicated no significant dispersion effect of the chemical systems while these particles were in suspension.

Table 12. Zeta Potential measurements for chemical admixtures

Sample no.	Zn $(NO_3)_2$ (0.1 wt%)	K(NO_3) (0.1 wt%)
	ZP (mV)	ZP (mV)
1	-5,45	-19,87
2	-1,59	-21,3
3	-2,76	-19,4
Average	-3.27	-20.19

6.2.2 *Mechanical Properties and Strength Development*

Compressive strength of selected mix designs is presented below in Figure 20. As observed, the strength development of geopolymer slurry at 80°C had a significant increase after 1 day, however the progress slows down after 3 days. According to Villarreal *et al.* [87] temperatures higher than 60°C can affect the formation of a complete oligomerization and polycondensation phases, which in turn affects the completion of the geopolymer matrix. Thus, this can be one reasoning to explain why at 80°C the compressive strength of geopolymer samples (Geo-Neat & Geo-K/Zn-3) were close to their counterparts cured at 70°C with a difference in compressive strength of around 5 MPa to each sample. These results were also supported by findings by Bakri *et al.* [88] where they cured fly ash-based geopolymer at temperatures ranging from 50°C to 80°C and the highest compressive strength was obtained with samples cured at 60°C. Alternatively, in the mix designs at hand, it was not noticeable the effect of poisoning influenced by the addition of $Zn(NO_3)_2$ which in turn raised the request for deeper understanding of the role of K^+ or $(NO_3)^-$ which acted as a counter for the poisoning by fastening the reaction rate in the polycondensation phase of the reaction as described in previous studies [89].
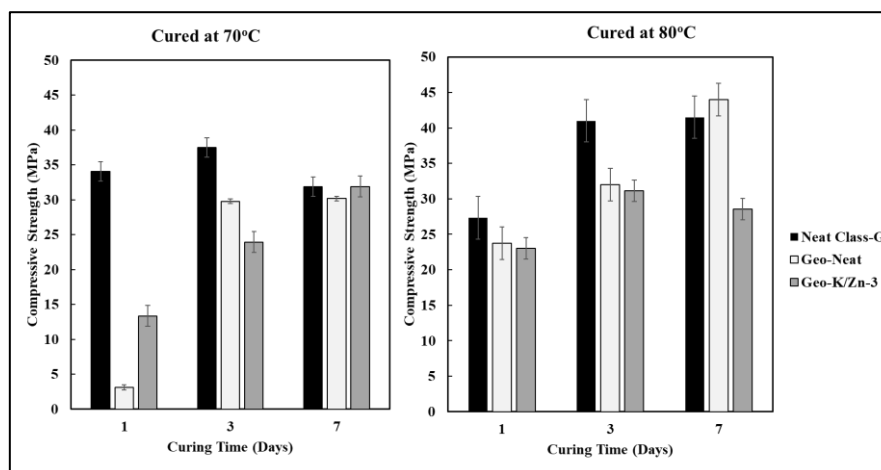
Figure 20. Compressive strength measurements after 1, 3, and 7 days of curing (Paper II)

Further analysis was conducted on mechanical properties to observe the effects of $Zn(NO_3)_2$ and $K(NO_3)$, in addition to the increase in curing temperature, on geopolymer slurry. Nondestructive strength development was measured to determine the starting time of strength development. Since sonic strength development equipment are designed for cement slurries, a correlation was developed from compressive strength results (Figure 20) which can be found in Appendix 2 (Figure 46). The sonic strength results are presented below in Figure 21. It can be observed that temperature had a significant effect to have a faster strength development since at 80^oC geopolymer samples started developing strength at around 1 hr while at 70^oC strength development time was between 2 to 4 hr. On the other hand, the effect of $K(NO_3)$ in fastening polycondensation phase was also recognized in strength development where Geo-K/Zn-3 samples, cured at both temperatures, were able to develop strength faster than Geo-Neat.

45
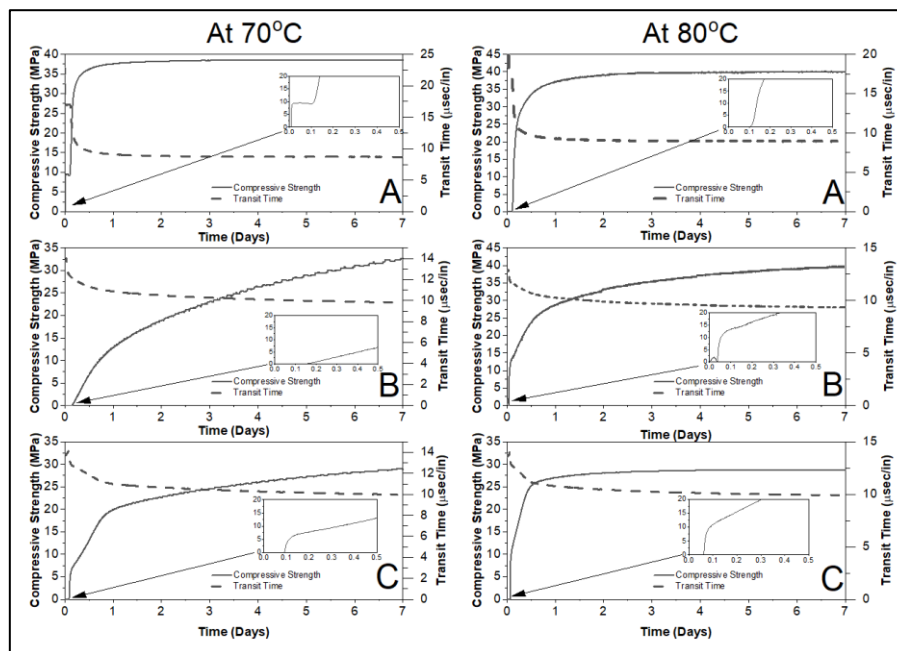
Figure 21. Sonic strength development measurements of (A) Neat
Class-G; (B) Geo-Neat; (C) Geo-K/Zn-3 (Paper II)

To conclude, $Zn(NO_3)_2$ and $K(NO_3)$ as chemical admixture exhibited superior properties for geopolymer systems which in turn triggers an interest in conducting more in-depth analysis of mechanical strength, hydraulic sealability, microstructure, and crystallography which leads eventually to the analysis of reaction mechanism and behavior.

6.3 In-Depth Analysis of $Zn(NO_3)_2$ in Geopolymer Slurries – Effect on Slurry properties, Mechanical Properties, and Microstructure (III)

To elaborate in-depth on the impact of utilizing $Zn(NO_3)_2$ and $K(NO_3)$ as chemical admixtures in geopolymer systems, it was of great importance to examine the manner these admixtures affect other properties from sealability and mechanical properties to microstructure

and crystallography. Extensive tests were performed in multiple curing periods of 1, 3, 7, 14, and 28 days to monitor the behavioral changes in the bulk matrix. This highlighted behavioral changes in intermediate stages of strength development and in turn exposed the material for relatively longer curing times in comparison to the work done in previous sections. In this section, the chemical composition was slightly differed from the previous section 6.2 due to uncontrollable changes in the BFS source from the supplier at the time Paper II was produced. The composition can be examined in Appendix 1. The mix designs' nomenclature and composition is presented in Table 13. The mix designs were tested and conditioned at a BHCT of 50°C, and were cured at BHST of 70°C for 1, 3, 7, 14, and 28 days at a curing pressure of 14 MPa. The slurry properties of the tested mix designs quite similar to the ones mentioned in section 6.1 and 6.2, thus to avoid repeatability of information this section will focus on tests linked to operation and repeatability, in addition to mechanical and microstructural analysis.

Table 13. Mix designs under study (Paper III)

Mix design	Sample Composition (wt. %)					K^+/Zn^{2+} Ratio
	Solid	Liquid	Total water	$K(NO_3)$	$Zn(NO_3)_2$	
Geo-Neat	66.23	33.77	22.13	-	-	-
Geo-Zn/K	66.23	33.77	22.13	0.075	0.3	0.25

6.3.1   Slurry Properties: Repeatability and On-Off Test

To guarantee that the mix designs with $Zn(NO_3)_2$ and $K(NO_3)$ have reproducible results several tests have been conducted in addition to the original tests. The results are presented below in Figure 22. The measurements were carried in an HPHT consistometer under the same conditions using the same source of raw material. The results highlight minor overall differences in consistency and setting time. The relative standard deviation was calculated based on differences in the time when

the slurry reaches 40 Bc where it was concluded that the deviation was around 5.13%. It was noted that although results were reproducible, however special care must be considered to the setting time profile (slurry going from 40 to 70 Bc) where some higher deviations can take place.
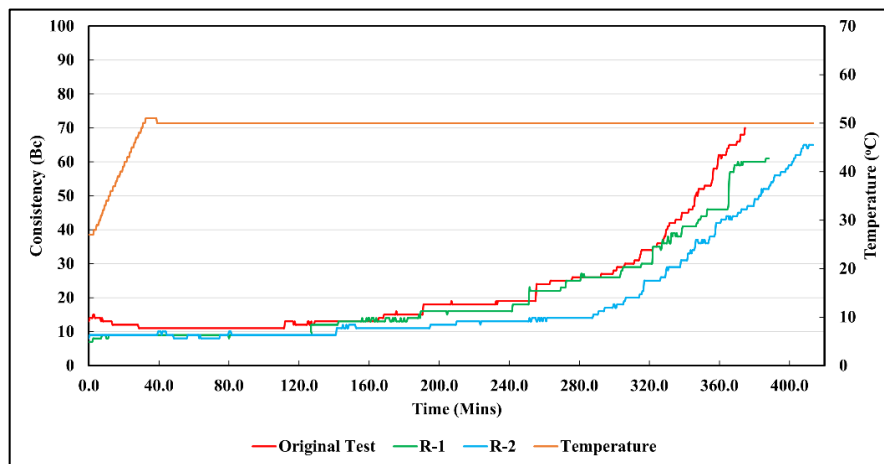
Figure 22. Repeatability tests for retarded mix design at BHCT of 50ºC and 14 MPa (Paper III)

In addition to repeatability tests, on-off tests have been conducted as well to mimic pause of circulation in field operations where two stops were made by shutting down the HPHT consistometer's motor, thus halting the shearing of the sample. Two stops were made, the first for 60 mins while the second was for 30 mins with a 20 mins difference in between. The results are presented in Figure 23. It was observed that the slurry quickly regained its natural consistency at the allocated testing time and quite close to the consistency measurement to the original test. This forwards a good figure of geopolymer applicability in the field where, in this case, the chemical admixtures maintained their role although interruptions were introduced to the system.
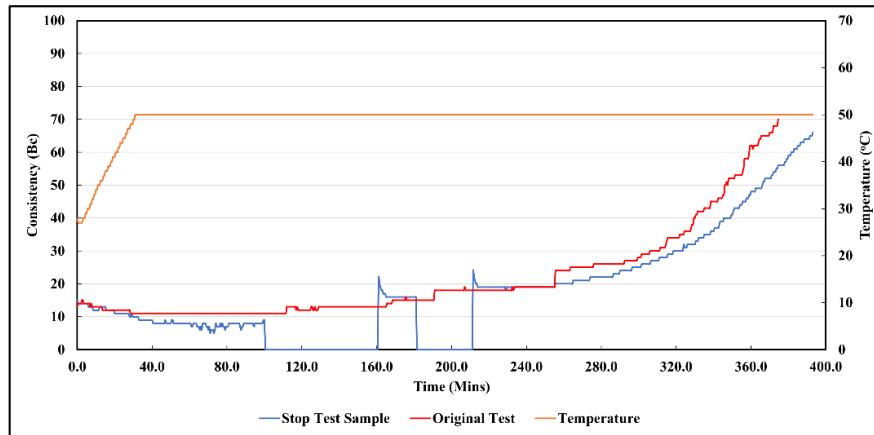
Figure 23. On-Off test of mix design at BHCT of 50ºC and 14 MPa
(Paper III)

6.3.2 Effect of Zn(NO₃)₂ and K(NO₃) on Mechanical Properties and Hydraulic Sealability

The compressive strength was measured up to 28 days and is presented in Figure 24. It can be observed that generally geopolymer samples increase in compressive strength over curing periods under confined temperature and pressure. However, it was evident that up to 14 days the poisoning effect of $Zn(NO_3)_2$ was obviously dominating Geo-Zn/K, but a slight increase has been recorded after 28 days in comparison to Geo-Neat. This indicates that the poisoning effect of chemical admixtures has a specific time window which afterwards becomes depleted, and the admixture completely incorporated into the geopolymer matrix.
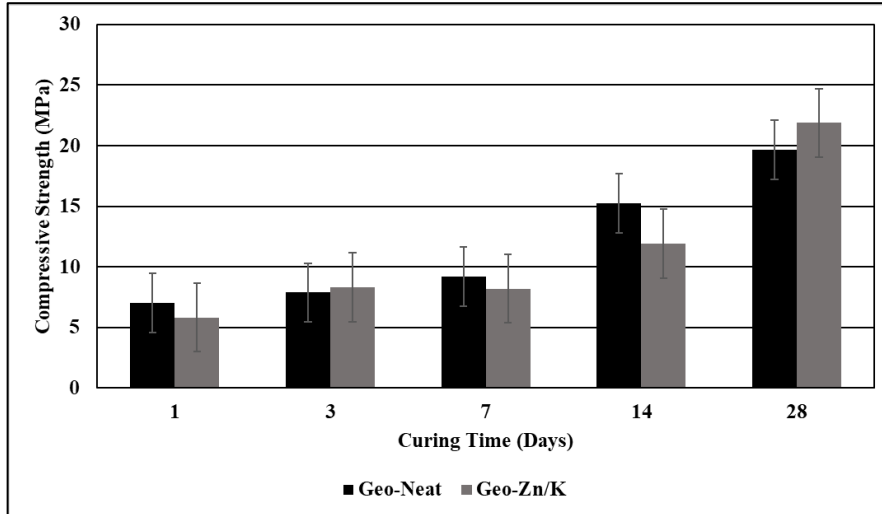
Figure 24. Compressive strength of mix designs cured at 70°C and 14 MPa up to 28 days (Paper III)

The tensile strength on the other hand, presented in Figure 25, had no clear indication of the manner $Zn(NO_3)_2$ and $K(NO_3)$ affected the tensile strength development up to the 28 days curing period. As a general observation, the tensile strength in both samples had close results indicating that the bulk matrix required modifications in chemical composition, either in terms of solid precursors or chemical admixtures, to uplift its performance. However, examining the Young's modulus in Figure 26, it was observed that tested mix designs had a low Young's modulus up to 28 days, which indicates increase of elasticity. Hence, this increase in elasticity contributes to the decrease in compressive and tensile strength properties in cementitious material [90].
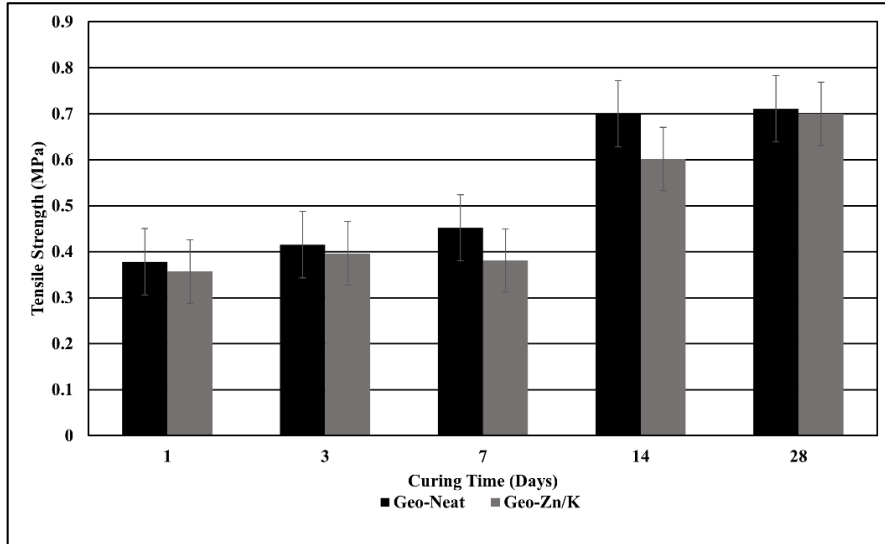
Figure 25. Tensile strength measurements of mix designs cured up to 28 days (Paper III)
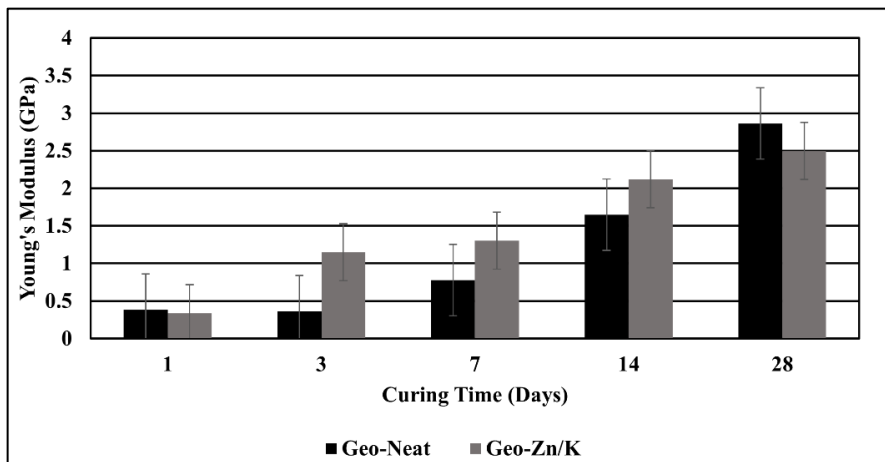
Figure 26. Young's modulus developed from compressive strength data for mix designs up to 28 days

Furthermore, hydraulic sealability was examined to test the material's ability to maintain sealability and zonal isolation properties. The test was

performed after curing for a period of 7 days under BHST of 70°C and pressure of 14 MPa. The results are presented in Figure 27. Fluctuations in flow rate can be observed in the early stages of testing due to differential pressure already existing between the pressure inside the test apparatus and the water pump. Flow was detected at a pressure of 1.5 MPa, however it is observed that a rapid increase was detected with Geo-Neat sample in comparison to a slow build up flow in Geo-Zn/K. This highlights a resistance by the bulk matrix to leakage occurring within. Carter *et al.* [91] highlighted the role of $Zn(NO_3)_2$ species as an expansive additive to cement which triggers a gas forming mechanism, mainly hydrogen, leading to an expansion effect in the bulk matrix while curing. The gas formation mechanism utilizing Al molecules which in turn are heavily available in geopolymer systems. In addition, following on Carter *et al.* [91] findings, the conditions of the reaction occurring from temperature, chemical composition, and pressure seem to have been in favor of triggering an expansion mechanism.
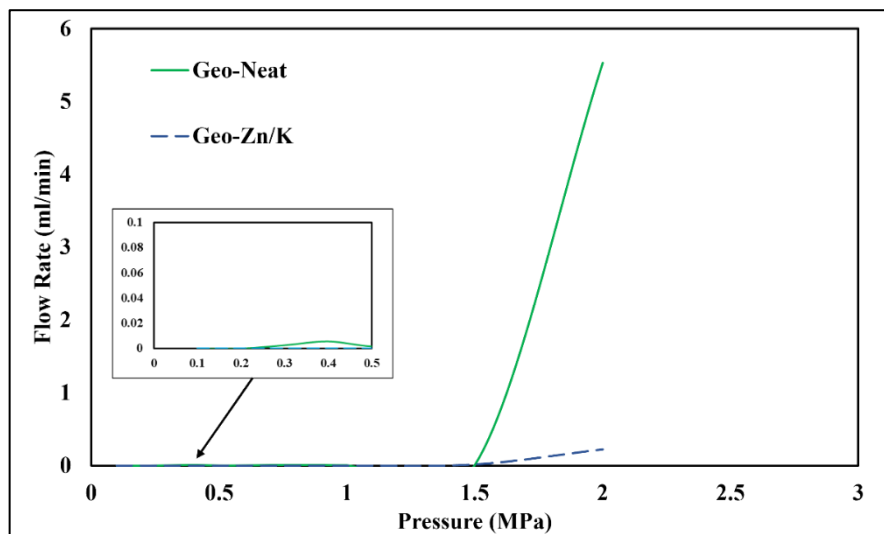
Figure 27. Hydraulic sealability results after 7 days of curing (Paper III)

6.3.3 Effect of Zn(NO₃)₂ and K(NO₃) on Crystallography and Microstructure

Phase changes present a valuable opportunity to examine alterations on minerology of material and inspect formation of foreign components which in turn can elevate or deteriorate properties of mix designs. XRD patterns for Geo-Neat and Geo-Zn/K are presented in Figure 28. Composition of available minerals is mentioned in Table 14. Samples were dominated by quartz and various species of albite, microcline, biotite, chamosite, and calcium zinc silicate available in a minor phase. These findings align with the work of Khalifeh *et al.* [92] done on rock-based geopolymers where quartz was found as a major phase and albite, in addition to microcline, was found as minor phases and not clearly detectable. Yet, the availability of albite and microcline benefits the development of zeolite phases which in turn explains the highly crystalline pattern obtained [92]. The zeolite formation have attributed to the development of compressive strength throughout the curing period since a relation between favorable reaction terms and composition can be established aiding the reaction [93]. On the other hand, the detection of calcium zincate phase at peak $27.8°$ leads on the probability of $Zn(NO_3)_2$ species' interaction with Ca molecules contributing to poisoning phenomenon inhibiting the reaction and causing retardation and weakening strength development. In literature, the main detected phases of Zn was in the form of zinc oxide (ZnO), but that was highly dependent on the nature of Zn additive utilized [55, 78]. Though a detection of calcium zinc silicate was present, nevertheless it was quite minor to be a conclusive finding. The weak presence of such peaks corresponded to the already limited amount of $Zn(NO_3)_2$ species (0.3 wt%) available in the mix design but still more in-depth analysis is required to understand the formation of these complex minerals and their corresponding chemical reactions. Last, the present compounds linked directly to the addition of $K(NO_3)$ species was not clearly foreseen on a phase change level, which raises interest in adapting to a different set of

53

characterization techniques or eliminating its presence and handle the consequences on setting time by adjusting the chemical composition of solid precursors or the addition of chemic admixtures that can act as a delayed accelerator.

Table 14. Mineral composition available in XRD patterns of Geo-Neat and Geo-Zn/K (III)

Mineral	Chemical Composition	Label
Quartz	SiO_2	Qz
Albite	$NaAlSi_3O_8$	Alb
Microcline	$KAlSi_3O_8$	Mic
Chamosite	$(Fe^{2+},Mg,Al,Fe^{3+})_6(Si,Al)_4O_{10}(OH,O)_8$	Ch
Biotite	$K(Mg,Fe)_3(AlSi_3O_{10})(F,OH)_2$	Bio
Calcium Zinc Silicate	$CaZnSi_3O_8$	CZ
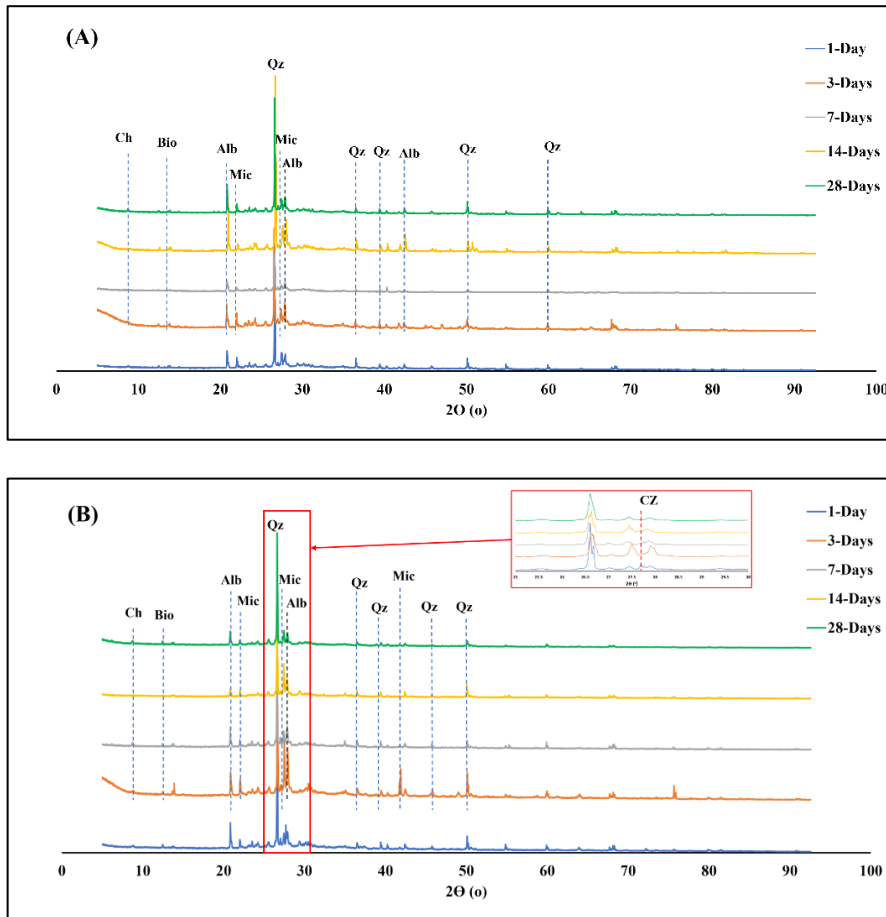
Figure 28. XRD patterns of Geo-Neat (A) and Geo-Zn/K (B) up to 28 days of curing (Paper III)

Furthermore, SEM imaging was performed to mix designs throughout the curing period. The images for Geo-Neat and Geo-Zn/K are presented below in Figure 29 and Figure 30, respectively. From the images it can be observed that unreacted particles (indicated in red arrow) became more incorporated into the bulk matrix and continue to react where it eventually depleted and formed a homogeneous structure as reported in previous geopolymer studies [17, 92]. Once more, like XRD patterns, the direct impact of $Zn(NO_3)_2$ and $K(NO_3)$ was not clearly detected from

SEM imaging. Thus, mapping imagery was conducted trying to get an overview of the overlapping spread of elements, in more particular Zn and Ca, following the point of interest starting from calcium zinc silicate phase detection in Geo-Zn/K. Mapping imagery at different curing phases is presented in Figure 31. The distribution of elements was overlapping with very low concentrations for Zn. Still the formation of Ca-Zn phases cannot be verified 100%. However, it questions the reaction mechanism $Zn(NO_3)_2$ species was undergoing and whether this interaction with Ca was the main effect imposed by $Zn(NO_3)_2$ or whether there was an interaction with the main reaction phases of Si and Al to be uncovered. This would necessitate the incorporation of new chemical reaction analysis techniques with a much-advanced approach to analyze the mechanistic behavior of Zn^{2+} species, which in turn would reveal the real nature of this poisoning phenomenon for curing.
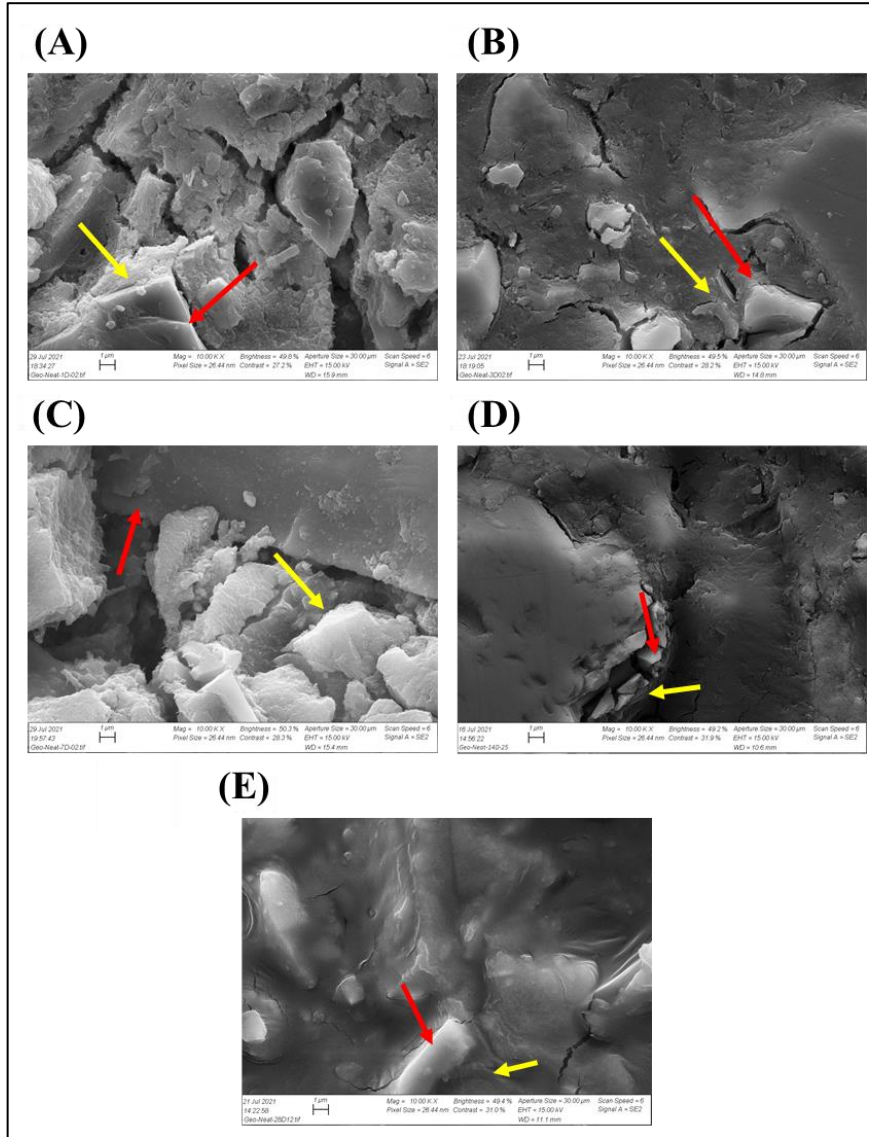
Figure 29. SEM results of Geo-Neat at (A) 1 day; (B) 3 days; (C) 7 days; (D) 14 days; (E) 28 days; Unreacted particles (red arrow) and binder formation (yellow arrow) (Paper III)
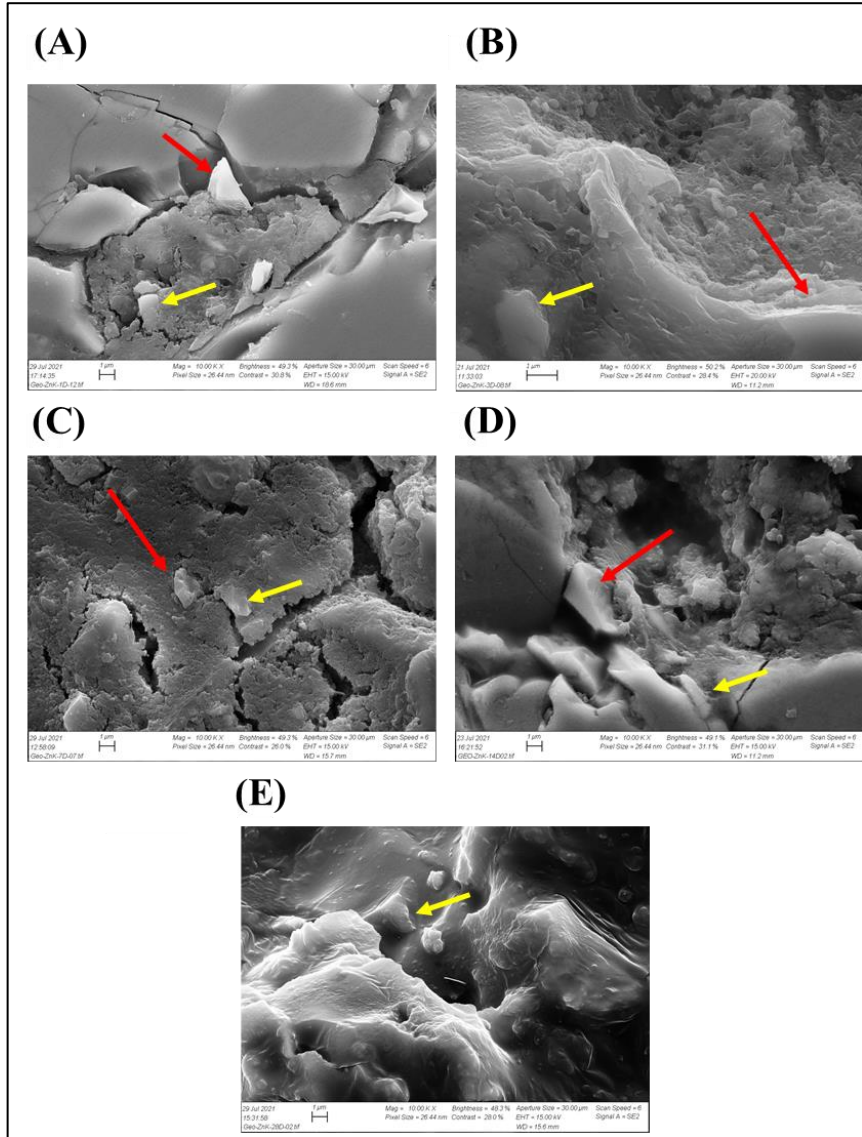
Figure 30. SEM results with range of 1 μm of Geo-Zn/K at (A) 1 day;
(B) 3 days; (C) 7 days; (D) 14 days; (E) 28 days; Unreacted particles
(red arrow) and binder formation (yellow arrow) (Paper III)
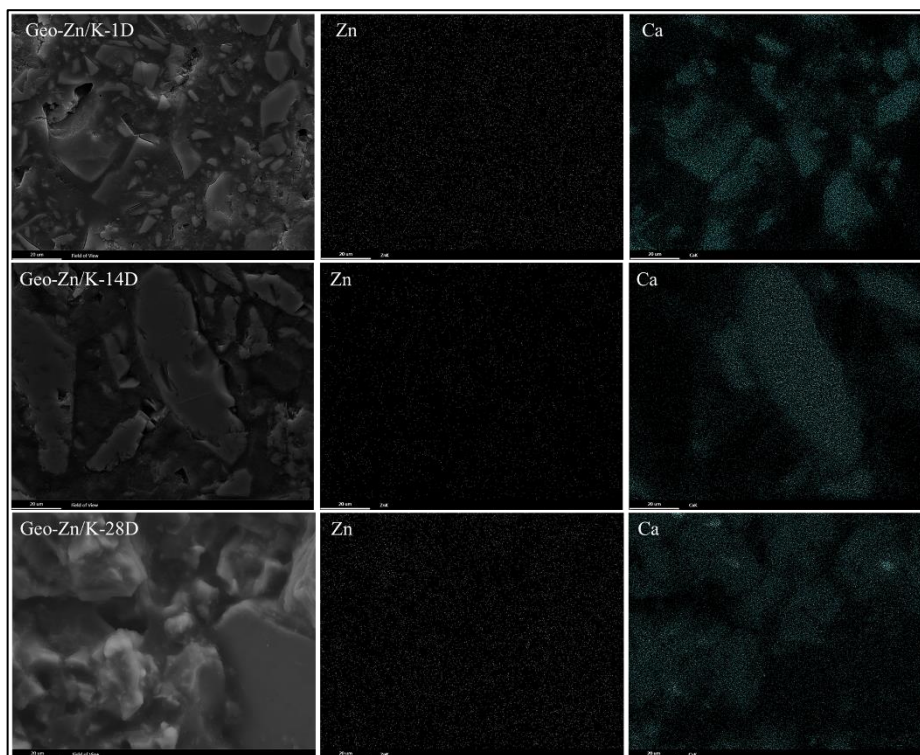
Figure 31. EDS-mapping analysis of of Zn and Ca for Geo-Zn/K for samples cured for 1,14, and 28 days (Paper III)

6.4 Mechanism of Reaction for Zn(NO₃)₂ Species in Geopolymer Systems (IV)

In the previous sections, the effect of chemical admixtures on physically observed properties whether workability or mechanical and microstructural properties was discussed. However, limited findings can be concluded regarding the effect of chemical admixtures on the reaction path. Observations from Paper III indicate no clear/solid reasoning could be concluded regarding the behavior of these admixtures, specifically $Zn(NO_3)_2$,on the reaction path and its working mechanism. Many reasonings can be attributed to these challenges such as the very small

amount of $Zn(NO_3)_2$ utilized, the complexity of the mix design system under study (minerology) and the nature of characterization techniques used for identification (such as XRD). Such challenges motivated the search of characterization techniques and methods that can eliminate the complexities of the system and simultaneously acquire accurate detection of reaction path with methods confirming the prior techniques used.

Zinc can exist in different forms and species some of which are soluble, and some are insoluble in water. Soluble Zn species such as zinc sulfate ($ZnSO_4$) and zinc chloride ($ZnCl_2$). The solubility of zinc depends on a variety of factors such as the pH of the solution, temperature, and presence of other dissolved compounds. For instance, at low pH values, Zn tends to be more soluble, whereas at high pH values, it tends to form insoluble hydroxide (OH^-) species [94]. Thus, the strategy would be to examine the behavior of Zn^{2+} ions, from Zn salts such as $Zn(NO_3)_2$, under the current system's pH so that a more inclusive conclusion can be made of the nature of reaction. Furthermore, the behavior of Zn^{2+} ions must be considered in its interaction with a Si & Al rich system. In previous studies, it was claimed that ZnO dissolves into Zn^{2+} and attaches itself to Ca^{2+} ions forming calcium zincate of which it was speculated that Zn^{2+} influenced the polymerization phase of the reaction [78, 95]. However, the fact that ZnO reacts with OH^- in alkali medium to form $Zn(OH)_2$ has been well documented in the literature which contradicts the proposes claim above [96, 97] . Nevertheless, to shed some light on the Zn^{2+} behavior in the system, the interaction with Q^{0-4} sites of SiO_4^- must be examined as the link to these sites was previously touched up on by Oretgo *et al.*[98].

In this section, retarding mechanism of $Zn(NO_3)_2$ was examined using density functional theory (DFT) calculations and confirming the reaction path by Raman Spectroscopy. Due to the geopolymer system's complexity, a lab-controlled system was created to maneuver the mineral complexity of precursors and pure lab-grade chemicals were used to

mimic the chemical composition of the original granite-based mix design, presented in Table 15, respectively. The details of the lab-controlled samples, composition, and type of chemical replacements are mentioned in Appendix 3 (Table 22, Table 23, & Table 24).

Table 15. Mix design of lab-controlled samples (Paper IV)

Mix design components (Wt%)				
Mix Design	Solid	Liquid	$Zn(NO_3)_2$	Number of molecules of Zn^{2+}
CNT-0%Zn	66.6	33.3	-	-
CNT-1%Zn	66.6	33.3	1	1.21×10^{22}

6.4.1 Density Functional Theory (DFT) Calculations: Isolation of Si, Al, & Zn molecules

The calculations of Gibbs free energy of reaction for dehydration reaction were based on the two dehydration reactions presented in Figure 32. These reactions were considered in this study due to the highly alkaline medium used producing the geopolymer system understudy (pH between 13 to 13.5).
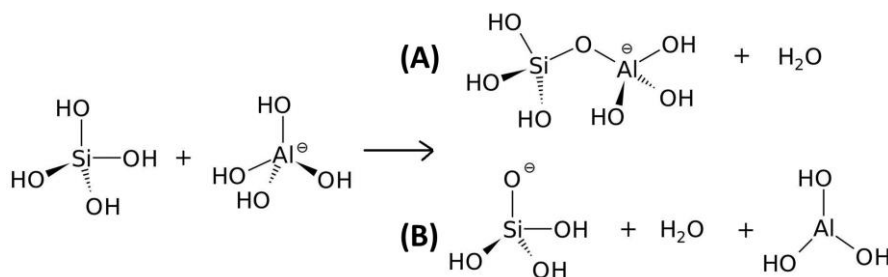
Figure 32.(A) Dehydration reaction with condensation ;(B) Dehydration reaction without condensation of the reactant species (Paper IV)

Through conducting DFT calculations based on the assumed dehydration reactions, fifteen reactions were concluded, and their Gibbs free energy

(Δ_rG) was calculated. Findings are presented in Table 16. The results suggest that the reaction driving force was associated with the formation of Al-O-Si linkage in the oligomer species and $[(OH)_3Al–O–Si(OH)_3]^-$. In addition, DFT calculations foresee the formation of Zn-O-Si linkage (reactions 5-9) which were favorable in terms of Gibbs free energy. However, the dehydration reactions seem to be only favorable with the presence of $[Zn(OH)_4]^{2-}$.

Table 16. Dehydration reactions and their associated Gibbs free energy (in kcal mol^{-1}) based on ωB97X-D/6–311 + G(3df.2p)//6–31 + G(d.p) level of theory (Paper IV)

	Condensation	Δ_rG
(1)	$[Al(OH)_4]^- + Si(OH)_4 \rightarrow [(OH)_3Al–O–Si(OH)_3]^- + H_2O$	−11.0
(2)	$[Al(OH)_4]^- + 2Si(OH)_4 \rightarrow [(OH)_2Al–(O–Si(OH)_3)_2]^- + 2H_2O$	−20.4
(3)	$[Al(OH)_4]^- + 3Si(OH)_4 \rightarrow [(OH)Al–(O–Si(OH)_3)_3]^- + 3H_2O$	−30.5
(4)	$[Al(OH)_4]^- + 4Si(OH)_4 \rightarrow [Al–(O–Si(OH)_3)_4]^- + 4H_2O$	−38.7
(5)	$[Zn(OH)_3]^- + Si(OH)_4 \rightarrow [(OH)_2Zn–O–Si(OH)_3]^- + H_2O$	−7.5
(6)	$[Zn(OH)_3]^- + 2Si(OH)_4 \rightarrow [(OH)Zn–(O–Si(OH)_3)_2]^- + 2H_2O$	−18.2
(7)	$[Zn(OH)_3]^- + 3Si(OH)_4 \rightarrow [Zn–(O–Si(OH)_3)_3]^- + 3H_2O$	−26.9
(8)	$[Zn(OH)_4]^{2-} + Si(OH)_4 \rightarrow [(OH)_3Zn–O–Si(OH)_3]^{2-} + H_2O$	−18.9
(9)	$[Zn(OH)_4]^{2-} + 2Si(OH)_4 \rightarrow [(OH)_2Zn–(O–Si(OH)_3)_2]^{2-} + 2H_2O$	−36.0
	Dehydration	
(10)	$[Al(OH)_4]^- + Si(OH)_4 \rightarrow [Al(OH)_3] + [Si(OH)_3O]^- + H_2O$	+35.0
(11)	$[Zn(OH)_3]^- + Si(OH)_4 \rightarrow [Zn(OH)_2] + [Si(OH)_3O]^- + H_2O$	+1.5
(12)	$[Zn(OH)_4]^{2-} + Si(OH)_4 \rightarrow [Zn(OH)_3]^- + [Si(OH)_3O]^- + H_2O$	−13.3
(13)	$[Al(OH)_4]^- + [(OH)_3Al–O–Si(OH)_3]^- \rightarrow [Al(OH)_3] + [(OH)_3Al–O–Si(OH)_2O]^{2-} + H_2O$	+44.5
(14)	$[Zn(OH)_3]^- + [(OH)_3Al–O–Si(OH)_3]^- \rightarrow [Zn(OH)_2] + [(OH)_3Al–O–Si(OH)_2O]^{2-} + H_2O$	+11.0
(15)	$[Zn(OH)_4]^{2-} + [(OH)_3Al–O–Si(OH)_3]^- \rightarrow [Zn(OH)_3]^- + [(OH)_3Al–O–Si(OH)_2O]^{2-} + H_2O$	−3.8

The optimized structures and their Gibbs free energy profiles of reactions (1), (8), and (12) are presented in Figure 33. In this model, condensation reactions from Al and Zn species were defined by mechanism analogous. These reactions were interlinked through the allure of hydrogen molecules between $Si(OH)_4$ and the available OH groups from either

$[Al(OH_4)]^-$ or $[Zn(OH_3)]^-$. Afterwards, these reactions release H_2O through the reactants' ($[Al(OH_4)]^-$ or $[Zn(OH_3)]^-$) condensation into $[(OH)_3Al–O–Si(OH)_3]^-$ and $[(OH)_2Zn–O–Si(OH)_3]^-$. From Figure 33 it can be observed that reactions (1) and (8) progress into a TS sited at 16.4 and 2.1 kcal mol^{-1} higher than the reactant's energy. This revealed a steric hindrance at the TS structures which can create different geometrical deformation as the case between $[Al (OH_4)]^-$ and $[Zn(OH_3)]^-$ where the first had a larger deformation in comparison to the later one. Moreover, the Int ($[Zn(OH_3)(OH_2)…OSi(OH)_3]^{2-}$) formed as a result of reaction (12), happened with no significant registered barriers of which $Si(OH)_4$ undertakes a hydrogen preoccupation process by the OH group originating from $[Zn(OH_4)]^-$. Later, this Int phase can either undergo a fragmentation process which yields products of $[Zn(OH)_3]^-$, $[Si(OH)_3O]^-$, and H_2O; or it can condense to yield $[(OH)_3Zn–O–Si(OH)_3]^{2-}$ and H_2O. These calculations highlight that reactions involving $[Zn(OH_4)]^{2-}$ anions were more feasible in terms of thermodynamics and kinetics in comparison to other available anions in the reaction.
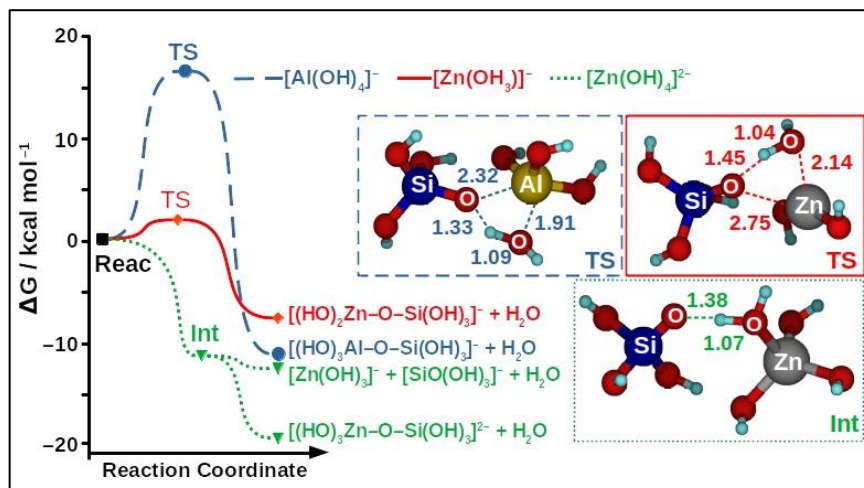
Figure 33. Optimized structures and their Gibbs free energy profiles. The Gibbs energy values (in kcal mol⁻) for each reaction profile were relative to the reactants (Reac). Structures of the transitions state (TS) and intermediate (Int) calculated at the ωB97X-D/6–31 +G(d.p) level of theory. Some relevant bond distances (in Å) were included in the structures. (Paper IV)

6.4.2 *Raman Spectroscopy: A Verification of Reaction Mechanism from Density Functional Theory Calculations*

Raman spectroscopy was carried out simultaneously with DFT calculations to comprehend the conclusions from the stated model. The use of controlled lab-samples proved highly reliable specially in removing the fluorescence effect of some the elements available in the granite-based geopolymer. Raman spectroscopy results are presented in Figure 34. The results concluded from DFT calculations (Figure 33) suggests Zn^{2+} species can trigger the formation of SiO_4-Q^3 species via a barrierless TS, which in turn will lead to higher formation of Q^3 species compared to samples without Zn^{2+} species. Here, Raman spectroscopy was utilized to provide evidence for this phenomenon where it can be

noticed from Figure 34 (A) and Figure 34 (B) that the sharp peaks at 1051 cm^{-1} and 1048 cm^{-1}, respectively, were associated to Si-O$^-$ vibrations where O$^-$ denotes a non-bridging O to the Q^3 sites [99]. One important observation to note is that the Q^3 bands have increased as the reaction progresses which indicates an OH$^-$ attaches on the Si network which produces increased amounts of unbounded O molecules into the system. To emphasis on the effect of Zn(NO$_3$)$_2$, it can be observed from Figure 34 (C) that the Q^3 peak have shifted to 1048 cm^{-1} which was a consequence of the charge transfer from Zn(OH)$_4$$^{2-}$ to SiO$_4$ which in turn weakness the Si-O bonds. The effect can be observed much clearly in Figure 35 where higher rate of Q^3 formation was detected because of adding Zn^{2+} species.

The unraveling of possible reaction pathway for Zn^{2+} species in the geopolymer system under study can help in unraveling other reaction mechanisms occurring in the system. This understanding would take the incorporation of chemical admixtures, with different roles, to the next level by considering how these different admixtures would behave together in a high pH medium. This would be discussed in the next section.
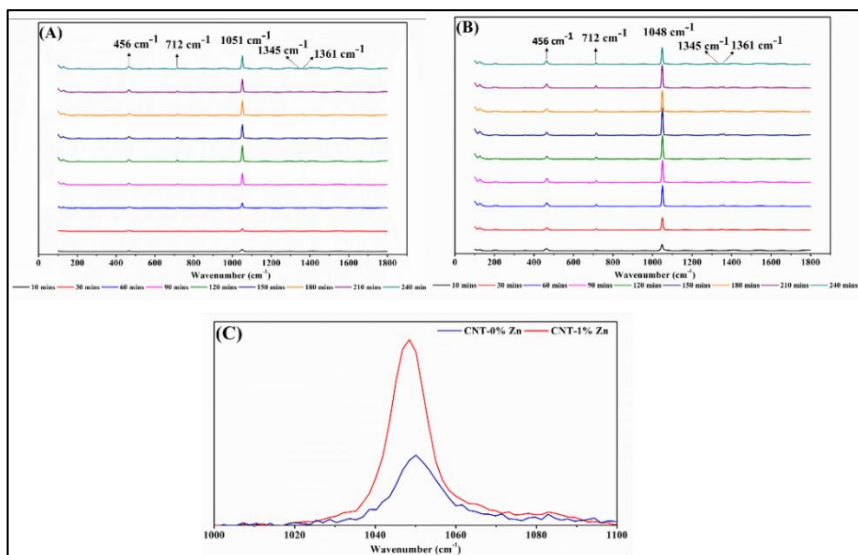
Figure 34. Raman spectra of tested samples (A) CNT-0%Zn; (B) CNT-0%Zn; (C) Overlay of Raman spectra of CNT-0%Zn and CNT-1%Zn at t = 10 min (Paper IV)
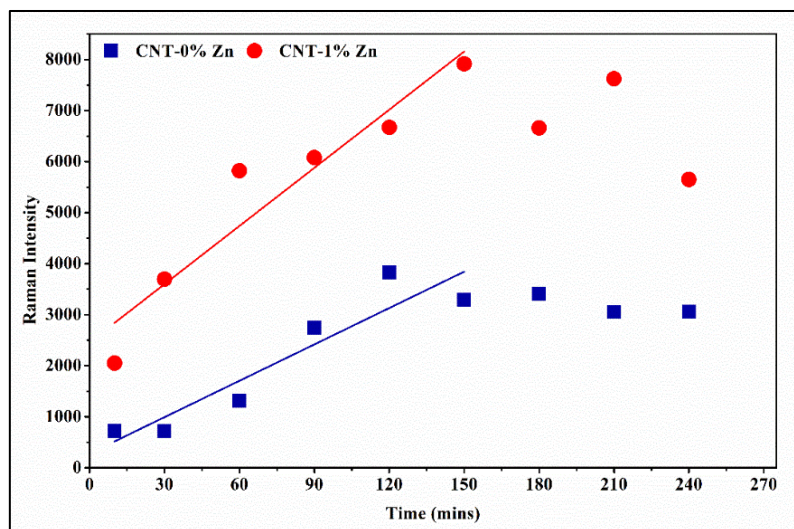
Figure 35. ''Q^3 band intensity as a function of time for geopolymer pastes CNT-0%Zn & CNT-1%Zn'' (Paper IV)

6.5 *Calcium and Sodium as Potential Strength Development Agents (V)*

Geopolymers utilized in high temperature applications dictate the use of retarders to ensure sufficient time to have the slurry pumped into the wellbore, in addition to the required safety margins. However, since the use of retarders will highly influence the bulk matrix, in the form of poisoning phenomenon, and the material may have a delayed strength development phase, which is not likeable from an operational perspective. Therefore, the idea of using strength development agents or delayed accelerators, in efforts to minimize the poisoning mechanism as much as possible, was implemented using Ca^{2+} and Na^{2+} species in the form of $CaCO_3$ and NaOH, respectively [65]. A combination of both elements was used to assist the bulk matrix in early strength development cured under a BHST of 80°C. Slurry and mechanical properties were examined to learn the effects of strength development agents on the geopolymer matrix. The mix design nomenclature and composition are presented in Table 17.

Table 17. Mix Design Composition (Paper V)

Mix Design	Solid|	Liquid	Molar Ratio	K(NO₃)	Zn(NO₃)₂	NaOH	CaCO₃
				Sample Composition (wt. %)				
Geo-Neat	66.23	33.77	2.4	-	-	-	-
Geo-Retarded	66.23	33.77	2.4	0.3	1.1	0.07	0.4

6.5.1 Impact of Strength Development Agents on Slurry Properties

At a BHCT of 60°C, more $Zn(NO_3)_2$ must be utilized to ensure adequate workability and setting time because of the effect of high temperature on setting time (Paper II). However, with this increase, a deterioration in the slurries ability to undergo a rather solid polycondensation phase can be observed in Figure 36. As presented, above 40 Bc the slurry faces a challenge in developing strength quickly, which indicates that the $Zn(NO_3)_2$ effect was overcoming the role of $CaCO_3$ and NaOH at this phase of study.
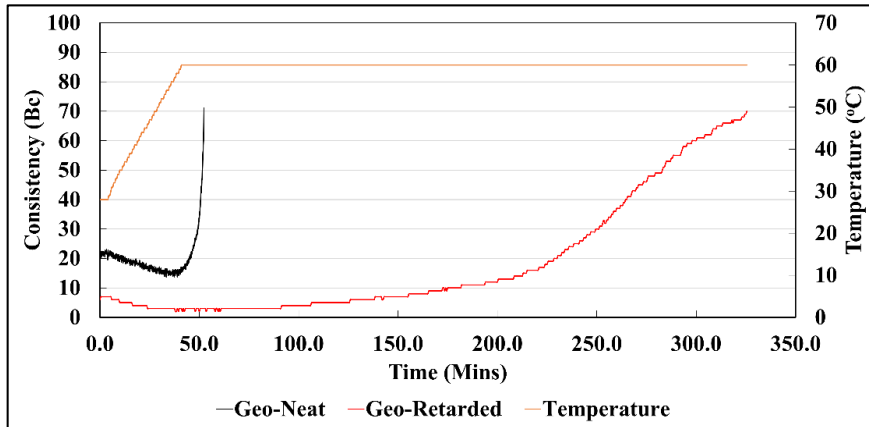
Figure 36. Consistency measurements of mix designs (Paper V)

6.5.2 Mechanical Properties: Efficiency of CaCO₃ and NaOH

In terms of strength of cured slurries, it was observed from Figure 37 that the retarded sample (Geo-Retarded) was heavily affected in comparison to the neat sample (Geo-Neat) after 1 day of curing. The situation changed after 3 days, where the retarded sample starts to regain strength and relatively match with neat sample while continuing with the same trend up to 7 days. Thus, the strength development agents did not provide

superior properties, but they managed to reduce the effect period of the poisoning mechanism imposed by $Zn(NO_3)_2$ species and reduced the poisoning time from 14 days to 7 days as was previously observed in paper III. It was suspected that the presence Ca^{2+} could yield some C-S-H gel phases through integrating into the bulk matrix, while Na^+ presence increased the count of Si monomers, through higher dissolution, which in turn gave the combined effect of altering the poisoning effect and reducing its lifespan in the bulk matrix [100-102]. However, no major strength development can be attributed to C-S-H gel phases in this case since, according to Puligilla *et al.* [103], C-S-H gels inhibit/delay the formation of K-A-S-H gels, the building blocks of geopolymer matrix, which can contribute highly to the strength development of the bulk matrix.
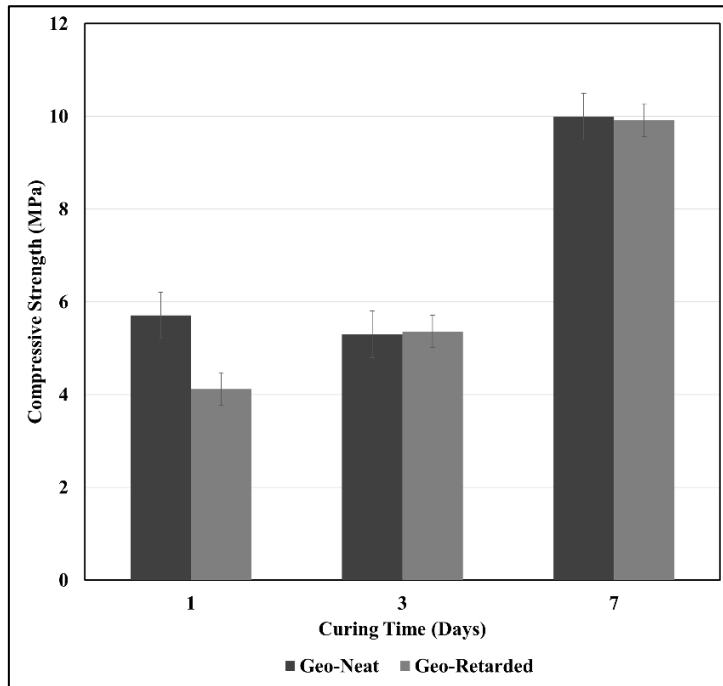
Figure 37. Compressive strength of mix designs of samples after 1, 3, and 7 days of curing (Paper V)

Although, having strength development agents would make one expect a sharp increase in the sonic strength development profiles (correlation for sonic strength in Appendix 2 (Figure 47) throughout curing time, however Figure 38 highlights a dip in strength development at the time after 2-3 days of curing. These dips were suspected to be the influence of molecular organization occurring in the inner structure which in turn widens the gap between molecules and results in increase in transit time. Still more investigation must be performed to guaranty the hypothesis's accuracy since the material achieved similar compressive strength after 3 days in comparison to the measurements after 1 day.
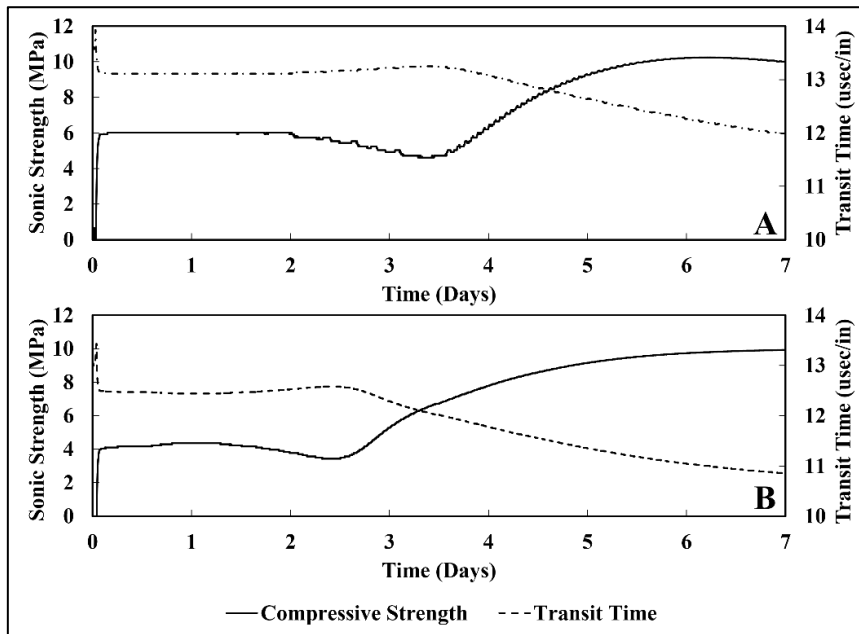
Figure 38. Sonic strength measurements of mix designs (A) Geo-Neat; (B) Geo-Retarded (Paper V)

The tensile strength of mix designs turned out quite different from compressive strength measurements in terms of trend of development throughout the curing period as presented in Figure 39. It cannot be accurately foreseen of why such trend appeared and what parameters

surround its existence due to the low measured values and the high probability in error measurement, which no solid conclusion can be drawn.
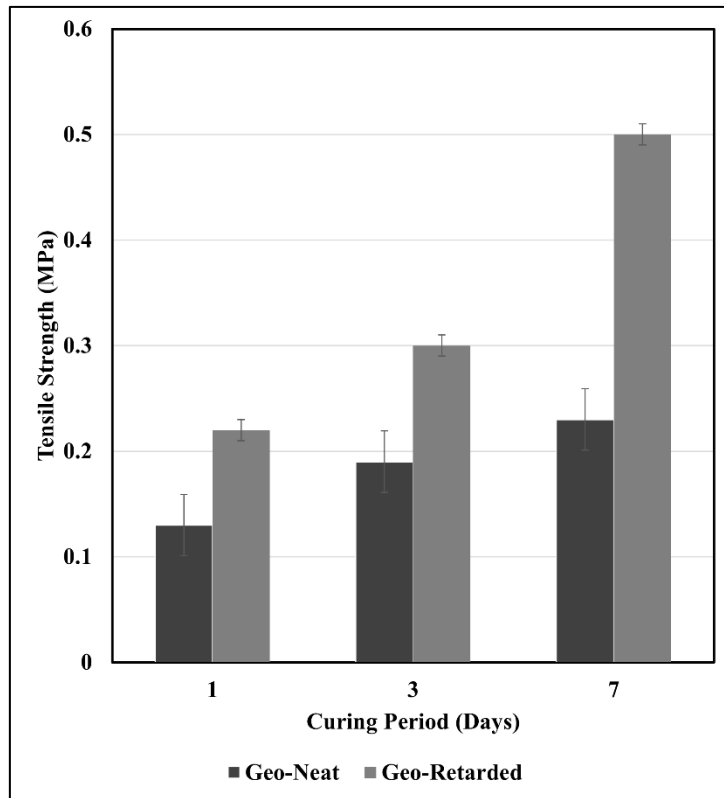
Figure 39. Tensile strength of tested mix designs samples after 1, 3, and 7 days of curing (Paper V)

6.6   *Developing Geopolymer Mix Designs – Applicable from Low to Elevated Temperature (VI)*

One aspect of developing cementitious material was not only to investigate the chemical admixtures that may be added to a dry blend but examine the parameters that surround the dry blend and modify the composition to be suitable for multiple ranges of applications. Like OPC,

72

the development of different blends for geopolymer material for the oil & gas industry can fasten the development of material and reduce operational cost by reducing the use of external chemical admixtures in the field.

In this section, three mix designs were developed and examined under a range of temperature from 5°C to 60°C of BHCT. The main difference was in the composition of mix designs where it was adjusted using CaO added to the dry blend mixture. The focus was on developing three classes of dry blends to meet applications of well cementing at shallow, intermediate, and production section of wellbores. These classes were catalogued based on their performance under the proposed conditions in Table 18 where the pressure and temperature were linked to the True Vertical Depth (TVD) to make the approach as close to North Sea field conditions. The chemical composition of mix designs under study can be found in Appendix 1 (Table 21). The mix design components and density (SG) are presented in Table 19.

Table 18. Mix designs and their allocated operational conditions (Paper VI)

Mix Design	TVD (m)	Pressure (MPa)	Temperature (°C)
M.D A	350	4.5	5
	530	5.5	10
	670	6.5	15
	800	8.0	20
M.D B	920	9.5	25
	1,090	11.5	30
	1,370	14.5	40
M.D C	1,655	17.5	50
	1,941	20.0	60

Table 19. Mix design composition under study (Paper VI)

	Slurry Design (wt. %)					
Mix Design	**Density (SG)**	**Solid**	**CaO**	**KOH (4M)**	**K_2OSiO_2**	**Solid/Liquid Ratio**
M.D A	1.88	69.5	3	30.5	-	2.28
M.D B	1.88	69.3	1	30.7	-	2.26
M.D C	1.98	66.7	-	-	33.3	2

6.6.1 Slurry Properties – Workability and Rheology

A main determining factor for the applicability of each mix design is workability/setting time. Measurements have been done relative to the assigned conditions (Table 18) as presented in Figure 40. It can be observed how temperature was a determining factor in the applicability of each mix design considering the setting time of each mix designs. The addition of CaO at low temperatures was highly beneficial to the

hardening of mix designs, at low temperatures, which facilitated the development of a hard structure [104, 105]. If the mix design can achieve hardening state, having an extended workability is an advantage that can reduce the use of chemical admixtures and allow fewer complex modifications to slurry properties.
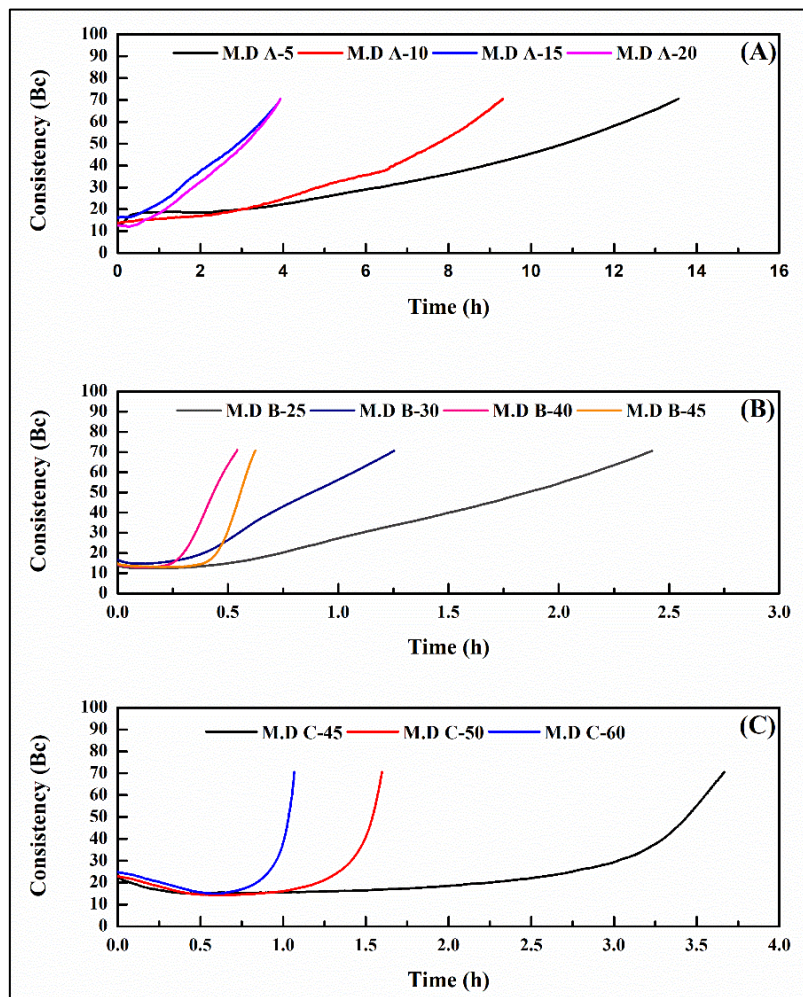
Figure 40. Workability measurements of (A) M.D A, (B) M.D B, and (C) M.D C (Paper VI)

Due to the sensitivity of some mix designs, viscosity ramp-down measurements of all mix designs are presented in Figure 41. It was noticed that with an increase in temperature, the slurry's viscosity was reduced due to the higher kinetic energy undergoing the reaction as seen with M.D A [106]. However, the other mix designs had an opposite trend with increasing temperature which can be attributed to the acceleration of material while the test was undergoing as in M.D B-40 and M.D C-60. These results were interlinked with the workability measurements where some mix designs were not pumpable more than one hour.
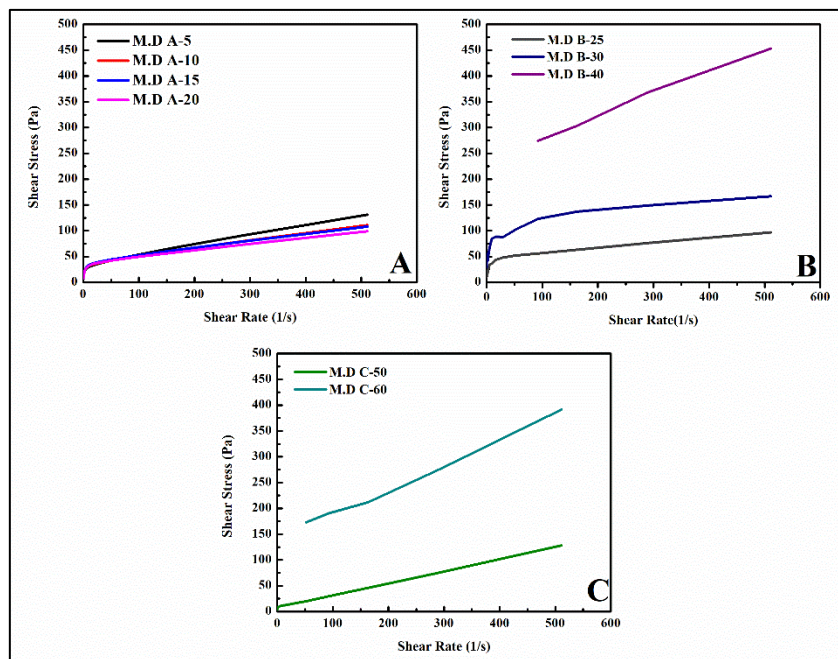
Figure 41. Viscosity measurements (Ramp-Down) (A) M.D A, (B) M.D B, and (C) M.D C (Paper VI)

Furthermore, these mix designs had a thixotropic behavior as observed from Figure 42 where the mix designs were examined at temperatures which separate their classification. The area between the curves present a thixotropic behavior of slurry [107]. These effects were linked to

chemical composition nature and the operating temperature tested upon, where this is seen as a positive behavior in slurries which can reduce fluid loss issues during operations [108].
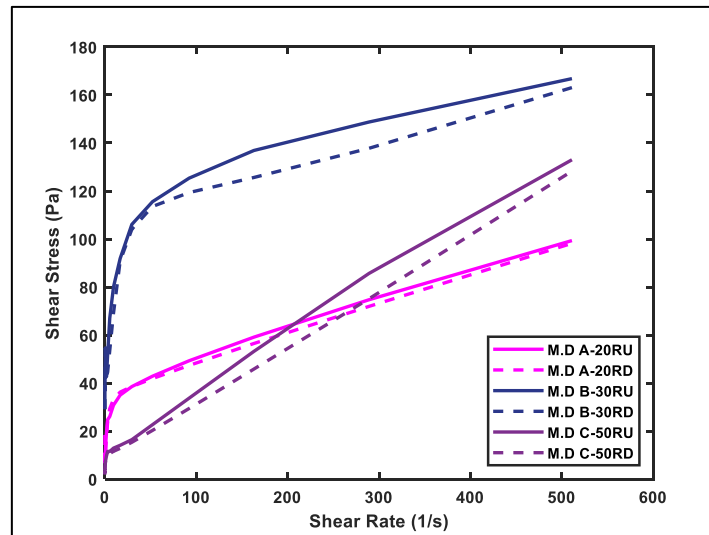
Figure 42. Ramp-up/down curves of mix designs at their intermediate temperatures (Paper VI)

6.6.2 Mechanical Properties: Variations Depending on Composition and Temperature

The compressive strength of mix designs is presented in Figure 43, where samples have been tested after 1 and 7 days of curing at the allocated operational temperatures. Noticeably, the mix design at low temperatures, M.D A, was able to develop strength although being at unfavorable conditions for reaction. Temperature has always been considered an important parameter to have a complete reaction, which in turn results in higher mechanical strength. In this case, M.D A has benefited from the higher Ca content in its composition where it contributes to achieving a high extent of reaction and leads to higher strength in the bulk matrix [109]. Furthermore, it was perceived that M.D

B-40 had the highest performance at 1 and 7 days of curing. This indicates that not only chemical composition, but also the thermodynamic parameters surrounding this reaction have all favored the reaction phases and resulted eventually in the highest compressive strength. This reasoning has been touched upon previously by Provis *et al.* [110] where they highlighted how at 40°C the kinetics of geopolymer reaction were highly favorable. Moving on to M.D C, it was noticed how although higher temperatures were utilized in curing, however, the compressive strength achieved was not the highest in those terms. This indicates that temperature alone was not enough to maintain/develop superior mechanical properties. The need for a firm balance between composition and the effect of thermodynamic parameters can result in achieving a reaction where its kinetics were more favorable, thus producing a highly developed reaction.
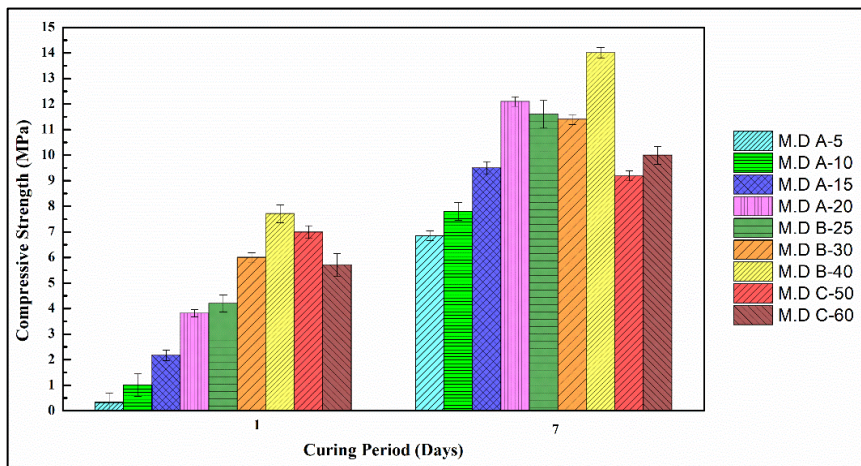
Figure 43. Compressive strength measurements of mix designs from 5 to 60°C (Paper VI)

6.6.3   *Crystallography of Mix Designs*

A comparative approach was performed to analyze the changes occurring in the solid precursor post reaction phase. To that end, the dry

78

blend of mix designs and the mix designs' outcome was analyzed using XRD and presented in Figure 44 & Figure 45 respectively. The mix designs M.D A, M.D B, and M.D C were cured for 7 days at 20, 40, & 60°C, respectively. Starting with the dry blend (Figure 44), it was observed that peaks of illite (IL) were consumed post reaction, whereas peaks of quartz (Qz), albite (Alb) and microcline (Mic) were consistent in their presence. However, it was noticed that no C-S-H peaks from the Ca content in M.D A and M.D B were visible. Still interestingly, the quartz peak of M.D B in Figure 45 shows higher consumption after 7 days in comparison to M.D A and M.D C. This runs along the observations of M.D B performance in compressive strength where M.D B-40 had the highest compressive strength throughout the curing periods. This is an additional indication that the chemical composition of M.D B and the allocated operational temperature have yielded favorable conditions for the geopolymer formation reaction.
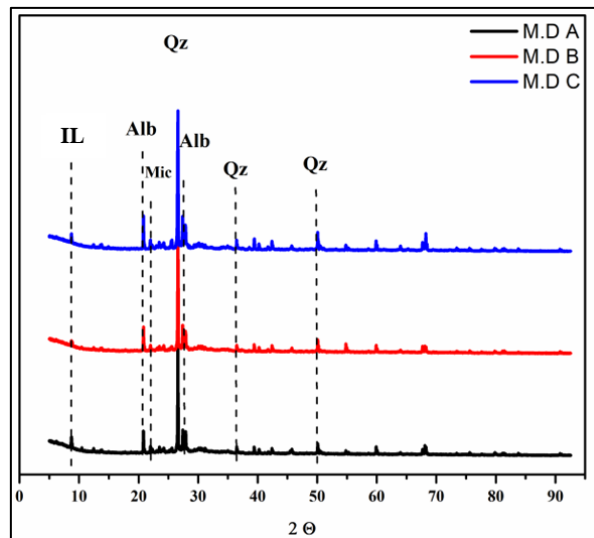
Figure 44. Crystallography of solid precursors mix of of M.D A, B, & C (Paper VI)
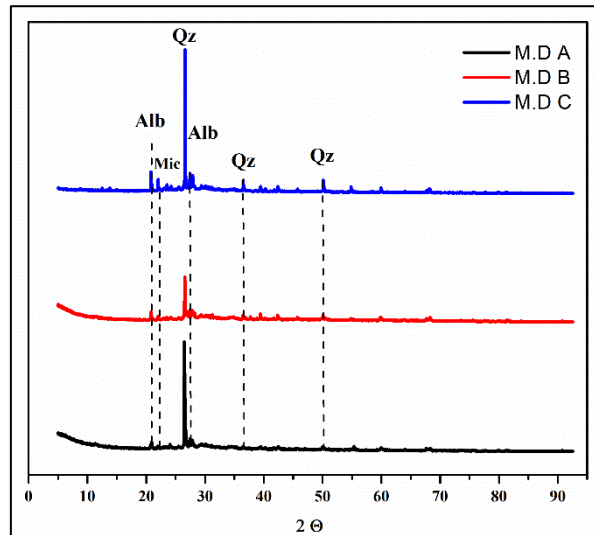
Figure 45. Crystallography of M.D A, M.D B, and M.D C after 7 days of curing at 20, 40, & 60ºC respectively (Paper VI)

7. Summary and Conclusion

7.1 Summary

Chemical admixtures for granite-based geopolymers have been developed and studied under a variety of operational conditions. Slurry properties from consistency to viscosity and mechanical properties from mechanical strength to microstructure were examined. A variety of chemical admixtures have been tested where $Zn(NO_3)_2$ and $K(NO_3)$ achieved the best results in terms of elongating workability and ensuring retardation. Furthermore, the effect of temperature was investigated on geopolymer mix designs, where a direct impact can be observed on slurry properties with the reduction in workability and fastening strength development process.

However, the disadvantage of using these admixtures was the poisoning phenomenon induced by Zn^{2+} species, which is the cause of the retardation. The phenomenon had a negative impact on mechanical properties where mix designs have struggled to reach high early mechanical strength. Still the poisoning effect seems to be active up to only 14 days of curing. After investigating this phenomenon on a microstructural level with no clear indications of the effect of Zn from a chemical reaction perspective, other methods were implemented to study the reaction. DFT calculations and Raman spectroscopy were used to observe the effects of Zn^{2+} species on a reaction level. The results highlight the effect on Q^3 species where shifts in wavelength can be observed from Raman spectroscopy measurements. These shifts were in parallel with the DFT calculations where it showed that SiO_4 reacts more rapidly with Zn^{2+} than with Al^{3+}, which indicates that the oligomerization phase requires more time to be complete, hence retardation phenomenon. This leads to the conclusion that Zn^{2+} ions were the responsible species for retarding the reaction despite the knowledge observed in literature.

The performance of Ca and Na species as strength development agents have been tested. It seems that the concentrations introduced were not adequate to guarantee a major strength development, however, they were adequate to pause the poisoning of Zn^{2+} species and help in the recovery of the bulk matrix. Nevertheless, more investigation must be done to recognize the synergy between chemical admixtures with different roles where the concentrations and operational conditions must be considered to guaranty maximum benefit of each.

To minimize the use of chemical admixtures, efforts were made to alter the mix designs by manipulating the composition by adding CaO into the dry solid blend. This allowed the development of three classes with differences in composition, mainly Ca content, which in turn provided mix designs for a temperature range of 5° to 60°C of BHCT. However, mix designs still require the utilization of chemical admixtures to be fully adequate for field applications.

7.2 *Conclusion*

The following conclusions can be drawn from this study:

- Zn^{2+} species has the potential to become a reliable retarder for geopolymers, however further development on strength developments agents may be necessary to handle the poisoning phenomenon imposed by zinc if high strength is required.
- Zn^{2+} ions react rapidly with SiO_4 compounds and causes a disruption in SiO_4 and Al^{3+} reactions, elongating the oligomerization phase in the reaction.
- The chemical admixtures understudy show reliability and repeatability in testing.
- Ca and Na species have the potential of becoming the antidote for using Zn, but still tuning to the concentrations must be done considering the reaction kinetics.

- The reliability on chemical admixtures can be reduced by manipulating the Ca content in the dry blend. However, this does not eliminate the need for chemical admixtures for further development.
- Temperature is a prime factor in controlling geopolymer reactions and the chemical admixtures' efficiency in the mix design.
- When alkali silicate solutions are used as a hardener, gelation of slurry due to stalling pumping operations will not be a concern for the slurry handling.

8. Research Contributions and Future Recommendations

The study focused on the development of granite-based geopolymers, which is a type of geopolymer produced in-house at the University of Stavanger. The work contributed to the development of chemical admixtures with the aim to implement geopolymers as a zonal isolation material in oil & gas applications under downhole conditions. The approach was a mixture between application characterization and analytical/scientific interpretation of the effect of chemical admixtures on granite-based geopolymer systems. It must be noted that granite as a main source of Si and Al rich material, has been rarely seen outside the research group at the University of Stavanger, which made the geopolymer system under study by itself to be viable and sustainable. Although the work focused on granite-based geopolymer, however the results can be beneficial and inspirational to develop chemical admixtures for geopolymers with other raw material basis. Each paper contributed to the work and helped in shaping the work as it is presented today. The following contributions can be assigned to each paper:

1. Paper I was the starting point of potential chemical admixtures with different acting roles. The results highlight Zn^{2+} and K^+ species as interesting chemical admixtures to act as retarders for the system under study.

2. Paper II highlighted the effect of different concentrations of Zn^{2+} and K^+ species on geopolymer systems, in addition the effect of temperature which indicated that higher dosages must be utilized to extend the pumping at higher temperatures. Also, temperature can play a major role in influencing the retarders' effect on the geopolymerization phase causing a variation in mechanical properties.

3. Paper III exhibited further investigation into the effect of Zn^{2+} and K^+ species on mechanical and morphological properties for a curing period up to 28 days under downhole conditions. The purpose was to explore the causation of the poisoning phenomenon shown using the chemical admixtures under study. However, due to the low concentrations of admixtures in the system, used techniques from XRD to SEM were not adequate to clearly observe the effect of Zn species and K species on the final bulk matrix.

4. Paper IV aimed to analyze and predict possible reaction paths of Zn^{2+} species, since it was the main acting agent in the retardation phenomenon, on the geopolymer system under study. Computational modeling and Raman Spectroscopy aided in the analysis of reaction steps and guaranteed a proper understanding of the system at hand. It must be noted that a new technique was used in geopolymer system analysis, which was to construct a control system using pure chemical components such as SiO_2, $Al(NO_3)_3 \cdot 9H_2O$, $FeSO_4$…etc. to mimic the original composition of granite-based geopolymers. This technique aimed to avoid structural complexities from used minerals and to avoid fluorescence effect in Raman Spectroscopy analysis. The results highlight the effect on Q^3 species where shifts in wavelength (cm^{-1}) can be observed from Raman spectroscopy measurements in comparison between samples with and without Zn^{2+} species. These shifts were in parallel with the DFT calculations where it showed that SiO_4 reacts more rapidly with Zn^{2+} than with Al^{3+}, which indicated that the oligomerization phase required more time to be complete, hence the retardation phenomenon. This led to the conclusion that Zn^{2+} ions were the responsible species for retarding the reaction despite the knowledge foreseen in literature.

5. Paper V presented a strategy for incorporating retarding agents with strength development agents, of Ca and Na origin, to

compensate for the poisoning effect imposed by retarders, specifically at elevated temperatures. The results confirmed that Ca and Na species can compensate the poisoning phenomenon in the short-term mechanical properties. However, further investigation is required to properly tune the concentrations of these admixtures together to create a cohesive interaction between all chemical admixtures in the system. In addition, it can be concluded that higher concentrations were required to further enhance the mechanical properties of geopolymer systems under study.

6. Paper VI presented a new track of development for granite-based geopolymers where instead of using chemical admixtures separately, the dry solid precursors were tuned to suit different well sections by adding CaO, thus creating different classes of geopolymer similar to OPC. This step furthers the effort of creating a cheap low carbon alternative material for OPC with a similar application approach to the oil & gas applications. The results highlight the importance of Ca content in connection to the operational temperature the slurry was being used at. Results concluded that it is vital to consider reaction kinetics in connection to composition and accompanying downhole conditions to develop proper classes of geopolymers for a variety of conditions and applications.

For future work, it is recommended that researchers focus on the optimum tuning of different chemical admixtures in a geopolymer system. Tuning of these admixtures can facilitate the application of geopolymer technology into the field and increase the understanding of possible reaction mechanisms where it is vital that admixtures do not counteract each other. In addition, since there are different sources of raw material for geopolymer technology, unifying the approach to develop universal chemical admixtures moves the technology a step closer towards commercialization and field applications.

86

9. References

[1] K. L. Scrivener and R. J. Kirkpatrick, "Innovation in use and research on cementitious material," *Cement and Concrete Research,* vol. 38, no. 2, pp. 128-136, 2008/02/01/ 2008, doi: https://doi.org/10.1016/j.cemconres.2007.09.025.

[2] V. Mancini, N. Verdone, A. Trinca, and G. Vilardi, "Economic, environmental and exergy analysis of the decarbonisation of cement production cycle," *Energy Conversion and Management,* vol. 260, p. 115577, 2022/05/15/ 2022, doi: https://doi.org/10.1016/j.enconman.2022.115577.

[3] IEA., "Low-Carbon Transition in the Cement Industry," 2018: IEA.

[4] G. C. Bye, *Portland cement: composition, production and properties*. Thomas Telford, 1999.

[5] R. M. Andrew, "Global CO2 emissions from cement production, 1928–2018," *Earth Syst. Sci. Data,* vol. 11, no. 4, pp. 1675-1710, 2019, doi: 10.5194/essd-11-1675-2019.

[6] F. Aslani, Y. Zhang, D. Manning, L. C. Valdez, and N. Manning, "Additive and alternative materials to cement for well plugging and abandonment: A state-of-the-art review," *Journal of Petroleum Science and Engineering,* vol. 215, p. 110728, 2022/08/01/ 2022, doi: https://doi.org/10.1016/j.petrol.2022.110728.

[7] M. Schneider, M. Romer, M. Tschudin, and H. Bolio, "Sustainable cement production—present and future," *Cement and Concrete Research,* vol. 41, no. 7, pp. 642-650, 2011/07/01/ 2011, doi: https://doi.org/10.1016/j.cemconres.2011.03.019.

[8] S. Prakash Chandar and R. Santhosh, "Partial replacement of cement with alternative cementitious material in the production of concrete: A review," *Materials Today: Proceedings,* 2022/09/16/ 2022, doi: https://doi.org/10.1016/j.matpr.2022.09.140.

[9] M. Khalifeh, J. Todorovic, T. Vrålstad, A. Saasen, and H. Hodne, "Long-term durability of rock-based geopolymers aged at downhole conditions for oil well cementing operations," *Journal*

of Sustainable Cement-Based Materials, vol. 6, no. 4, pp. 217-230, 2017.

[10] M. Sugumaran, "Study on effect of low calcium fly ash on geopolymer cement for oil well cementing," in *SPE/IATMI Asia Pacific Oil & Gas Conference and Exhibition*, 2015: OnePetro.

[11] M. Khalifeh, H. B. Motra, A. Saasen, and H. Hodne, "Potential Utilization for a Rock-Based Geopolymer in Oil Well Cementing," in *International Conference on Offshore Mechanics and Arctic Engineering*, 2018, vol. 51296: American Society of Mechanical Engineers, p. V008T11A037.

[12] P. Duxson, A. Fernández-Jiménez, J. L. Provis, G. C. Lukey, A. Palomo, and J. S. J. van Deventer, "Geopolymer technology: the current state of the art," *Journal of Materials Science,* vol. 42, no. 9, pp. 2917-2933, 2007/05/01 2007, doi: 10.1007/s10853-006-0637-z.

[13] M. N. S. Hadi, N. A. Farhan, and M. N. Sheikh, "Design of geopolymer concrete with GGBFS at ambient curing condition using Taguchi method," *Construction and Building Materials,* vol. 140, pp. 424-431, 2017/06/01/ 2017, doi: https://doi.org/10.1016/j.conbuildmat.2017.02.131.

[14] B. Prabu, A. Shalini, and J. Kumar, "Rice husk ash based geopolymer concrete-a review," *Chem. Sci. Rev. Lett,* vol. 3, pp. 288-294, 2014.

[15] J. Davidovits, "Geopolymer Chemistry and Applications. 4-th edition," *J. Davidovits.–Saint-Quentin, France,* 2015.

[16] P. D. Silva, K. Sagoe-Crenstil, and V. Sirivivatnanon, "Kinetics of geopolymerization: Role of Al2O3 and SiO2," *Cement and Concrete Research,* vol. 37, no. 4, pp. 512-518, 2007/04/01/ 2007, doi: https://doi.org/10.1016/j.cemconres.2007.01.003.

[17] M. Khalifeh, A. Saasen, H. Hodne, and H. B. Motra, "Laboratory evaluation of rock-based geopolymers for zonal isolation and permanent P&A applications," *Journal of Petroleum Science and Engineering,* vol. 175, pp. 352-362, 2019/04/01/ 2019, doi: https://doi.org/10.1016/j.petrol.2018.12.065.

[18] L. K. Turner and F. G. Collins, "Carbon dioxide equivalent (CO2-e) emissions: A comparison between geopolymer and OPC cement concrete," *Construction and Building Materials,* vol. 43,

pp. 125-130, 2013/06/01/ 2013, doi: https://doi.org/10.1016/j.conbuildmat.2013.01.023.

[19] M. Khalifeh, A. Saasen, H. Hodne, R. Godøy, and T. Vrålstad, "Geopolymers as an alternative for oil well cementing applications: A review of advantages and concerns," *Journal of Energy Resources Technology,* vol. 140, no. 9, 2018.

[20] E. Eid, H. Tranggono, M. Khalifeh, S. Salehi, and A. Saasen, "Impact of Drilling Fluid Contamination on Performance of Rock-Based Geopolymers," *SPE Journal,* vol. 26, no. 06, pp. 3626-3633, 2021, doi: 10.2118/205477-pa.

[21] J. Davidovits, "Geopolymers: inorganic polymeric new materials," *Journal of Thermal Analysis and calorimetry,* vol. 37, no. 8, pp. 1633-1656, 1991.

[22] G. Davis, C. Montes, and S. Eklund, "Preparation of lunar regolith based geopolymer cement under heat and vacuum," *Advances in Space Research,* vol. 59, no. 7, pp. 1872-1885, 2017/04/01/ 2017, doi: https://doi.org/10.1016/j.asr.2017.01.024.

[23] K. A. Komnitsas, "Potential of geopolymer technology towards green buildings and sustainable cities," *Procedia Engineering,* vol. 21, pp. 1023-1032, 2011/01/01/ 2011, doi: https://doi.org/10.1016/j.proeng.2011.11.2108.

[24] H. Xu and J. Van Deventer, "The geopolymerisation of alumino-silicate minerals," *International journal of mineral processing,* vol. 59, no. 3, pp. 247-266, 2000.

[25] J. Van Jaarsveld, J. Van Deventer, and G. Lukey, "The effect of composition and temperature on the properties of fly ash-and kaolinite-based geopolymers," *Chemical Engineering Journal,* vol. 89, no. 1-3, pp. 63-73, 2002.

[26] D. Hardjito, S. Wallah, D. Sumajouw, and B. Rangan, "Brief review of development of geopolymer concrete," in *8th CANMET/ACI International Conference on fly ash, silica fume, slag and natural pozzolans in concrete. Las Vegas (USA)*, 2004.

[27] V. Glukhovsky, "Ancient, modern and future concretes," in *Proceedings of the First International Conference on Alkaline Cements and Concretes*, 1994: Kiev, Ukraine, pp. 1-9.

[28] A. Palomo, A. Fernández-Jimenez, and G. Kovalchuck, "Some key factors affecting the alkali activation of fly ash," in *2nd*

International Symposium of Non-Traditional Cement and Concrete, 2005.

[29]   J. L. Provis and S. A. Bernal, "Geopolymers and Related Alkali-Activated Materials," *Annual Review of Materials Research,* vol. 44, no. 1, pp. 299-327, 2014, doi: 10.1146/annurev-matsci-070813-113515.

[30]   F. Pacheco-Torgal, J. Labrincha, C. Leonelli, A. Palomo, and P. Chindaprasit, *Handbook of alkali-activated cements, mortars and concretes*. Elsevier, 2014.

[31]   J. Davidovits, "Ancient and modern concretes: what is the real difference," *Concrete International,* vol. 9, pp. 12-23, 12/01 1987.

[32]   A. Fernández-Jiménez and A. Palomo, "Characterisation of fly ashes. Potential reactivity as alkaline cements☆," *Fuel,* vol. 82, no. 18, pp. 2259-2265, 2003.

[33]   T. Antonic, A. Cizmek, C. Kosanovic, and B. Subotic, "Dissolution of amorphous aluminosilicate zeolite precursors in alkaline solutions. I: Kinetics of the dissolution," *Journal of the Chemical Society. Faraday transactions,* vol. 89, no. 11, pp. 1817-1822, 1993.

[34]   A. Hajimohammadi and J. S. J. van Deventer, "Dissolution behaviour of source materials for synthesis of geopolymer binders: A kinetic approach," *International Journal of Mineral Processing,* vol. 153, pp. 80-86, 2016/08/10/ 2016, doi: https://doi.org/10.1016/j.minpro.2016.05.014.

[35]   P. M. Dove and N. Han, "Kinetics of mineral dissolution and growth as reciprocal microscopic surface processes across chemical driving force," in *AIP Conference Proceedings*, 2007, vol. 916, no. 1: American Institute of Physics, pp. 215-234.

[36]   S. Sprung, "Cement," in *Ullmann's Encyclopedia of Industrial Chemistry*.

[37]   J. W. Bullard *et al.*, "Mechanisms of cement hydration," *Cement and Concrete Research,* vol. 41, no. 12, pp. 1208-1223, 2011/12/01/ 2011, doi: https://doi.org/10.1016/j.cemconres.2010.09.011.

[38]   P. Barret, D. Ménétrier, and D. Bertrandie, "Mechanism of C3S dissolution and problem of the congruency in the very initial

period and later on," *Cement and Concrete Research,* vol. 13, no. 5, pp. 728-738, 1983.

[39]   H. Jennings and P. Pratt, "An experimental argument for the existence of a protective membrane surrounding Portland cement during the induction period," *Cement and Concrete Research,* vol. 9, no. 4, pp. 501-506, 1979.

[40]   Z.-Q. Wu and J. Young, "The hydration of tricalcium silicate in the presence of colloidal silica," *Journal of materials science,* vol. 19, no. 11, pp. 3477-3486, 1984.

[41]   E. B. Nelson, *Well cementing*. Newnes, 1990.

[42]   P. C. Hewlett, *Cement admixtures: uses and applications*. Longman Scientific & Technical, 1988.

[43]   U. Rattanasak, K. Pankhet, and P. Chindaprasirt, "Effect of chemical admixtures on properties of high-calcium fly ash geopolymer," *International Journal of Minerals, Metallurgy, and Materials,* vol. 18, no. 3, p. 364, 2011/05/29 2011, doi: 10.1007/s12613-011-0448-3.

[44]   T. Phoo-ngernkham, P. Chindaprasirt, V. Sata, S. Hanjitsuwan, and S. Hatanaka, "The effect of adding nano-SiO2 and nano-Al2O3 on properties of high calcium fly ash geopolymer cured at ambient temperature," *Materials & Design,* vol. 55, pp. 58-65, 2014/03/01/ 2014, doi: https://doi.org/10.1016/j.matdes.2013.09.049.

[45]   G. D. Bhavsar, K. R. Talavia, D. P. Suthar, M. B. Amin, and A. A. Parmar, "Workability properties of geopolymer concrete using accelerator and silica fume as an admixture," *International Journal for Technological Research in Engineering,* vol. 1, no. 8, pp. 541-544, 2014.

[46]   D. Jeon, Y. Jun, Y. Jeong, and J. E. Oh, "Microstructural and strength improvements through the use of Na2CO3 in a cementless Ca(OH)2-activated Class F fly ash system," *Cement and Concrete Research,* vol. 67, pp. 215-225, 2015/01/01/ 2015, doi: https://doi.org/10.1016/j.cemconres.2014.10.001.

[47]   G. Yu and Y. Jia, "Preparation of geopolymer composites based on alkali excitation," *Arabian Journal of Geosciences,* vol. 14, no. 7, p. 600, 2021/03/24 2021, doi: 10.1007/s12517-021-06908-8.

[48]   D. Manmohan and P. Mehta, "Influence of pozzolanic, slag, and chemical admixtures on pore size distribution and permeability of hardened cement pastes," *Cement, Concrete and Aggregates,* vol. 3, no. 1, pp. 63-67, 1981.

[49]   G. Brearley, "Third CANMET/ACI international conference on superplasticisers and other chemical admixtures in concrete. 4–6 October 1989, Ottawa, Canada," *Cement and Concrete Composites,* vol. 12, no. 2, pp. 140-141, 1990/01/01/ 1990, doi: https://doi.org/10.1016/0958-9465(90)90052-Y.

[50]   Y. Du *et al.*, "The Effect of Magnesium Chloride on the Macroscopic and MI-Croscopic Properties of Phosphate Cement-Based Materials," *Coatings,* vol. 12, no. 3, p. 370, 2022. [Online]. Available: https://www.mdpi.com/2079-6412/12/3/370.

[51]   J. S. J. Van Deventer, D. Feng, and P. Duxson, "Dry mix cement composition, methods and systems involving same," ed: Google Patents, 2010.

[52]   L. Coppola *et al.*, "The combined use of admixtures for shrinkage reduction in one-part alkali activated slag-based mortars and pastes," *Construction and Building Materials,* vol. 248, p. 118682, 2020/07/10/ 2020, doi: https://doi.org/10.1016/j.conbuildmat.2020.118682.

[53]   B. S. Umniati, P. Risdanareni, and F. T. Z. Zein, "Workability enhancement of geopolymer concrete through the use of retarder," *AIP Conference Proceedings,* vol. 1887, no. 1, p. 020033, 2017/09/29 2017, doi: 10.1063/1.5003516.

[54]   N. N. Zulkarnain, N. Shafiq, S. H. Abd Rahman, and S. A. Farhan, "Lignosulfonate as a retarder in geopolymer cement for oil well cementing: Effect on compressive strength," *Materials Today: Proceedings,* vol. 66, pp. 2986-2989, 2022/01/01/ 2022, doi: https://doi.org/10.1016/j.matpr.2022.06.572.

[55]   L. Wang, D. A. Geddes, B. Walkley, J. L. Provis, V. Mechtcherine, and D. C. Tsang, "The role of zinc in metakaolin-based geopolymers," *Cement and Concrete Research,* vol. 136, p. 106194, 2020.

[56]   Y. Liu, Z. Qin, and B. Chen, "Experimental research on magnesium phosphate cements modified by red mud," *Construction and Building Materials,* vol. 231, p. 117131,

2020/01/20/ 2020, doi: https://doi.org/10.1016/j.conbuildmat.2019.117131.

[57] W. S. Pitcher, *The nature and origin of granite*. Springer Science & Business Media, 1997.

[58] T. O. Richter *et al.*, "The Avaatech XRF Core Scanner: technical description and applications to NE Atlantic sediments," *Geological Society, London, Special Publications,* vol. 267, no. 1, pp. 39-50, 2006.

[59] I. W. Croudace, A. Rindby, and R. G. Rothwell, "ITRAX: description and evaluation of a new multi-function X-ray core scanner," *Geological Society, London, Special Publications,* vol. 267, no. 1, pp. 51-63, 2006.

[60] G. J. Weltje, M. R. Bloemsma, R. Tjallingii, D. Heslop, U. Röhl, and I. W. Croudace, "Prediction of Geochemical Composition from XRF Core Scanner Data: A New Multivariate Approach Including Automatic Selection of Calibration Samples and Quantification of Uncertainties," in *Micro-XRF Studies of Sediment Cores: Applications of a non-destructive tool for the environmental sciences*, I. W. Croudace and R. G. Rothwell Eds. Dordrecht: Springer Netherlands, 2015, pp. 507-534.

[61] S. P. S. MAAL0E, "The Iddefjord granite: geology and age," Norges Geologiske Undersøkelse Bergen, Norway, 1990 1990.

[62] N. N. Greenwood and A. Earnshaw, *Chemistry of the Elements*. Elsevier, 2012.

[63] I. Yuksel, "12 - Blast-furnace slag," in *Waste and Supplementary Cementitious Materials in Concrete*, R. Siddique and P. Cachim Eds.: Woodhead Publishing, 2018, pp. 361-415.

[64] P. Nath and P. K. Sarker, "Effect of GGBFS on setting, workability and early strength properties of fly ash geopolymer concrete cured in ambient condition," *Construction and Building Materials,* vol. 66, pp. 163-171, 2014/09/15/ 2014, doi: https://doi.org/10.1016/j.conbuildmat.2014.05.080.

[65] M. Soutsos, A. P. Boyle, R. Vinai, A. Hadjierakleous, and S. J. Barnett, "Factors influencing the compressive strength of fly ash based geopolymers," *Construction and Building Materials,* vol. 110, pp. 355-368, 2016/05/01/ 2016, doi: https://doi.org/10.1016/j.conbuildmat.2015.11.045.

[66]   J. E. Oh, P. J. M. Monteiro, S. S. Jun, S. Choi, and S. M. Clark, "The evolution of strength and crystalline phases for alkali-activated ground blast furnace slag and fly ash-based geopolymers," *Cement and Concrete Research,* vol. 40, no. 2, pp. 189-196, 2010/02/01/ 2010, doi: https://doi.org/10.1016/j.cemconres.2009.10.010.

[67]   M. B. Haha, B. Lothenbach, G. Le Saout, and F. Winnefeld, "Influence of slag chemistry on the hydration of alkali-activated blast-furnace slag—Part I: Effect of MgO," *Cement and Concrete Research,* vol. 41, no. 9, pp. 955-963, 2011.

[68]   A. Gholampour and T. Ozbakkaloglu, "Performance of sustainable concretes containing very high volume Class-F fly ash and ground granulated blast furnace slag," *Journal of Cleaner Production,* vol. 162, pp. 1407-1417, 2017/09/20/ 2017, doi: https://doi.org/10.1016/j.jclepro.2017.06.087.

[69]   R. API, "10B-2," *Recommended Practice for Testing Well Cements,* 2018.

[70]   R. API, "API TR 10TR7," *Mechanical Behavior of Cement,* 2017.

[71]   A. A. S. f. T. a. Materials, "ASTM D3967-16, Standard Test Method for Splitting Tensile Strength of Intact Rock Core Specimens," 2016.

[72]   B. D. Cullity, *Elements of X-ray Diffraction.* Addison-Wesley Publishing, 1956.

[73]   U. Holzwarth and N. Gibson, "The Scherrer equation versus the'Debye-Scherrer equation'," *Nature nanotechnology,* vol. 6, no. 9, pp. 534-534, 2011.

[74]   M. e. Frisch *et al.*, "Gaussian 16," ed: Gaussian, Inc. Wallingford, CT, 2016.

[75]   M. Khalifeh, "Materials for optimized P&A performance: Potential utilization of geopolymers," 2016.

[76]   L. N. Assi, E. Deaver, and P. Ziehl, "Using sucrose for improvement of initial and final setting times of silica fume-based activating solution of fly ash geopolymer concrete," *Construction and Building Materials,* vol. 191, pp. 47-55, 2018/12/10/ 2018, doi: https://doi.org/10.1016/j.conbuildmat.2018.09.199.

[77]   F. F. Ataie, M. C. G. Juenger, S. C. Taylor-Lange, and K. A. Riding, "Comparison of the retarding mechanisms of zinc oxide and sucrose on cement hydration and interactions with supplementary cementitious materials," *Cement and Concrete Research,* vol. 72, pp. 128-136, 2015/06/01/ 2015, doi: https://doi.org/10.1016/j.cemconres.2015.02.023.

[78]   N. Garg and C. E. White, "Mechanism of zinc oxide retardation in alkali-activated materials: an in situ X-ray pair distribution function investigation," *Journal of Materials Chemistry A,* vol. 5, no. 23, pp. 11794-11804, 2017.

[79]   M. Lizcano, H. S. Kim, S. Basu, and M. Radovic, "Mechanical properties of sodium and potassium activated metakaolin-based geopolymers," *Journal of Materials Science,* vol. 47, no. 6, pp. 2607-2616, 2012/03/01 2012, doi: 10.1007/s10853-011-6085-4.

[80]   C. Desbats-Le Chequer and F. Frizon, "Impact of sulfate and nitrate incorporation on potassium-and sodium-based geopolymers: geopolymerization and materials properties," *Journal of materials science,* vol. 46, pp. 5657-5664, 2011.

[81]   S. D. Kinrade and D. L. Pole, "Effect of alkali-metal cations on the chemistry of aqueous silicate solutions," *Inorganic Chemistry,* vol. 31, no. 22, pp. 4558-4563, 1992.

[82]   I. A. Frigaard, K. G. Paso, and P. R. de Souza Mendes, "Bingham's model in the oil and gas industry," *Rheologica Acta,* vol. 56, no. 3, pp. 259-282, 2017.

[83]   P. Duxson, S. W. Mallicoat, G. C. Lukey, W. M. Kriven, and J. S. van Deventer, "The effect of alkali and Si/Al ratio on the development of mechanical properties of metakaolin-based geopolymers," *Colloids and Surfaces A: Physicochemical and Engineering Aspects,* vol. 292, no. 1, pp. 8-20, 2007.

[84]   P. Duxson, J. Provis, G. Lukey, J. Van Deventer, F. Separovic, and Z. Gan, "39K NMR of free potassium in geopolymers," *Industrial & engineering chemistry research,* vol. 45, no. 26, pp. 9208-9210, 2006.

[85]   A. A. Siyal, K. A. Azizli, Z. Man, and H. Ullah, "Effects of Parameters on the Setting Time of Fly Ash Based Geopolymers Using Taguchi Method," *Procedia Engineering,* vol. 148, pp. 302-307, 2016/01/01/ 2016, doi: https://doi.org/10.1016/j.proeng.2016.06.624.

[86]   F. Varenne *et al.*, "Standardization and validation of a protocol of zeta potential measurements by electrophoretic light scattering for nanomaterial characterization," *Colloids and Surfaces A: Physicochemical and Engineering Aspects,* vol. 486, pp. 218-231, 2015/12/05/ 2015, doi: https://doi.org/10.1016/j.colsurfa.2015.08.044.

[87]   M. S. Muñiz-Villarreal *et al.*, "The effect of temperature on the geopolymerization process of a metakaolin-based geopolymer," *Materials Letters,* vol. 65, no. 6, pp. 995-998, 2011/03/31/ 2011, doi: https://doi.org/10.1016/j.matlet.2010.12.049.

[88]   A. M. M. A. Bakria, H. Kamarudin, M. BinHussain, I. K. Nizar, Y. Zarina, and A. R. Rafiza, "The Effect of Curing Temperature on Physical and Chemical Properties of Geopolymers," *Physics Procedia,* vol. 22, pp. 286-291, 2011/01/01/ 2011, doi: https://doi.org/10.1016/j.phpro.2011.11.045.

[89]   D. Sabitha, J. K. Dattatreya, N. Sakthivel, M. Bhuvaneshwari, and S. A. J. Sathik, "Reactivity, workability and strength of potassium versus sodium-activated high volume fly ash-based geopolymers," *Current Science,* vol. 103, no. 11, pp. 1320-1327, 2012. [Online]. Available: http://www.jstor.org.ezproxy.uis.no/stable/24089151.

[90]   N. Jafariesfad, M. R. Geiker, Y. Gong, P. Skalle, Z. Zhang, and J. He, "Cement sheath modification using nanomaterials for long-term zonal isolation of oil wells: Review," *Journal of Petroleum Science and Engineering,* vol. 156, pp. 662-672, 2017/07/01/ 2017, doi: https://doi.org/10.1016/j.petrol.2017.06.047.

[91]   L. Carter, H. Waggoner, and C. George, "Expanding cements for primary cementing," *Journal of Petroleum Technology,* vol. 18, no. 05, pp. 551-558, 1966.

[92]   M. Khalifeh, A. Saasen, T. Vrålstad, H. B. Larsen, and H. Hodne, "Experimental study on the synthesis and characterization of aplite rock-based geopolymers," *Journal of Sustainable Cement-Based Materials,* vol. 5, no. 4, pp. 233-246, 2016/07/03 2016, doi: 10.1080/21650373.2015.1044049.

[93]   E. Prud'homme, P. Michaud, E. Joussein, and S. Rossignol, "Influence of raw materials and potassium and silicon concentrations on the formation of a zeolite phase in a geopolymer network during thermal treatment," *Journal of Non-*

Crystalline Solids, vol. 358, no. 16, pp. 1908-1916, 2012/08/15/ 2012, doi: https://doi.org/10.1016/j.jnoncrysol.2012.05.043.

[94]   J. O. M. Bockris, Z. Nagy, and A. Damjanovic, "On the Deposition and Dissolution of Zinc in Alkaline Solutions," *Journal of The Electrochemical Society,* vol. 119, no. 3, p. 285, 1972/03/01 1972, doi: 10.1149/1.2404188.

[95]   X. Cong, W. Zhou, X. Geng, and M. Elchalakani, "Low field NMR relaxation as a probe to study the effect of activators and retarders on the alkali-activated GGBFS setting process," *Cement and Concrete Composites,* vol. 104, p. 103399, 2019/11/01/ 2019, doi: https://doi.org/10.1016/j.cemconcomp.2019.103399.

[96]   A. Degen and M. Kosec, "Effect of pH and impurities on the surface charge of zinc oxide in aqueous solution," *Journal of the European Ceramic Society,* vol. 20, no. 6, pp. 667-673, 2000/05/01/ 2000, doi: https://doi.org/10.1016/S0955-2219(99)00203-4.

[97]   H. C. H. Hahne and W. Kroontje, "Significance of pH and Chloride Concentration on Behavior of Heavy Metal Pollutants: Mercury(II), Cadmium(II), Zinc(II), and Lead(II)," *Journal of Environmental Quality,* vol. 2, no. 4, pp. 444-450, 1973, doi: https://doi.org/10.2134/jeq1973.00472425000200040007x.

[98]   J. D. Ortego, Y. Barroeta, F. K. Cartledge, and H. Akhter, "Leaching effects on silicate polymerization. An FTIR and silicon-29 NMR study of lead and zinc in portland cement," *Environmental Science & Technology,* vol. 25, no. 6, pp. 1171-1174, 1991/06/01 1991, doi: 10.1021/es00018a024.

[99]   C. Rtischerl, E. Mielcarekl, J. Wongpaz, and F. J. W. Lutz, "New Insights on Geopolymerisation Using Molybdate, Raman, and Infrared Spectroscopy," *Strategic Materials and Computational Design, Volume 31, Issue 10,* no. 10, p. 17, 2010.

[100] C. K. Yip, G. C. Lukey, J. L. Provis, and J. S. J. van Deventer, "Effect of calcium silicate sources on geopolymerisation," *Cement and Concrete Research,* vol. 38, no. 4, pp. 554-564, 2008/04/01/ 2008, doi: https://doi.org/10.1016/j.cemconres.2007.11.001.

[101] J. van Jaarsveld and J. Van Deventer, "Effect of the alkali metal activator on the properties of fly ash-based geopolymers,"

Industrial & engineering chemistry research, vol. 38, no. 10, pp. 3932-3941, 1999.

[102] K. Komnitsas and D. Zaharaki, "Geopolymerisation: A review and prospects for the minerals industry," *Minerals engineering,* vol. 20, no. 14, pp. 1261-1277, 2007.

[103] S. Puligilla, X. Chen, and P. Mondal, "Does synthesized C-S-H seed promote nucleation in alkali activated fly ash-slag geopolymer binder?," *Materials and Structures,* vol. 52, no. 4, p. 65, 2019/06/17 2019, doi: 10.1617/s11527-019-1368-3.

[104] D. L. Kong and J. G. Sanjayan, "Effect of elevated temperatures on geopolymer paste, mortar and concrete," *Cement and concrete research,* vol. 40, no. 2, pp. 334-339, 2010.

[105] P. Rovnaník, "Effect of curing temperature on the development of hard structure of metakaolin-based geopolymer," *Construction and building materials,* vol. 24, no. 7, pp. 1176-1183, 2010.

[106] M. N. Agista, M. Khalifeh, and A. Saasen, "Evaluation of Zonal Isolation Material for Low Temperature Shallow Gas Zone Application," in *SPE Asia Pacific Oil & Gas Conference and Exhibition*, 2022, vol. Day 2 Tue, October 18, 2022, D021S009R005, doi: 10.2118/210751-ms. [Online]. Available: https://doi.org/10.2118/210751-MS

[107] G. H. Tattersall and P. F. Banfill, *The rheology of fresh concrete* (no. Monograph). 1983.

[108] A. Fomenkov, I. Pinigin, M. Mikliayev, and A. Fedyanin, "Using Thixotropic Cement Slurry for Lost Circulation Control: Case History, Volga-Urals Region," in *SPE Russian Petroleum Technology Conference*, 2019: OnePetro.

[109] J. Temuujin, A. Van Riessen, and R. Williams, "Influence of calcium compounds on the mechanical properties of fly ash geopolymer pastes," *Journal of hazardous materials,* vol. 167, no. 1-3, pp. 82-88, 2009.

[110] J. Provis and C. Rees, "Geopolymer synthesis kinetics," in *Geopolymers*: Elsevier, 2009, pp. 118-136.

Appendix 1 – Chemical Composition of Mix Designs

Table 20. Chemical composition of addressed mix designs

Paper\Element	SiO₂	Al₂O₃	Fe₂O₃	CaO	MgO	Na₂O	K₂O	TiO₂	MnO	SrO	BaO	S²⁻	LOI	Reference to Section
I	63.10	12.97	1.49	9.94	4.54	2.34	3.81	0.8	0.19	0	0	0.61	0.8	6.1
II	60.02	10.88	0.58	15.04	8.07	1.84	1.62	1.15	0.01	0.01	0.01	0.61	0.15	6.2
III	63.10	12.97	1.49	9.94	4.54	2.34	3.81	0.8	0.19	0	0	0.61	0.8	6.3
IV	63.10	12.97	1.49	9.94	4.54	2.34	3.81	0.8	0.19	0	0	0.61	0.8	6.3
V	63.10	12.97	1.49	9.94	4.54	2.34	3.81	0.8	0.19	0	0	0.61	0.8	6.4

Table 21. Chemical Composition of mix designs mentioned in section
6.6

Mix Design	SiO₂	Al₂O₃	Fe₂O₃	CaO	MgO	Na₂O	K₂O	TiO₂	MnO	SrO	BaO	S²⁻	LOI
MD A	62.01	9.84	0.42	16.74	5.73	1.76	1.79	1.01	0.001	0.001	0	0.52	0.13
MD B	62.51	9.92	0.43	16.06	5.78	1.78	1.81	1.02	0.01	0.01	0	0.58	0.13
MD C	69.75	10.02	0.58	10.21	3.72	2.33	2.41	0.67	0.01	0.01	0.01	0.37	0.2

Appendix 2 – Sonic Strength Correlations
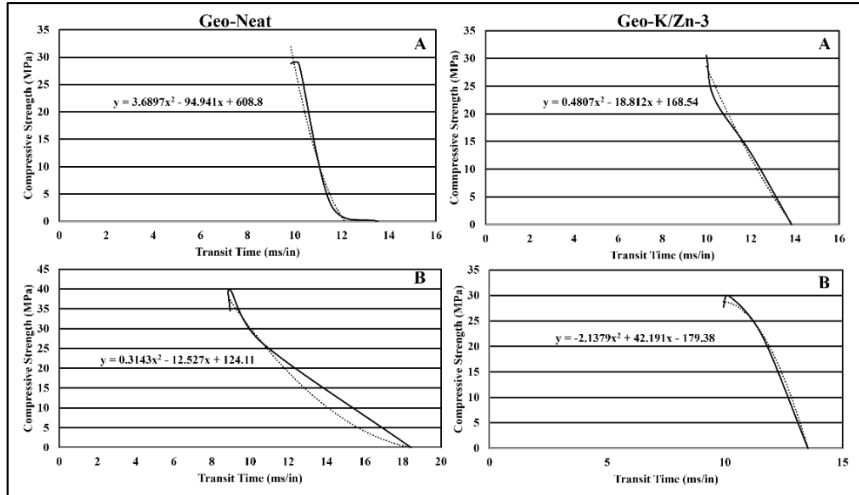
Figure 46. Sonic strength correlations Paper (II)
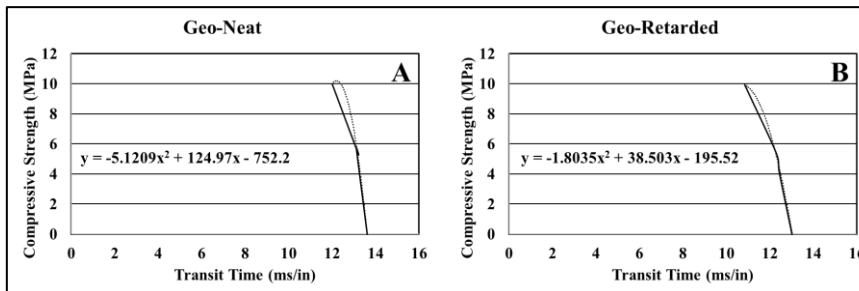
Figure 47. Sonic strength correlations Paper (V)

Appendix 3 – Lab Control Samples Composition (IV)

Table 22. Elemental composition considered for engineering the lab-controlled samples (Paper IV)

	To be considered in the reactants' composition							Not to be considered due to low concentrations				
Composition W%	SiO₂	Al₂O₃	Fe₂O₃	CaO	MgO	Na₂O	K₂O	TiO₂	MnO	SrO	BaO	LOI	Total
	63	13	1.5	10	4.5	2.34	3.81	0.8	0.19	0.01	0.01	0.72	100

Table 23. List of chemical replacement for each element in the original composition (Paper IV)

Component in compositions	Chemical replacement	Chemical formula	Number of molecules
Si	Silica flour	SiO_2	$4.423 \times 10^{+24}$
Al	Aluminum Nitrate Nanohydrate	$Al(NO_3)_3 \cdot 9H_2O$	$5.358 \times 10^{+23}$
Fe	Iron (II) Sulfate	$FeSO_4$	$3.94 \times 10^{+22}$
Ca	Calcium Hydroxide	$Ca(OH)_2$	$7.47 \times 10^{+23}$
Mg	Magnesium Oxide	MgO	$4.75 \times 10^{+23}$
Na	Sodium Hydroxide	$NaOH$	$1.59 \times 10^{+23}$
K	Potassium Hydroxide	KOH	$1.71 \times 10^{+23}$
Zn	Zinc Nitrate Hexhydrate	$Zn(NO_3)_2.6H_2O$	$1.21 \times 10^{+22}$

Table 24. Detailed composition of lab-controlled samples (Paper IV)

Components (Purity > 90%)	Mix design components (g)	
	CNT-0%Zn	CNT-1%Zn
SiO_2	44.13	44.13
$Al(NO_3)_3 \cdot 9H_2O$	18.96	18.96
$FeSO_4$	0.99	0.99
$Ca(OH)_2$	9.19	9.19
MgO	3.18	3.18
NaOH	1.06	1.06
KOH	1.59	1.59
$Zn(NO_3)_2.6H_2O$	-	0.79
Total	79.1	79.89

Appendix 4 – Paper I

Impact of Admixtures on Pumpability and Short-Term Mechanical
Properties of Rock-Based Geopolymer Designed for Zonal Isolation
and Well Abandonment

Fawzi Chamssine, Pedram Gargari, and Mahmoud Khalifeh

Paper OTC-31880-MS presented at the Offshore Technology
Conference, Texas, USA, 5th of May 2022

Appendix 5 – Paper II

EFFECTS OF TEMPERATURE AND CHEMICAL ADMIXTURES
ON THE PROPERTIES OF ROCK-BASED GEOPOLYMERS
DESIGNED FOR ZONAL ISOLATION AND WELL
ABANDONMENT

Fawzi Chamssine, Mahmoud Khalifeh, Elsayed Eid, Mona Wetrhus
Minde, Arild Saasen

Appendix 6 – Paper III

Effect of Zn^{2+} and K^+ as Retarding Agents on Rock-Based
Geopolymers for Downhole Cementing Operations

Fawzi Chamssine, Mahmoud Khalifeh, Arild Saasen

Effect of Zn^{2+} and K^+ as Retarding Agents on Rock-Based Geopolymers for Downhole Cementing Operations

Fawzi Chamssine[1]
Department of Energy and Petroleum Engineering,
Faculty of Science & Technology,
University of Stavanger,
4036 Stavanger, Norway
e-mail: fawzi.chamssine@uis.no

Mahmoud Khalifeh
Department of Energy and Petroleum Engineering,
Faculty of Science & Technology,
University of Stavanger,
4036 Stavanger, Norway
e-mail: mahmoud.khalifeh@uis.no

Arild Saasen
Department of Energy and Petroleum Engineering,
Faculty of Science & Technology,
University of Stavanger,
4036 Stavanger, Norway
e-mail: arild.saasen@uis.no

Geopolymer material has a potential to function alongside Portland Cement as an efficient cementitious material for well cementing and plug and abandonment applications. Geopolymer material requires retarding agents to be displaced into the well while considering the properties required to maintain efficient zonal isolation through superior mechanical properties. Chemical admixtures affect the material structure and can, in some cases, jeopardize material integrity if not engineered properly to suite downhole conditions. The present article shows the effect of Zn^{2+} and K^+ species have as retarding agents on slurry, mechanical, and microstructural properties. The approach has been carried out to obtain a preliminary overview of how retarding agents can behave in mix design slurries where eventually sealing performance was examined. Samples were cured and examined for periods of 1, 3, 7, 14, and 28 days at downhole conditions. The results obtained confirm a retardation effect by the addition of Zn^{2+} and K^+ species and some shortcomings in early strength development due to a poisoning mechanism by Zn^{2+} species. This phenomenon indicates the formation of Ca-Zn phase that can hinder the nucleation of the geopolymeric gel structure. No significant effects were observed on the microstructural development throughout the curing period. The effect of Zn^{2+} species was also observed in increasing threshold for hydraulic sealability. It may be concluded that the tested retarding agents require furthermore development to minimize shortcomings in mechanical properties specifically early strength development. [DOI: 10.1115/1.4053710]

Keywords: geopolymers, zinc retarder, workability, strength development, sealability, petroleum engineering, petroleum wells-drilling/production/construction

1 Introduction

Alternative materials to Ordinary Portland Cement (OPC) have been studied throughout the past decades motivated by improving performance properties, lower cost, and lower environmental impact through the reduction in emission of greenhouse gases (e.g., CO_2, NO_x) [1]. One of the suggested materials is an alternative to OPC known as geopolymers [2–4]. These materials were first introduced by Joseph Davidovits in the 1970s as a material with potential properties to replace OPC [5–10]. Multiple studies presented some plausible shortcomings of OPC, which are related to the short- and long-term performance of OPC at operational conditions [11–19]. Thus, geopolymers have attracted the petroleum industry specifically due to the lower environmental impact during production, outstanding short- and long-term performance, and lower production cost by lowering taxable carbon emissions [20,21]. To create a lateral comparison, it is important to test geopolymer slurries at real field conditions to observe the closest effect of these conditions while testing on a lab-scale. The use of retarding agents is vital to make this material pumpable in cementing operations. Elevated downhole temperatures contribute in higher activation energy levels to geopolymer material, but at the same time limit material's applications specifically in well cementing operations [22]. Previous studies exhibited the effect of Zn^{2+} in retarding chemical reactions in geopolymer systems [23,24], thus workability of material can be increased to achieve sufficient time

for displacement from surface to target downhole area. On the other hand, K^+ was utilized as a delayed accelerator to guaranty material setting and boost mechanical properties by allowing a controlled gelation reaction [25,26].

In the present study, zinc (Zn) and potassium (K) Nitrate have been used as chemical admixtures to adjust the slurry properties to prolong pumpability of the rock-based geopolymer for intermediate cementing operations. To address the objective of this study, two mix designs, a neat recipe, and a retarded recipe, were investigated under bottomhole circulating and static temperature and elevated pressure. The geopolymer material was prepared for downhole cementing operations in accordance with the set of tests presented in Fig. 1. Hydraulic sealability was conducted at the end to guaranty that material's integrity is not compromised due to the influence of retarding agents.

2 Materials and Methods

2.1 Materials and Mixing Procedure. The solid precursor used in this study was an aluminosilicate rich rock powder primarily made of granite, normalized with other precursors having reactive properties. The precursor was designed to have a low calcium content (<10 wt%). The solid precursor's composition is presented in Table 1. Potassium silicate solution with a modular ratio of 2.21 was used as the activating hardener phase. Distilled water was used to adjust total water content, viscosity of the slurries, and as a medium to introduce the chemical admixtures. Zinc nitrate hexahydrate ($N_2O_6Zn.6H_2O$) and potassium nitrate (KNO_3) were used, both with a purity of 99%. The amount of added chemical admixtures was adjusted to have a K^+/Zn^{2+} ratio of 0.25. The mix design of the neat sample (Geo-Neat) and retarded sample (Geo-Zn/K) is presented in Table 2. The used ratio was
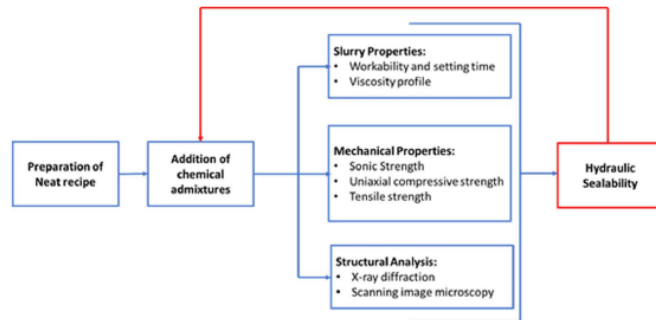
124

Fig. 1 Applied strategy for testing chemical admixtures in cementitious material slurries on a laboratory scale

experimentally concluded after running several tests and past experiences using the combination of both Zn^{2+} and K^+ species [27].

The slurries were prepared with a solid to liquid ratio of 2.07. The mixing was carried out using a Waring high-speed blender with an OFITE control pad following the API RP 10B-2 recommendations [28].

2.1.1 Conditioning. Prior to some tests, conditioning of mix designs was conducted using an OFITE atmospheric consistometer (Model 60) following API RP 10B-2 recommendations [28]. Conditioning was performed at bottomhole circulating temperature (BHCT) of 50 °C and 150 rounds per minute (rpm), for a period of 30 min after reaching the desired BHCT. The purpose behind this process is to match the circulating slurry conditions and prepare it to match the static curing conditions to avoid any thermal shock to the slurry.

2.2 Slurry Properties

2.2.1 Workability and Setting Time. An OFITE HPHT consistometer (Model 2040) was used to examine the workability and setting time at a BHCT of 50 °C and pressure of 14 MPa. The temperature was ramped up at a rate of 1 °C/min and the pressure was ramped up from atmospheric to 14 MPa in a period of 10 min. The standard for workability was set from the starting point until 40 BC while setting time was from 40 BC to 100 BC following API RP 10-B2 recommendations [28].

2.2.2 Viscosity Measurements. Viscosity was measured using an OFITE Model 900 viscometer while tested at a BHCT of 50 °C. Ideally, these measurements should have been performed under pressure. To fulfill standard requirements, a large annular gap was necessary. Hence, the option was to use an atmospheric viscometer (OFITE Model 900 Rotational Viscometer). Addition of pressure would generally increase the viscosity slightly as the

Table 1 Solid phase composition

Chemical element	wt%
SiO_2	63.10
Al_2O_3	12.97
Fe_2O_3	1.49
CaO	9.94
MgO	4.54
Na_2O	2.34
K_2O	3.81
TiO_2	0.80
MnO	0.19
LOI	0.80
Total	100

liquid phase is compressed and the efficient solid's fraction is slightly increased. The slurries were conditioned prior to testing.

2.3 Mechanical Properties

2.3.1 Sonic Strength. An OFITE Model 4005 automated twin cell ultrasonic cement analyzer (UCA) was used to examine the early strength development of the slurries. A sonic signal is emitted through the sample where the transit time of the signal is recorded [16]. Upon phase changes and setting, the velocity of transit time (time for sound to travel through the slurry) is increased. A correlation was used to convert the transit time recordings to sonic compressive strength. Since the default correlation is based on OPC parameters, a specific correlation was developed for geopolymer material using the results from the uniaxial compressive strength tests. The strength development was measured continuously for a period of 28 days at bottomhole static temperature (BHST) of 70 °C and pressure of 14 MPa.

Table 2 Mix design of tested slurries

Mix design	Sample composition (wt%)					
	Solid	Liquid	Total water	K^+	Zn^{2+}	K^+/Zn^{2+} ratio
GEO-Neat	66.23	53.77	22.13	–	–	–
GEO-Zn/K	66.23	53.77	22.13	0.075	0.3	0.25

125
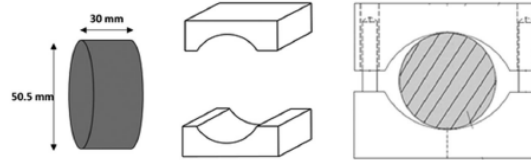
Fig. 2 Indirect tensile strength setup
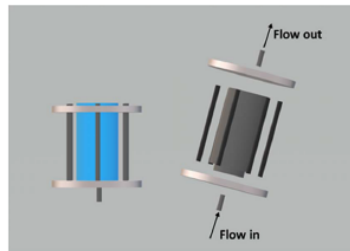
Fig. 3 Hydraulic sealability setup

were cured at BHST of 70 °C and pressure of 14 MPa. The loading rate was selected to be 30 kN/min set at a force-controlled mode. Per curing period, three samples were tested, and the average compressive strength was calculated. The slurries were conditioned prior to curing.

2.3.3 Indirect Tensile Test (Brazilian Test). A Zwick/Roell Z050 material testing equipment was used to examine the tensile strength. Samples were cured at BHST of 70 °C and pressure of 14 MPa. Cured samples were cut in a disc-like shape having a thickness of 30 mm approximately. For each curing interval, four samples were prepared and tested to minimize any possible measurement error where the average tensile strength was calculated. The samples were later placed vertically in the setup described in Fig. 2. The compression load was 50 N/sec where the results were used to calculate the tensile strength based on Eq. (1) [30]. The average of the tested four samples was calculated and presented in the results. The slurries were conditioned prior to curing

$$\text{Tensile strength} = 1.2 \, \frac{F}{\pi d l} \qquad (1)$$

2.3.2 Uniaxial Compressive Strength. The uniaxial compressive strength (UCS) tests were conducted using a Toni Technik-H mechanical tester in accordance with API TR 10TR7:2017 [29]. Cylindrical plastic molds of 50 mm diameter and 10 mm length were filled with slurries and positioned in cylindrical pressurized autoclaves filled with water where later a pressure buildup was applied using a Teledyne ISCO pump (Model 260D). Samples

2.3.4 Hydraulic Sealability. To understand impact of the used admixtures on sealability (the objective using zonal isolation materials) of the final product, hydraulic integrity test was concluded. A cylindrical steel tube (KF HUP S355J2H) with diameter 82 mm and height of 150 mm and roughness of 1 μm of Ra was used to measure hydraulic sealability. The tube had a 2 side caps tightened with

Fig. 4 Workability and gelation time at BHCT of 50 °C and pressure of 14 MPa

126

Fig. 5 Viscosity profile at 50 °C BHCT

metal bolts; the setup is presented in Fig. 3. Samples were conditioned prior of placement in the setup and cured for 7 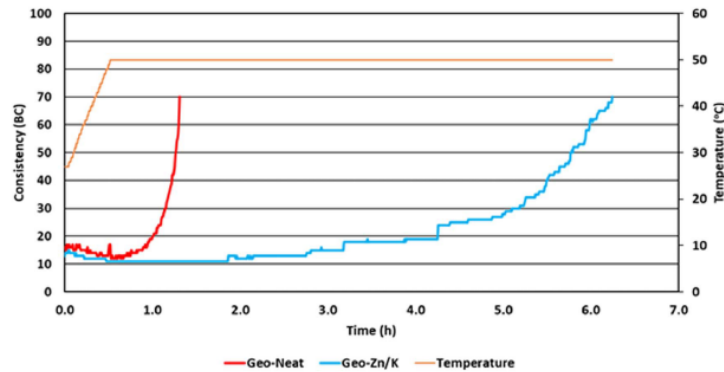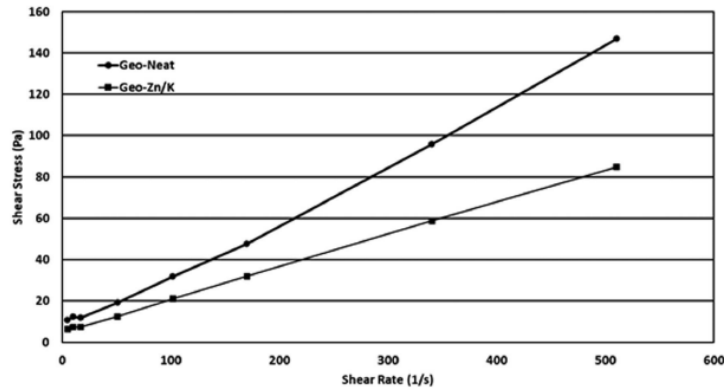days at BHST of 70 °C and pressure of 14 MPa. The test setup was designed to pump water from the bottom, using a linear gradual increase in pressure, where any water out would be detected by a flowmeter connected to the top outlet of the setup. After breaking sealability, the pressure and amount of water escaping the setup was recorded.

2.4 Composition and Structural Analysis

2.4.1 Phase Change. After curing samples, it is expected that there are multiple crystalline phase changes affected by temperature, pressure, and the chemical composition used. These changes were observed throughout the curing periods using a Bruker-AXS Micro-diffractometer D8 Advance, which uses a CuKα radiation (40.0 kV, 25.0 mA) with a 2θ range from 5 deg to 92 deg with 1 deg/min step and 0.010 deg increment. Samples collected from UCS tests were crushed and grounded into powder manually and drying was conducted at 40 °C in a vacuum oven for 24 h to avoid any solid–gas reaction and ensure the removal of water particles.

2.4.2 Microstructure Analysis. Scanning electron microscopy was conducted using a Gemini Supra 35VP (ZEISS) to examine microstructure post curing phase. Samples were retrieved from cured samples, cut into thin sections (thickness 1–2 mm), and emerged in epoxy to avoid any phase change or solid–gas, solid–solid reactions. The samples were smoothed and coated under vacuum with a palladium (Pd) layer of 10 nm prior to examination.

3 Results and Discussions

3.1 Workability and Gelation Time. The consistency profiles of geopolymer samples, both the neat and with chemical admixtures, are presented in Fig. 4. It was observed that the Geo-Neat had a workability period of approximately 1.2 h (h) (~73 min) and a gelation time of around 0.1 h (~6 min). On the other hand, the addition of Zn^{2+} and K^+ species created a retarding effect making the workability reach around 5.5 h (~330 min) and a setting time of around 0.74 h (~44 min). It has been observed that the combination of Zn^{2+} and K^+ has created a retarding effect in comparison with Geo-Neat sample by extending workability from ~1.22 h to ~5.5 h. Cavallotti et al. [31] showed that Zn^{2+} species
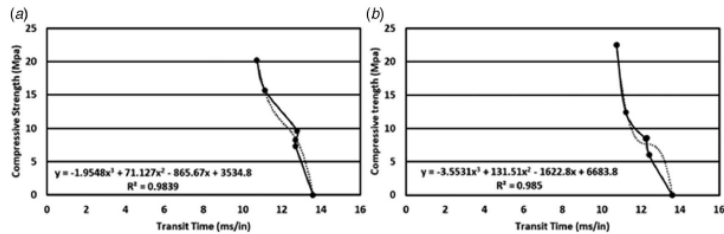
Fig. 6 Uniaxial compressive strength plotted versus the transit time for (a) Geo-Neat and (b) Geo-Zn/K

127
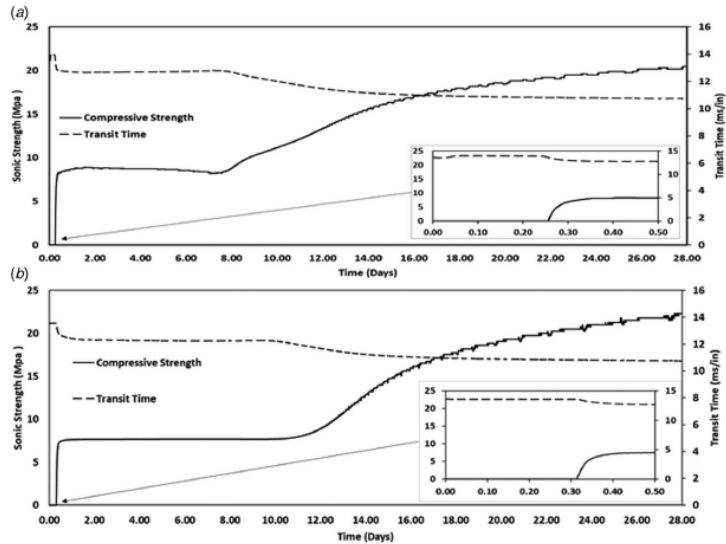
Fig. 7   UCA measurements for (a) Geo-Neat and (b) Geo-Zn/K

has a tendency to engage in hydroxylated alumina. In addition, it has the tendency to capture OH^- groups and produce zinc hydroxide (ZnO), which contributes to the poisoning effect. The current geopolymer system contains CaO by 9.94 wt% and high concentrations of OH^- which imply the possible formation of a Ca-Zn phase (Ca $(Zn(OH)_3)_2.2H_2O$). Such effects have been reported in previous studies of Zn effects in cement systems and alkali-activated systems [32,33]. Garg and White [34] investigated the effect of zinc oxide (ZnO) on high/low Ca alkali-activated system. They were able to correlate the effect of Zn^{2+} species on prolonging setting time of high Ca systems while not observing any significant effect on low calcium content systems. Their conclusion mainly focused on the
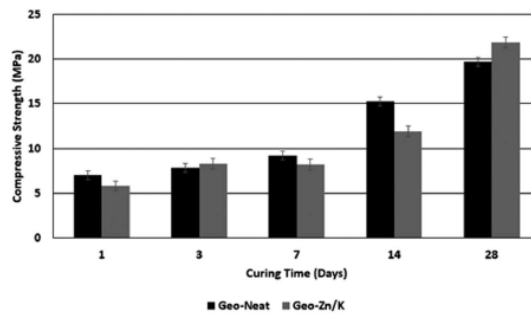
Fig. 8   Average UCS measurements of mix designs up to 28 days

128
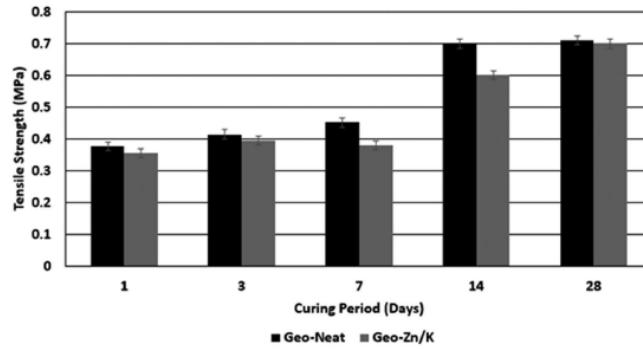
Fig. 9   Average tensile strength of mix designs

formation of Ca-Zn phases, which have the ability of poisoning C-(N)-A-S-H gel where Zn is incorporated homogenously through a "Ca depletion" mechanism where the development of Ca-Zn phases infects local undersaturated pore solutions which evidently leads to the retardation effect. In addition to the Zn's effect on Ca contained in the system, it has been found that incorporate with alkali activators, whether sodium (Na) or K-based systems, can also happen. A study by Wang et al. [35] indicates that Zn in geopolymer systems can inhibit alkali-activation reactions through the formation of metastable K/Na-Zn phases, which does not have any significant effect on primary products of N-(K)-A-S-H structure. This was concluded by investigating $Q^4(4Al)$ and $Q^4(3Al)$ through ^{29}Si MAS NMR spectra, which

indicated the increase in number of $Q^4(4Al)$ sites leading to a decrease in the Si/Al ratio that point to the phenomena created by the partial replacement of Zn^{2+} for Na^+/K^+. N-(K)-A-S-H gels are intermediate products before the 3D network of geopolymers are completed [36]. However, in alkali-activated based systems, N-(K)-C-A-S-H phases are the final product. These observations support the retardation phenomena caused by Zn^{2+} ions.

3.2 Viscosity Profile. Geopolymer mix designs exhibit a non-Newtonian fluid behavior with the presence of yield stress as shown in Fig. 5. The shear stress of Geo-Neat was larger than the shear stress of the Geo-Zn/K slurry at the different evaluated shear
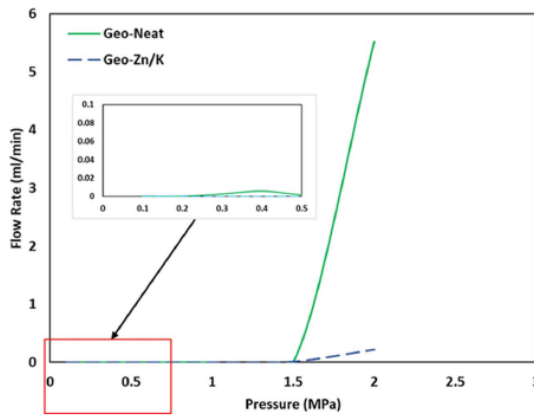
Fig. 10   Hydraulic sealability test results for clean steel casing

129
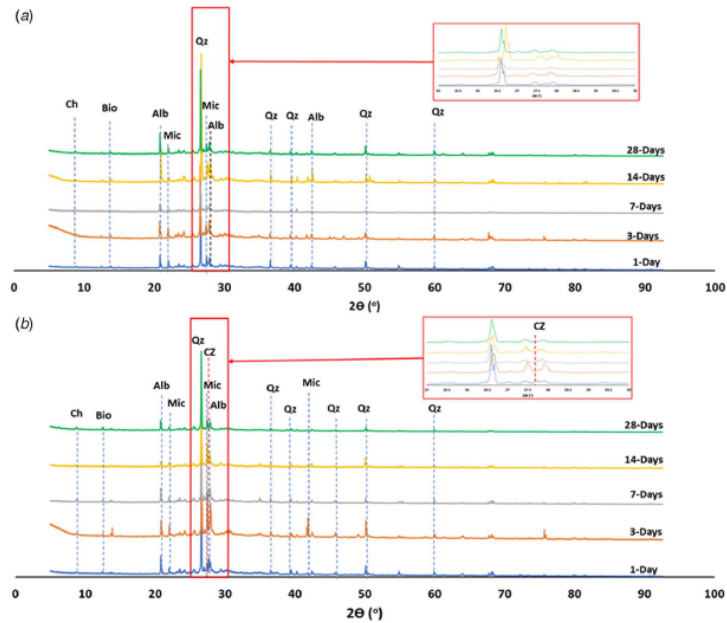
Fig. 11 XRD measurements of cured (*a*) Geo-Neat and (*b*) Geo-Zn/K up to 28 days

rates. By the addition of chemical admixtures, a reduction in viscosity can be observed for all the applied shear rates. Thus, it might be concluded that the chemical stability of the geopolymer colloidal system was affected by the addition of chemical admixtures.

3.3 Ultrasonic Cement Analyzer. The UCA was designed to measure sonic strength of OPC by detecting the travel time of ultrasound waves through the sample and applying a predetermined algorithm to estimate the sonic strength. Thus, a custom algorithm was developed by plotting the UCS data versus transit time. Afterward, the created algorithm was introduced to the UCA to convert the recorded transit time to sonic strength (see Fig. 6).

The sonic strength development for Geo-Neat and Geo-Zn/K was measured for a period of 28 days and under BHST conditions (70 °C and 14 MPa), presented in Fig. 7. It has been observed for Geo-Neat, the initial strength development starts after ∼6 h from initial mixing ($t = 0$), stabilizing for around 7 days at around 8 MPa of compressive strength and then increase gradually to reach around 20 MPa after 28 days. On the other hand, Geo-Zn/K started to develop strength after ∼7.5 h, maintaining a compressive strength of around 6 MPa for 11 days and then gradually increase to reach a compressive strength of around 21 MPa.

The effect of Zn^{2+} ions can be attributed to the similar poisoning phenomena mentioned in the *workability and gelation time* section,

where Zn/K poisoning have occurred to the nucleation sites of N(K)-A-S-H gel of which the geopolymerization reaction was delayed due to the formation of Ca-Zn [35]. The differences surrounding the early strength development between Geo-Neat and Geo-Zn/K, ∼1.5 h, indicates a delay in setting and hardening process.

3.4 Uniaxial Compressive Strength. The average compressive strength of mix designs for a period up to 28 days is shown in Fig. 8. It was observed that the compressive strength, elasticity, and tensile strength are interlinked properties where the increase elasticity of cementitious material can contribute in decreasing the

Table 3 Mineral composition extracted from XRD patterns of cured mix designs up to 28 days

Mineral	Chemical composition
Quartz	SiO_2
Albite	$NaAlSi_3O_8$
Microcline	$KAlSi_3O_8$
Chamosite	$(Fe^{2+},Mg,Al,Fe^{3+})_6(Si,Al)_4O_{10}(OH,O)_8$
Biotite	$K(Mg,Fe)_3(AlSi_3O_{10})(F,OH)_2$
Calcium Zinc Silicate	$CaZnSi_3O_8$

130

Fig. 12   SEM images (range of 20 μm) of Geo-Neat at (*a*) 1 day, (*b*) 3 days, (*c*) 7 days, (*d*) 14 days, and (*e*) 28 days; red square highlighting the focus area; red arrow for unreacted particles

compressive and tensile strength properties required to maintain zonal isolation [37]. This behavior is instinct of all cementitious materials unless reinforcements are used in the structure of the material. The results show that the compressive strength of Geo-Neat gradually increased throughout the curing period while maintaining a close compressive strength of around 8 to 9 MPa during the first 7 days reaching to ∼20 MPa after 28 days. On the other hand, the compressive strength of Geo-Zn/K was following an increasing trend, similar to Geo-Neat's trend, starting from around ∼6 MPa after 1 d to reach around 21 MPa after 28 days. It

is evident from the results presented in Fig. 8 that the addition of Zn^{2+} and K^+ species have reduced the compressive strength development of geopolymer samples in the early stages up to 14 days. The presence of Zn^{2+} species has a poisoning effect on geopolymer systems as discussed previously. In the presented chemical system, it is believed that the Zn^{2+} species have negatively affected the development of 3D networks by inhibiting the formation of geopolymer gels and slowing the condensation process [38]. Many researchers have examined the influence of increasing the weight of Zn^{2+} species (≤10 wt%) to improve the compressive strength

131

Fig. 13 SEM images (range of 1 μm) of Geo-Neat at (*a*) 1 day, (*b*) 3 days, (*c*) 7 days, (*d*) 14 days, and (*e*) 28 days; red arrow for unreacted particles and yellow arrow for binder formation

of geopolymer systems [38,39]; while this can be an interesting point to improve the compressive strength of the mix design discussed in the study, the effect on slurry properties, specifically workability, should be taken into account.

3.5 Indirect Tensile Test (Brazilian Test). The tensile strength measurements for mix designs are presented in Fig. 9. It

has been observed that both mix designs had a relatively increasing tensile strength starting from ~0.38 MPa reaching to around ~0.7 MPa. Although no clear indication of how the addition of Zn^{2+} and K^+ species may affect the tensile strength in long-term periods, it may be pointed out the trend seen by Geo–Zn/K at early stages of which shows a delay in the strength development. The reality of downhole conditions can exert force on different directions to the cement sheath, jeopardize the integrity of the
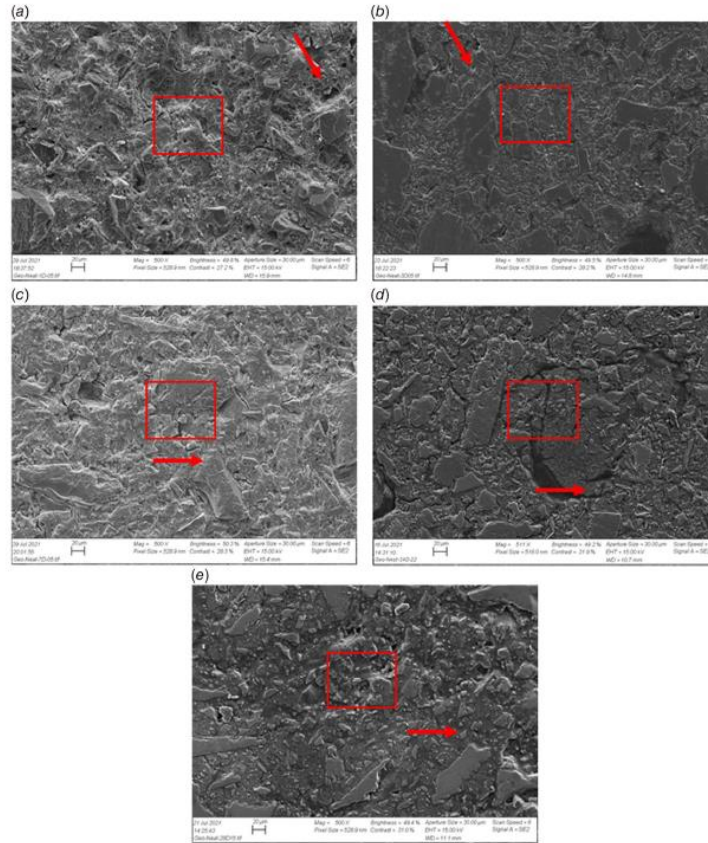
132
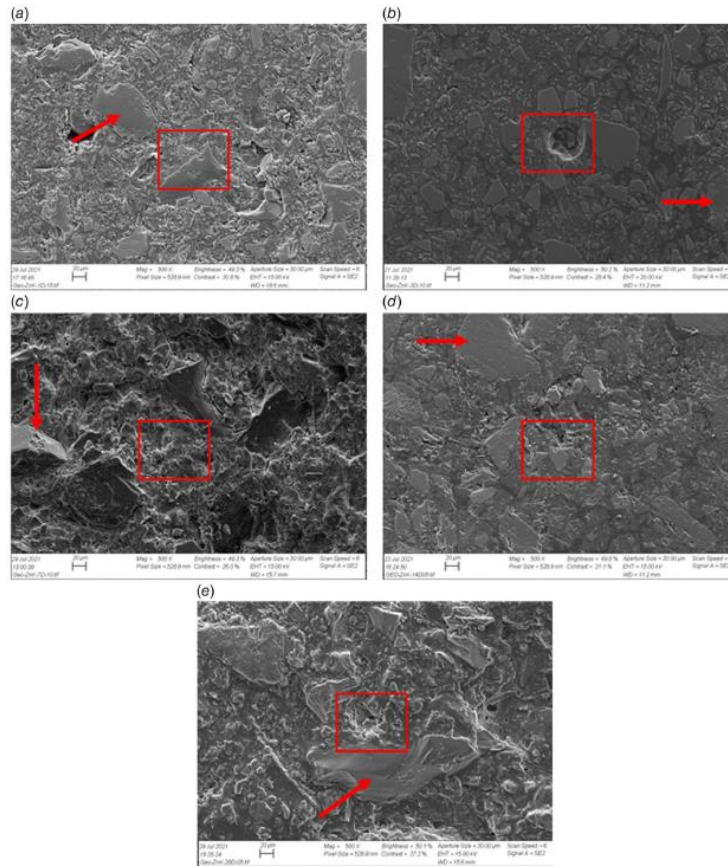
Fig. 14 SEM images (range of 20 μm) of Geo-Zn/K at (a) 1 day, (b) 3 days, (c) 7 days, (d) 14 days, and (e) 28 days; red square highlighting the focus area; red arrow for unreacted particles

cementitious material, and eventually the integrity of production operations. The forces applied over the cement sheath may lead to having low tensile strength or debonding/poor bonding of cementitious material to casing [40]. The effect of Zn^{2+} and K^+ species on the tensile strength throughout the curing periods can be linked as well to the poisoning effect of Zn^{2+} species, which was highlighted in Sec. 3.4. The effect of chemical admixtures specifically Zn^{2+}

species seems to be highly significant when it comes to mechanical properties development.

3.6 Hydraulic Sealability. The test was conducted to examine the material's ability to maintain sealability at the interface of barrier material and casing systems to ensure that the admixtures
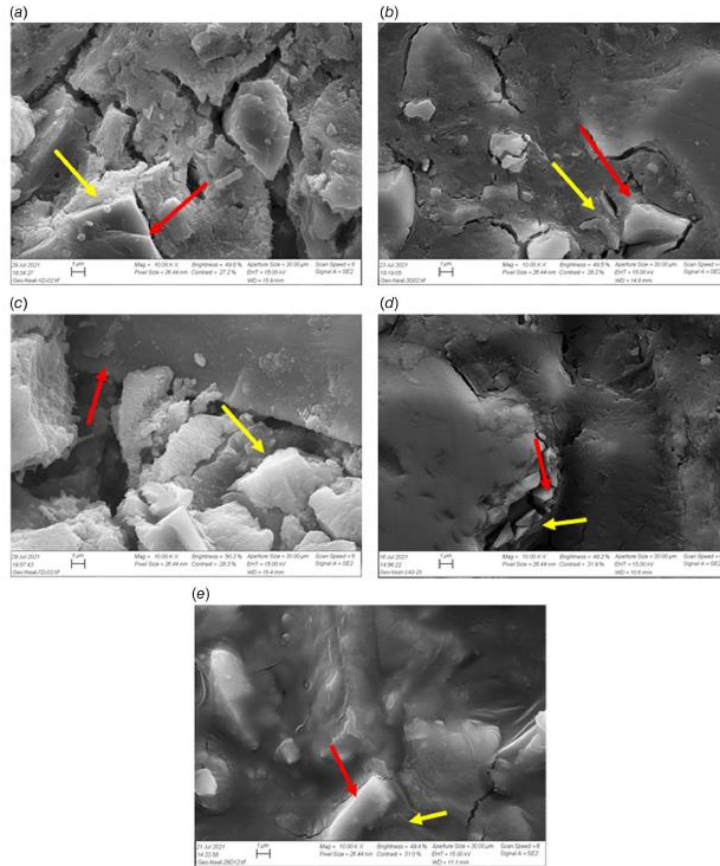
133
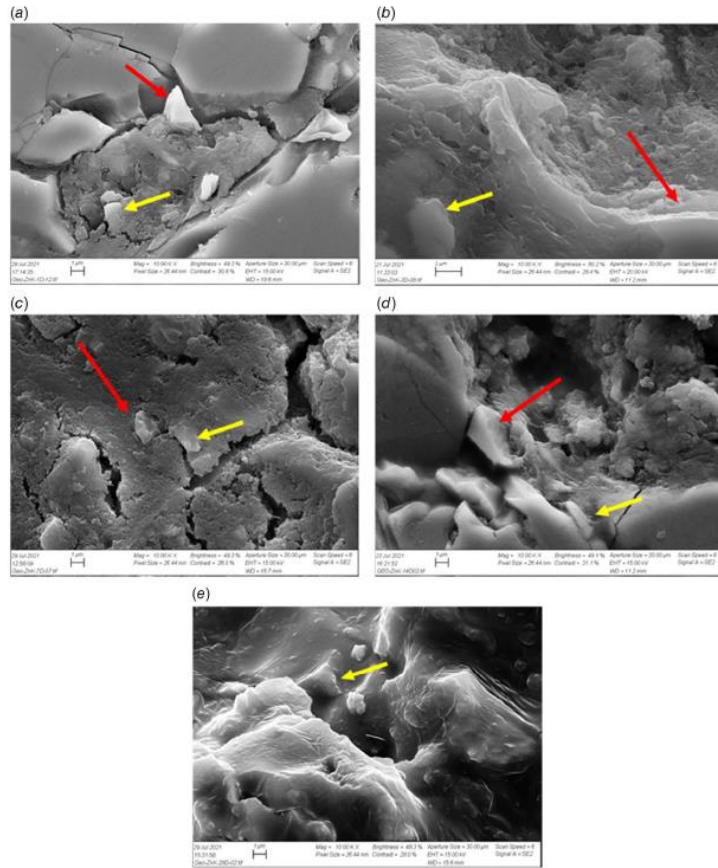
Fig. 15 SEM images (range of 1 μm) of Geo-Zn/K at (*a*) 1 day, (*b*) 3 days, (*c*) 7 days, (*d*) 14 days, and (*e*) 28 days; red arrow for unreacted particle and yellow arrow for binder formation

do not impact the main function of the barrier. The results of hydraulic sealability examination are presented in Fig. 10, where the water flowrate (ml/min) is presented versus the pressure (bar). For Geo-Neat, it has been observed that the hydraulic sealability has been compromised at a pressure of around ~0.3 MPa. Some minor fluctuations have been observed and may be attributed to the differential pressure between the water pump and the pressure already existing inside the hydraulic sealability test. On the other hand,

Geo-Zn/K failed hydraulic integrity at ~1.5 MPa where the initial flowrate indications were recorded. These observations indicate a significant effect of using Zn^{2+} and K^+ species as chemical admixtures on the material's ability to resist leakage. The higher sealability exhibited by Geo-Zn/K mix design can be attributed to the effect of Zn^{2+} species on the geopolymer system under study. The use of Zn has been recognized previously by Carter et al. [41] to be an effective additive in the expansion of cement, due to the gas forming

134
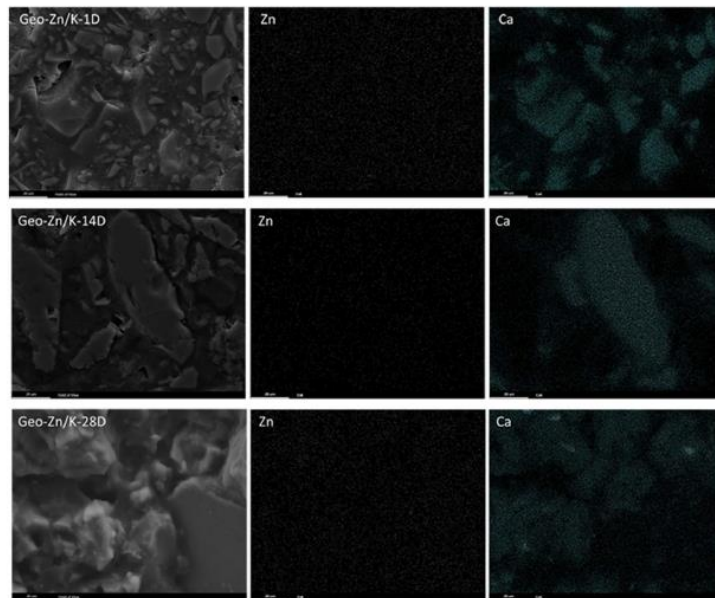
Fig. 16   SEM mapping imagery of Zn and Ca for Geo-Zn/K 1, 14, and 28 days

mechanism, which Zn eases in cementitious systems. Gas forming expansion happens due to the interaction between additive species, in this study Zn^{2+} species, and the alkali molecules in the cementitious medium where relatively small hydrogen gas bubbles are formed. The reaction occurs in the presence of Al particles, which are available in abundance in the system under study. Correlating to Carter et al. [41] conclusions, it seems that the conditions of this chemical reaction whether they are temperature, pressure, or chemical system were in favor for an expansion mechanism to be triggered by the presence of Zn^{2+} species. It should be noted that further consideration of this expansion phenomena should be examined considering the kinetics of the reaction and identifying the role of K^+ species, which was not highlighted during this study due to the very little amount used in the chemical system presented.

3.7   Phase Change. X-Ray diffraction (XRD) patterns of the cured samples of Geo-Neat and Geo-Zn/K are presented in Figs. 11(a) and 11(b). The main phase recorded in both patterns was Quartz (Qz) with the presence of minor phases of albite (Alb), microcline (Mic), chamosite (Ch), biotite (Bio) and minor presence of calcium zinc silicate (CZ) peak in Geo-Zn/K samples. The composition of the mentioned minerals is presented in Table 3. Similar trends have been observed throughout the XRD patterns of both cured mix designs, where Qz was constantly decreasing in peak intensity indicating the consumption of Si by the geopolymer binder. The presence of Alb and Mic peaks in K-activated system favors the formation of

zeolite phases which can explain the crystalline pattern obtained from the XRD results [17]. Thus, the increase in mechanical properties (e.g., compressive and tensile strengths) can be attributed to the formation of these zeolite phases. A study by Prud'homme et al. [42] investigated the effect of raw material and Si properties on the formation of zeolite phases in geopolymer material. It was determined that the properties of raw material and type of activator play a major role in the formation of zeolite phase. It can be concluded that in this geopolymer system properties of raw material may have favored the formation of a crystalline phase, mainly composed of zeolite, considering the enhancement of mechanical properties observed throughout the curing period. The effect of Zn^{2+} species was observed by detecting calcium zinc silicate (CZ) phase at peak 27.8 deg where the peak was minor in comparison to other existing peaks such as microcline and albite. The minor presence of such peaks can be attributed to the limited amount of Zn^{2+} species (0.3 wt%) used in the mix design (Table 2). In previous studies, Zn was detected mainly in the form of zinc oxide (ZnO), but that was highly dependent on the type of Zn used [34,35]. Although a CZ peak is present, it is still not a definite indication of the form/structure of the mineral formed and would require much thorough characterization to clearly identify the type of Ca-Zn phases formed with in Geo-Zn/K mix designs.

3.8   Microstructure Analysis. The scanning electronic microscopic (SEM) images of samples cured for a period up to 28 days

135

are presented in Figs. 12 and 13 for Geo-Neat and in Figs. 14 and 15 for Geo-Zn/K. It must be noted that the samples were collected through cutting from cured mold samples prepared for UCS tests to minimize any cracks caused by mechanical forces. The images present areas in the range of 20 μm presented for each curing period of every sample. The areas of focus and interest were marked with the red box (Figs. 12 and 14). The SEM images show significant change in microstructure between early curing periods (up to 7 days) and long curing periods (up 28 days). The visualization of unreacted aluminosilicate particles aligns with previous studies, where the presence of these unreacted particles was confirmed by having a plate-shaped structure around empty areas [43–45]. Throughout the SEM images, it can be noticed that a more homogeneous structure was formed as the curing time progresses which explains the increase in mechanical properties of the samples. The effect of Zn^{2+} species and K^+ species was not detected in the SEM images where this may be attributed to the low amount of chemical admixtures used in Geo-Zn/K. The identification of these phenomena will require more advanced techniques to compensate the current angular resolution from the XRD.

Mapping imagery in Fig. 16 shows a homogeneous distribution of Zn and Ca throughout Geo-Zn/K samples. The distribution of these elements was overlapping, though with much less concentration of Zn, which gives the presumption of chemical interactions occurring between these two elements. The formation of Ca-Zn phases cannot be verified from these imageries but raises the question of how these elements are interacting, what type of chemical structures are present, and what retardation mechanism is truly occurring throughout the chemical system and its poisoning effects during the curing period. To tackle these questions, advanced techniques such as solid Mass-NMR must be applied, especially due to the low amount of chemical admixtures introduced to this geopolymer chemical system.

4 Conclusion

Rock-based geopolymer systems with Zn^{2+} and K^+ species as retarding agents were examined under downhole conditions using a testing matrix developed to initially test material on a lab-scale under field conditions. Retardation was achieved by using Zn^{2+} species while the effect of K^+ species was not observed clearly due to the little amount introduced in the system. The chemical admixtures reduced the viscosity profile of the investigated slurry. Through the examination of mechanical properties, a delay in early strength development has been observed up to until 14 days due to a poisoning phenomenon, which was anticipated to be a result of the development of Ca-Zn phases that hurdles the nucleation and formation of geopolymeric structure. Composition analysis combined with SEM images showed the development of new crystalline phases and an ongoing reaction slowly incorporating particles into the binder structure throughout the curing period. More thorough characterization techniques are required to validate the presence of Ca-Zn phases and point out any other poisoning phases that might have developed throughout the reaction. The development of chemical admixtures for geopolymer systems opens the door to more tailored solutions that can fit with the assigned bottomhole conditions to ensure a systematic synergy between slurry, mechanical, and structural properties which can ease any future application of the material.

Acknowledgment

Funding Data

Conflict of Interest

There are no conflicts of interest.

References

[1] Pacheco-Torgal, F., Labrincha, J., Leonelli, C., Palomo, A., and Chindaprasit, P., 2014, *Handbook of Alkali-Activated Cements, Mortars and Concretes*, Elsevier, New York.

[2] Provis, J. L., Fernández-Jiménez, A., Kamseu, E., Leonelli, C., and Palomo, A., 2014, "Binder Chemistry—Low-Calcium Alkali-Activated Materials," *Alkali Activated Materials: State-of-the-Art Report, RILEM TC 224-AAM*, J. L. Provis, and J. S. J. van Deventer, eds., Springer Netherlands, Dordrecht, pp. 93–123.

[3] Duxson, P., Fernández-Jiménez, A., Provis, J. L., Lukey, G. C., Palomo, A., and van Deventer, J. S. J., 2007, "Geopolymer Technology: The Current State of the Art," J. Mater. Sci., 42(9), pp. 2917–2933.

[4] Bernal, S. A., Provis, J.L., and Fernandez-Jimenez, A., 2014, *Alkali Activated Materials: State-of-the-Art Report, RILEM TC 224-AAM*, J. L. Provis, and J. S. J. van Deventer, eds., Springer Netherlands, Dordrecht, pp. 59–91.

[5] Davidovits, J., 2005, Geopolymer, Green Chemistry and Sustainable Development Solutions: Proceedings of the World Congress Geopolymer 2005, Geopolymer Institute.

[6] Davidovits, J., 2015, *Geopolymer Chemistry and Applications*, 4th ed., Geopolymer Institute, France.

[7] Davidovits, J., 1994, "Properties of Geopolymer Cements," First International Conference on Alkaline Cements and Concretes, Ukraine, pp. 131–149.

[8] Davidovits, J., 1991, "Geopolymers: Inorganic Polymeric New Materials," J. Therm. Anal. Calorim., 37(8), pp. 1633–1656.

[9] Davidovits, J., 1987, "Ancient and Modern Concretes: What is the Real Difference," Concr. Int., 9(12), pp. 12–23.

[10] Davidovits, J., 1994, "Global Warming Impact on the Cement and Aggregates Industries," World Resour. Rev., 6(2), pp. 263–278.

[11] Khalifeh, M., 2016, "Materials for Optimized P&A Performance: Potential Utilization of Geopolymers," Ph.D. Thesis, http://hdl.handle.net/11250/2396282.

[12] Khalifeh, M., Hodne, H., Saasen, A., Integrity, O., and Eduok, E. I., 2016, "Usability of Geopolymers for Oil Well Cementing Applications: Reaction Mechanisms, Pumpability, and Properties," The SPE Asia Pacific Oil & Gas Conference and Exhibition, Perth, Australia.

[13] Khalifeh, M., Motra, H. B., Saasen, A., and Hodne, H., 2018, "Potential Utilization for a Rock-Based Geopolymer in Oil Well Cementing," International Conference on Offshore Mechanics and Arctic Engineering, Madrid, Spain, American Society of Mechanical Engineers, vol. 51296, p. V008T11A037.

[14] Khalifeh, M., Saasen, A., Hodne, H., Godøy, R., and Vrålstad, T., 2018, "Geopolymers as an Alternative for Oil Well Cementing Applications: A Review of Advantages and Concerns," ASME J. Energy Resour. Technol., 140(9), p. 092801.

[15] Khalifeh, M., Saasen, A., Hodne, H., and Motra, H. B., 2019, "Laboratory Evaluation of Rock-Based Geopolymers for Zonal Isolation and Permanent P&A Applications," J. Pet. Sci. Eng., 175, pp. 352–362.

[16] Khalifeh, M., Saasen, A., Vrålstad, T., and Hodne, H., 2014, "Potential Utilization of Class C Fly Ash-Based Geopolymer in Oil Well Cementing Operations," Cem. Concr. Compos., 53, pp. 10–17.

[17] Khalifeh, M., Saasen, A., Vrålstad, T., Larsen, H. B., and Hodne, H., 2016, "Experimental Study on the Synthesis and Characterization of Aplite Rock-Based Geopolymers," J. Sustainable Cem.-Based Mater., 5(4), pp. 233–246.

[18] Salehi, S., Khattak, M. J., Ali, N., Ezeakacha, C., and Saleh, F. K., 2018, "Study and Use of Geopolymer Mixtures for Oil and Gas Well Cementing Applications," ASME J. Energy Resour. Technol., 140(1), p. 012908.

[19] Salehi, S., Khattak, M. J., Rizvi, H., Karbalaei, S., and Kiran, R., 2017, "Sensitivity Analysis of Fly Ash Geopolymer Cement Slurries: Implications for Oil and Gas Wells Cementing Applications," J. Nat. Gas Sci. Eng., 37, pp. 116–125.

[20] Salehi, S., Ali, N., Khattak, M., and Rizvi, H., 2016, "Geopolymer Composites," SPE Annual Technical Conference and Exhibition, Dubai, UAE, Society of Petroleum Engineers.

[21] Chen, L., Wang, H., Xin, J., Wu, X., Wang, W., Zhao, H., Kong, L., and Xu, C., 2011, "Research on Techno-Economic Performance of the Geopolymeric Cement With Oil Shale Residue and Slag," New Build. Mater., 3.

[22] Mobili, A., Belli, A., Giosuè, C., Bellezze, T., and Tittarelli, F., 2016, "Metakaolin and Fly Ash Alkali-Activated Mortars Compared With Cementitious Mortars at the Same Strength Class," Cem. Concr. Res., 88, pp. 198–210.

[23] Alex, T. C., Kalinkin, A. M., Nath, S. K., Gurevich, B. I., Kalinkina, E. V., Tyukavkina, V. V., and Kumar, S., 2013, "Utilization of Zinc Slag Through Geopolymerization: Influence of Milling Atmosphere," Int. J. Miner. Process., 123, pp. 102–107.

[24] Nath, S. K., 2020, "Fly ash and Zinc Slag Blended Geopolymer: Immobilization of Hazardous Materials and Development of Paving Blocks," J. Hazard. Mater., 387, p. 121673.

[25] Duxson, P., Provis, J., Lukey, G., Van Deventer, J., Separovic, F., and Gan, Z., 2006, "39K NMR of Free Potassium in Geopolymers," Ind. Eng. Chem. Res., 45(26), pp. 9208–9210.

[26] Lizcano, M., Kim, H. S., Basu, S., and Radovic, M., 2012, "Mechanical Properties of Sodium and Potassium Activated Metakaolin-Based Geopolymers," J. Mater. Sci., 47(6), pp. 2607–2616.

[27] Charmasine, F., Khalifeh, M., Eid, E., Minde, M. W., and Saasen, A., 2021, "Effects of Temperature and Chemical Admixtures on the Properties of Rock-Based Geopolymers Designed for Zonal Isolation and Well Abandonment," ASME 2021 40th International Conference on Ocean, Offshore and Arctic Engineering, Online Conference, vol. 10, Petroleum Technology, p. V010T11A031.

[28] American Petroleum Institute, 2013, API RP 10B-2, 2nd ed., Recommended Practice for Testing Well Cements.

[29] American Petroleum Institute, 2017, API TR 10TR7, 1st ed., Mechanical Behavior of Cement.

[30] American Society for Testing and Materials, 2016, ASTM D-3967-16, Standard Testing Method for Splotting Tensile Strength of Intact Rock Core Specimens.

[31] Cavallotti, R., Goniakowski, J., Lazzari, R., Jupille, J., Koltsov, A., and Loison, D., 2014, "Role of Surface Hydroxyl Groups on Zinc Adsorption Characteristics on α-Al2O3(0001) Surfaces: First-Principles Study," J. Phys. Chem. C, 118(25), pp. 13578–13589.

[32] Tommaseo, C., and Kersten, M., 2002, "Aqueous Solubility Diagrams for Cementitious Waste Stabilization Systems. 3. Mechanism of Zinc Immobilization by Calcium Silicate Hydrate," Environ. Sci. Technol., 36(13), pp. 2919–2925.

[33] Yousuf, M., Mollah, A., Hess, T. R., Tsai, Y.-N., and Cocke, D. L., 1993, "An FTIR and XPS Investigations of the Effects of Carbonation on the Solidification/Stabilization of Cement Based Systems-Portland Type V With Zinc," Cem. Concr. Res., 23(4), pp. 773–784.

[34] Garg, N., and White, C. E., 2017, "Mechanism of Zinc Oxide Retardation in Alkali-Activated Materials: An in Situ X-Ray Pair Distribution Function Investigation," J. Mater. Chem. A, 5(23), pp. 11794–11804.

[35] Wang, L., Geddes, D. A., Walkley, B., Provis, J. L., Mechtcherine, V., and Tsang, D. C., 2020, "The Role of Zinc in Metakaolin-Based Geopolymers," Cem. Concr. Res., 136, p. 106194.

[36] Yang, J., Li, D., and Fang, Y., 2017, "Synthesis of Nanoscale CaO-Al2O3-SiO2-H2O and Na2O-Al2O3-SiO2-H2O Using the Hydrothermal Method and Their Characterization," Materials, 10(7), p. 695. https://www.mdpi.com/1996-1944/10/7/695

[37] Jafariesfad, N., Geiker, M. R., Gong, Y., Skalle, P., Zhang, Z., and He, J., 2017, "Cement Sheath Modification Using Nanomaterials for Long-Term Zonal Isolation of Oil Wells: Review," J. Pet. Sci. Eng., 156, pp. 662–672.

[38] Zailan, S. N., Bouaissi, A., Mahmed, N., and Abdullah, M. M. A. B., 2020, "Influence of ZnO Nanoparticles on Mechanical Properties and Photocatalytic Activity of Self-Cleaning ZnO-Based Geopolymer Paste," J. Inorg. Organomet. Polym. Mater., 30(6), pp. 2007–2016.

[39] Zidi, Z., Ltifi, M., Ayadi, Z. B., Mir, L. E., and Nóvoa, X., 2020, "Effect of Nano-ZnO on Mechanical and Thermal Properties of Geopolymer," J. Asian Ceram. Soc., 8(1), pp. 1–9.

[40] Kamali, M., Khalifeh, M., Saasen, A., Godøy, R., and Delabroy, L., 2021, "Alternative Setting Materials for Primary Cementing and Zonal Isolation—Laboratory Evaluation of Rheological and Mechanical Properties," J. Pet. Sci. Eng., 201, p. 108455.

[41] Carter, L., Waggoner, H., and George, C., 1966, "Expanding Cements for Primary Cementing," J. Pet. Technol., 18(5), pp. 551–558.

[42] Prud'homme, E., Michaud, P., Joussein, E., and Rossignol, S., 2012, "Influence of Raw Materials and Potassium and Silicon Concentrations on the Formation of a Zeolite Phase in a Geopolymer Network During Thermal Treatment," J. Non-Cryst. Solids, 358(16), pp. 1908–1916.

[43] Duxson, P., Provis, J. L., Lukey, G. C., Mallicoat, S. W., Kriven, W. M., and van Deventer, J. S. J., 2005, "Understanding the Relationship Between Geopolymer Composition, Microstructure and Mechanical Properties," Colloids Surf. A, 269(1), pp. 47–58.

[44] Duxson, P., Lukey, G., Separovic, F., and Van Deventer, J., 2005, "Effect of Alkali Cations on Aluminum Incorporation in Geopolymeric Gels," Ind. Eng. Chem. Res., 44(4), pp. 832–839.

[45] Xu, H., and Van Deventer, J. S. J., 2002, "Microstructural Characterisation of Geopolymers Synthesised From Kaolinite/Stilbite Mixtures Using XRD, MAS-NMR, SEM/EDX, TEM/EDX, and HREM," Cem. Concr. Res., 32(11), pp. 1705–1716.

137

Appendix 7 – Paper IV

Retarding mechanism of Zn^{2+} species in geopolymer material using
Raman spectroscopy and DFT calculations

Fawzi Chamssine, Luiz H. S. Gasparotto , Miguel Angelo Fonsecade
Souza , Mahmoud Khalifeh & Julio Cezar de Oliveira Freitas

scientific reports

Check for updates

OPEN

Retarding mechanism of Zn²⁺ species in geopolymer material using Raman spectroscopy and DFT calculations

Fawzi Chamssine[1]✉, Luiz H. S. Gasparotto[2], Miguel Angelo Fonsecade Souza[2], Mahmoud Khalifeh[1] & Julio Cezar de Oliveira Freitas[2]

Geopolymers are the most promising alternative to Ordinary Portland Cement for oil-well cementing and well abandonment. To that end, the slurry needs a required pumping time ensured by the addition of retarders. Although zinc has been widely known to prolong the setting time of geopolymers, its mechanism of action has yet to be fully elucidated. It is herein hypothesized that zinc ions impede the first stages of silicate oligomerization (Si–O–Al), culminating in longer setting times. Pumping time measurements showed that $Zn(NO_3)_2$ delayed the setting time by 5 h in comparison to the zinc-less sample. DFT calculations revealed $Si(OH)_4$ to react with $[Zn(OH)_4]^{2-}$ via a barrierless transition state, evidencing a kinetic ground for the retardation effect. Additionally, Raman spectroscopy corroborated the DFT results by showing that Q^3 species in the proposed mechanism are formed more rapidly in the presence of zinc ions than in its absence.

Geopolymers are an alternative cementitious material with the potential of replacing Ordinary Portland Cement (OPC) in both construction and oil & gas applications. The applicability of this material into oil and gas has been under research in the past period since its production has a lower carbon footprint and maintains superior properties over OPC specifically in long term periods[1–3]. However, to apply such material in cementing and well abandonment operations, chemical admixtures such as retarders must be used to delay setting and guaranty a safe period for displacement into wellbores[4]. Geopolymer formation from solid materials is a complex, multi-step process roughly comprising i) alkaline depolymerization of the poly(siloxo) framework and dissolution of aluminum ii) formation of monomers and oligomers from ortho-sialate $(OH)_3^-$ Si–O–Al–$(OH)_3$, and iii) poly-condensation into higher oligomers and polymeric 3D networks[5,6]. Advantageously, it has been demonstrated that the degree of polymerization/depolymerization of glasses and geopolymers can be determined via Raman spectroscopy[7]. In essence, SiO_4 species in a silica network differ from each other spectroscopically according to the number of sharing oxygen atoms. An isolated SiO_4, for instance, is referred to as Q^0 due to its lack of sharing oxygen. A Q^1 entity denotes, in turn, a SiO_4 with one sharing oxygen in the network. The reasoning extends then to Q^2, Q^3, and Q^4 meaning two, three, and four sharing oxygen atoms, respectively. Upon contacting glass or a silica-rich mineral with an alkaline environment it is expected that the amount of Q^0–Q^1 species increase with time due to silica depolymerization, a phenomenon that can be tracked since each Q^n species appear at distinct frequencies in the Raman spectrum[7–9].

Zinc (Zn^{2+}) species, as a retarder, have been under study where its mechanistic and kinetic aspects have been taken into consideration[10–13]. Zinc oxide (ZnO), for instance, is thought to dissolve into Zn^{2+} which prolongs the setting time by sequestering calcium ions (Ca^{2+}) and forming calcium zincate $[Ca(Zn(OH)_3)_2.2H_2O]^{11}$. This is also the conclusion reached by Cong et al.[14], who only speculated that Zn^{2+} could have had an effect on the condensation polymerization. The possibility of Zn^{2+} playing a role in the early stages of the geopolymerization should not be overlooked. Zeng et al.[15] demonstrated the synthesis of a coagulant based on poly-zinc-silicate to yield a complex compound with mainly zinc-silicon polymeric species rather than a simple mixture of raw materials. Upon studying the impact of Zn^{2+} and lead (Pb^{+2}) ions on OPC, Oretgo et al.[16] discovered Zn^{2+} ions to retard the silicate polymerization. The authors demonstrated, via NMR, a high proportion of Q^0 and Q^1 species after curing OCP with Zn^{2+} ions, implying a low degree of polymerization of SiO_4 units.

[1]Department of Energy and Petroleum Engineering, Faculty of Science and Technology, University of Stavanger, 4036 Stavanger, Norway. [2]Universidade Federal do Rio Grande do Norte, UFRN, Natal 59078-970, Brazil. ✉email: fawzi.chamssine@uis.no
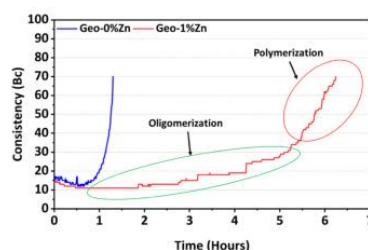
139

Figure 1. Effect of Zn^{2+} species on pumping time of granite-based geopolymer—oligomerization and polycondensation phases highlighted for Geo-1%Zn.

The present study intends to shed light on the mechanism via which Zn^{2+} retards the geopolymerization reaction. The insight of this work resides in regarding the Zn^{2+}, in the form of $[Zn(OH)_4]^{2-}$ due to the high pH, as a reactant that is inserted into monomers and oligomers to hamper momentarily the progression of the reaction. Density Functional Theory (DFT) calculations revealed that SiO_4 reacts more quickly with $[Zn(OH)_4]^{2-}$ via a step with a barrierless transition state, meaning that the reaction between $Si(OH)_4$ and $[Zn(OH)_4]^{2-}$ is kinetically more feasible in comparison to that between $Si(OH)_4$ and $Al[(OH)_4]^-$. Raman results revealed that the presence of Zn^{2+} led to a higher rate of initial depolymerization of the poly(siloxo) framework, which supports the DFT proposition.

Results and discussion

Retardation phenomenon: granite-based geopolymer slurry. The impact of retardation phenomena in geopolymer material can be initially observed through pumping time measurements as described in previous studies by Chamssine et al.[1,4,17]. The retardation phenomenon can be observed through consistency measurements of slurries that show the behavior of material under different conditions. In this case, pumpability into an oil & gas well. The pumping time of the granite-based geopolymer slurries Geo-0%Zn and Geo-1%Zn is presented in Fig. 1. It can be observed that the addition of Zn^{2+} species (Geo-1%Zn) delays the pumping time by around 5 h in comparison to the neat sample (Geo-0%Zn), which reached its maximum after around 1 h. It can be perceived that the oligomerization phase was highly extended due to the presence of Zn^{2+} species. A poisoning phenomenon of the reaction can be concluded from Fig. 1, where the oligomerization and polycondensation phase was also affected. Previously, different reasonings have been given to explain behavior of Zn^{2+} in silica-rich geopolymer systems. Wang et al.[10] analyzed the role of ZnO on metakaolin based geopolymer material. They concluded that the presence of ZnO have created metastable "Na/K-Zn" phase materials (Na^+ and K^+ sourced from the alkali activator), which have a prolonging effect on setting time. Their study also included the investigation of $Q^4(3Al)$ and $Q^4(4Al)$ sites using NMR spectra. A decrease in the Si/Al ratio was observed due to the increase in number of $Q^4(4Al)$ sites. It has been foreseen that not only Q^4 sites to be affected, but rather also the possibility of having a deviation in Q^3 sites' development, which can as well be sites to investigate while the reaction is developing[18].

Computational model. The calculated *Gibbs* free energy of reaction ($\Delta_r G$) for fifteen dehydration reactions involving the $Si(OH)_4$, $[Al(OH)_4]^-$, $[Zn(OH)_3]^-$, and $[Zn(OH)_4]^{2-}$ monomers (and also some oligomers) are presented in Table 1. The condensation reaction (reaction 1) between $Si(OH)_4$ and $[Al(OH)_4]^-$ monomers is exergonic by 11.0 kcal mol^{-1}. Besides, condensation reactions to yield the $(OH)_2Al-(O-Si(OH)_3)_2$, $(OH)Al-(O-Si(OH)_3)_3$, and $Al-(O-Si(OH)_3)_4$ oligomers are exergonic by 20.4, 30.5, and 38.7 kcal mol^{-1}, respectively (reactions 2–4 in Table 1). These results suggest that the formation of the Al–O–Si linkage at the $[(OH)_3Al-O-Si(OH)_3]^-$ (*ortho*-sialate) and oligomers species, which is the driving force of the reaction, is in line with the explanation previously given that the geopolymerization mechanism must occur through the condensation of oligomers[19].

The calculations also predict the formation of the Zn–O–Si linkage which is favorable in terms of the *Gibbs* energy. Condensation reactions from the $[Zn(OH)_3]^-$ and $[Zn(OH)_4]^{2-}$ species are all exergonic (reactions 5–9), suggesting that Zn–O–Si units can be incorporated into the polymeric framework. However, the dehydration reactions without the condensation of the reactant species are only favorable for reactions involving the $[Zn(OH)_4]^{2-}$ specie (reactions 10–15). Indeed, the reactions 12 and 15 are computed to be exergonic by 13.3 and 3.8 kcal mol^{-1}. Figure 2 depicts the *Gibbs* energy profiles and the relevant optimized structures calculated for the $[Al(OH)_4]^- + Si(OH)_4$, $[Zn(OH)_3]^- + Si(OH)_4$, and $[Zn(OH)_4]^{2-} + Si(OH)_4$ reactions. In our model, the condensation reactions from the $[Al(OH)_4]^-$ and $[Zn(OH)_3]^-$ anionic species are described by mechanism analogous. The reactants are linked to each other by the attraction between hydrogens from the $Si(OH)_4$ specie

140

		$\Delta_r G$
	Condensation	
(1)	$[Al(OH)_4]^- + Si(OH)_4 \rightarrow [(OH)_3Al-O-Si(OH)_3]^- + H_2O$	−11.0
(2)	$[Al(OH)_4]^- + 2Si(OH)_4 \rightarrow [(OH)_2Al-(O-Si(OH)_3)_2]^- + 2H_2O$	−20.4
(3)	$[Al(OH)_4]^- + 3Si(OH)_4 \rightarrow [(OH)Al-(O-Si(OH)_3)_3]^- + 3H_2O$	−30.5
(4)	$[Al(OH)_4]^- + 4Si(OH)_4 \rightarrow [Al-(O-Si(OH)_3)_4]^- + 4H_2O$	−38.7
(5)	$[Zn(OH)_3]^- + Si(OH)_4 \rightarrow [(OH)_2Zn-O-Si(OH)_3]^- + H_2O$	−7.5
(6)	$[Zn(OH)_3]^- + 2Si(OH)_4 \rightarrow [(OH)Zn-(O-Si(OH)_3)_2]^- + 2H_2O$	−18.2
(7)	$[Zn(OH)_3]^- + 3Si(OH)_4 \rightarrow [Zn-(O-Si(OH)_3)_3]^- + 3H_2O$	−26.9
(8)	$[Zn(OH)_4]^{2-} + Si(OH)_4 \rightarrow [(OH)_3Zn-O-Si(OH)_3]^{2-} + H_2O$	−18.9
(9)	$[Zn(OH)_4]^{2-} + 2Si(OH)_4 \rightarrow [(OH)_2Zn-(O-Si(OH)_3)_2]^{2-} + 2H_2O$	−36.0
	Dehydration	
(10)	$[Al(OH)_4]^- + Si(OH)_4 \rightarrow [Al(OH)_3] + [Si(OH)_3O]^- + H_2O$	+ 35.0
(11)	$[Zn(OH)_3]^- + Si(OH)_4 \rightarrow [Zn(OH)_2] + [Si(OH)_3O]^- + H_2O$	+ 1.5
(12)	$[Zn(OH)_4]^{2-} + Si(OH)_4 \rightarrow [Zn(OH)_3]^- + [Si(OH)_3O]^- + H_2O$	−13.3
(13)	$[Al(OH)_4]^- + [(OH)_3Al-O-Si(OH)_3]^- \rightarrow [Al(OH)_3] + [(OH)_3Al-O-Si(OH)_2O]^{2-} + H_2O$	+ 44.5
(14)	$[Zn(OH)_3]^- + [(OH)_3Al-O-Si(OH)_3]^- \rightarrow [Zn(OH)_2] + [(OH)_3Al-O-Si(OH)_2O]^{2-} + H_2O$	+ 11.0
(15)	$[Zn(OH)_4]^{2-} + [(OH)_3Al-O-Si(OH)_3]^- \rightarrow [Zn(OH)_3]^- + [(OH)_3Al-O-Si(OH)_2O]^{2-} + H_2O$	−3.8

Table 1. *Gibbs* free energy of reaction ($\Delta_r G$. in kcal mol^{-1}) computed at the ωB97X-D/6–311 + G(3df.2p)//6–31 + G(d.p) level of theory. For the oligomers is being considered the condensation from 1 to 4 Si(OH)$_4$ species.
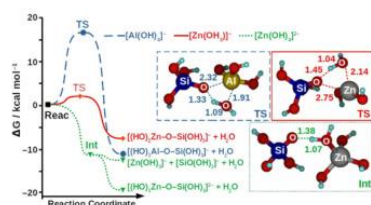
Figure 2. Left: *Gibbs* energy profiles calculated at the ωB97X-D/6–311 + G(3df.2p)//6–31 + G(d.p) method for the $[Al(OH)_4]^- + Si(OH)_4$, $[Zn(OH)_3]^- + Si(OH)_4$. and $[Zn(OH)_4]^{2-} + Si(OH)_4$ reactions. The *Gibbs* energy values (in kcal mol$^-$) for each reaction profile are relative to the reactants (Reac). Structures of the transition states (TS) and intermediate (Int) calculated at the ωB97X-D/6–31 + G(d.p) level of theory. Some relevant bond distances (in Å) are included in the structures.

and OH groups from the ionic specie, $[Al(OH)_4]^-$ or $[Zn(OH)_3]^-$. Then, the two reactants condense to form the $[(OH)_3Al-O-Si(OH)_3]^-$ and $[(OH)_2Zn-O-Si(OH)_3]^-$ species, respectively, with concomitant to release the H$_2$O molecule. Based on Fig. 2, it should be pointed out that the $[Al(OH)_4]^- + Si(OH)_4$ and $[Zn(OH)_3]^- + Si(OH)_4$ reactions proceed through a transition state (TS) located at 16.4 and 2.1 kcal mol^{-1} above the reactants' energy, respectively. The origin of the difference between these reaction barriers can be attributed to steric hindrance at the TS structures. As shown in Fig. 2, the TS of the reaction with the $[Al(OH)_4]^-$ specie involves a greater geometrical deformation when compared to the TS of the reaction with $[Zn(OH)_3]^-$.

On the contrary to what is computed for the Si(OH)$_4$ + $[Al(OH)_4]^-$/$[Zn(OH)_3]^-$ reactions, the mechanism of the reaction between $[Zn(OH)_4]^{2-}$ and Si(OH)$_4$ species is predicted to proceed by the initial formation of the $[Zn(OH)_3)(OH)_2]...OSi(OH)_3]^{2-}$ intermediate (Int). The formation of the Int occurs virtually barrierless, where the Si(OH)$_4$ specie undergoes a hydrogen abstraction process by the OH group from the $[Zn(OH)_4]^{2-}$ (Fig. 2). Then, the Int can either condense to form the $[(OH)_4Zn-O-Si(OH)_3]^{2-} + H_2O$ products or fragment to yield the $[Zn(OH)_3]^- + [SiO(OH)_3]^- + H_2O$ products. According to our calculations, the reactions involving the $[Zn(OH)_4]^{2-}$ anions are kinetically and thermodynamically more feasible than that reaction with other anions.

Raman spectroscopy. Raman spectroscopy has proven to be a valuable tool in the study of geopolymers[8,9]. An advantageous feature is that their Raman spectra can be compared with those of SiO$_4$ glasses[7]. SiO$_4$ glass

141

creation relies on the condensation of isolated SiO_4 tetrahedra (referred to as Q^0) by linking to each other via sharing one to four oxygen atoms (Q^1–Q^4). Since differently bonded tetrahedra have distinct Raman signatures in the range of 1000 cm^{-1}–1100 cm^{-1}, variations in that region may be used to track the SiO_4 depolymerization required for geopolymer formation[7]. Interestingly, the computational chemistry results in Fig. 2 hints to the formation of Q^3 species via a barrierless TS that appears only in the presence of Zn^{2+}. It is then conceivable that Zn^{2+} would lead to a higher rate of Q^3 formation in geopolymers when compared to their no Zn counterparts (CNT-0%Zn), which would support the mechanism determined by computational chemistry. This hypothesis has been verified by means of Raman spectroscopy with results shown in Fig. 3. Typical bands of quartz (silica flour) are probed at initial stages of geopolymerization (without Zn^{2+} at this point): 207 cm^{-1} (Si–O–Si bond twisting), 355 cm^{-1} (SiO_4 bending), and 456 cm^{-1} (bending of O–Si–O)[20], which tend to vanish due to quartz consumption. Vibrations at 712 cm^{-1}, 1345 cm^{-1}, and 1361 cm^{-1} refer to CO_3^{-2} in calcite as a consequence of natural carbonation[21], which is known to take place in cementitious materials such as OPC[22]. Regarding geopolymers, the reaction between CO_2 from the air and OH$^-$ produces Ca and sodium (Na) carbonates[23,24]. It is important to notice that the bands assigned to carbonate display no clear tendency over time, which is expected given that the variable amount of CO_2 in the atmosphere leads to an uncontrolled carbonation process. The most important feature of Fig. 3A is the sharp peak at 1051 cm^{-1} related to a Si–O- vibration with O$^-$ denoting a non-bridging oxygen within a Q^3 species[8,25]. Another important characteristic is that the Q^3 band initially increases with time (up to 150 min), meaning that OH$^-$ attacks the Si network to produce increasing amounts of unbounded oxygen. It is important to emphasize that the increase in intensity of the peak at 1051 cm^{-1} is not a result of any artifact since; i) the time of laser illumination and laser potency were the same for all samples (ruling out intensity variation due to heating effects), ii) the illuminated spot of the sample was always the same (same area probed), and iii) there is no contribution of carbonation in the wavenumber region of interest[25]. Upon addition of 1% of Zn to the mixture (Fig. 3B), the respective overlaying Raman spectrum in Fig. 3C reveals a clear shift towards lower frequencies (now centered at 1048 cm^{-1}) as a consequence of weakened Si–O force due to charge transfer from $Zn(OH)_4^{2-}$ to SiO_4. The negative charge transferred to tetrahedra accumulates preferentially on Si atoms leading to a decrease in the Si–O coulombic interaction[26]. When comparing Q^3 peaks, Fig. 4 clearly attests that the addition of 1% of Zn culminates in a higher rate of Q^3 formation. The slopes of the straight lines from t = 0 to t = 150 min are 23.75 and 37.97 for mixtures without and with Zn^{2+}, respectively. Both curves reach the steady state at 150 min, a situation in which the rate of Q^3 formation is counterbalanced by the emergence of oligomers and subsequently geopolymer.

Materials and methods

Material and mixing process. A granite-based aluminosilicate-rich solid precursor has been used to exemplify the retardation effect of Zn^{2+}. The precursor was designed with a low Ca content composition (< 10 wt.%) as presented in Table 2. A 2.21 potassium silicate solution with molar ratio of 2.21 was used as an activating hardener. Zinc nitrate hexahydrate ($Zn(NO_3)_2.6H_2O$) was used as the source of Zn^{2+} species. The mix design of slurries is presented in Table 3.

Control system (CNT): lab scale chemical components. In this study, a controlled system has been constructed using pure components that can replace certain compositions from the original granite-based precursor (presented in Table 2). The components have a purity of over 90%. The composition of the solid phase of the controlled system (CNT) is presented in Table 4, and list of chemical replacements used is presented in Table 5. The purpose behind using such a system is to isolate complex minerals and create a controlled system where the reaction progression can be monitored throughout time. Zn^{2+} species, in the form of $Zn(NO_3)_2.6H_2O$, were also used to mimic retardation with a similar 1 wt% as in the original mix design. In order to accurately mimic the designated components' behavior, the number of molecules of Si, Al, Fe, Ca, Mg, Na, and K was calculated and implemented with the proposed chemical replacements[27] (Table 5).

Two samples were developed, CNT-0%Zn & CNT-1%Zn, where the former contains no Zn^{2+} species while the latter contains 1wt% of Zn. The composition of CNT-0%Zn & CNT-1%Zn solid phases are mentioned in Table 6, while the total mix designs are presented in Table 7. The alkaline hardener phase, a 4 M potassium hydroxide (KOH) solution, was produced with KOH laboratory grade pellets and distilled water. The use of KOH in this system was implemented where it can avoid polycondensation and coagulants where it can start to form instantly after introduction of potassium silicate solution to the solid phase with free Ca^{2+} species. This phenomenon was reported in a study by Nachbaur et al.[28] where authors examined the electrokinetic properties which interfere with the suspension of silicates in early age hydration. They concluded that the presence of high Ca content in the composition can cause coagulation of Ca_3SiO_5 particles due to the low zeta potential under these conditions.

Samples were prepared by dry mixing of the solid components first followed by the addition of alkaline solution (4 M KOH). The solid-to-liquid ratio was around 2.0 (Table 7). Initially, hand mixing was applied for 2 min (mins), then the apparatus was moved to a Hamilton Beach mixer with a single spindle for 60 s. The material had a honey-like consistency at the end of mixing.

Testing and characterization methods. *Consistency Measurements.* An OFITE HPHT consistometer (Model 2040) was used to examine the pumping and setting time at a BHCT of 50 °C and pressure of 2000 psi. The standard for pumping time was set from the starting point until 40 BC while setting time was from 40 to 100 Bc following API RP 10-B2 recommendations[29]. This test was performed only on granite-based geopolymer slurry.

142

Appendix
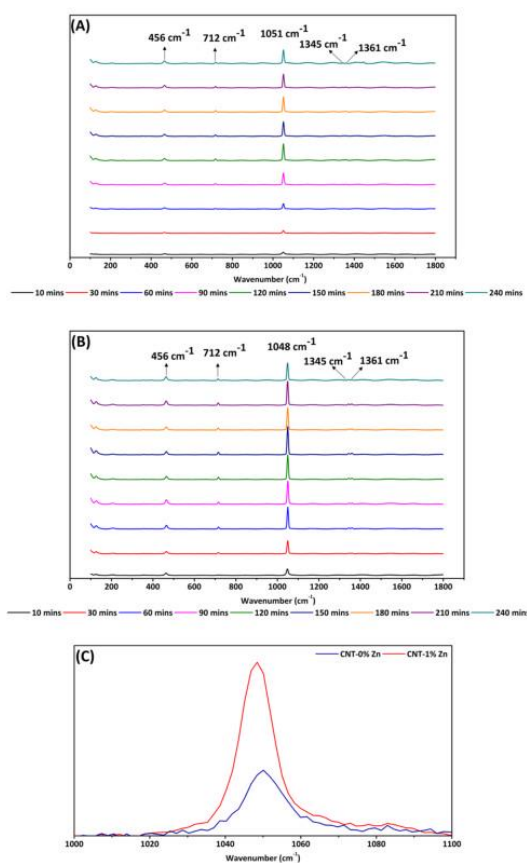
Figure 3. (**A**) Raman spectra of CNT-0%Zn; (**B**) Raman spectra of CNT-0%Zn; (**C**) Overlay of Raman spectra from geopolymer pastes having CNT-0%Zn and CNT-1%Zn (t = 10 min).

Raman Spectroscopy. Geopolymer paste, of the controlled system samples (CNT), was analyzed using Raman Spectroscopy. Spectra from 400 to 4000 cm^{-1} were examined using a LabRAM HR Evolution using a 532 nm diode laser operating at 25 mW. Spectra were collected at 30 min time interval. Freshly mixed geopolymer paste was analyzed at time (t) 0 and transported to a nearby oven operating at 50 °C. Thus, maintaining the reaction temperature like the one in the consistometer.

143
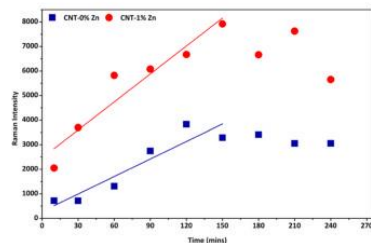
Figure 4. Q^3 band intensity as a function of time for geopolymer pastes CNT-0%Zn & CNT-1%Zn.

Chemical element	wt.%
SiO_2	63.10
Al_2O_3	12.97
Fe_2O_3	1.49
CaO	9.94
MgO	4.54
Na_2O	2.34
K_2O	3.81
TiO_2	0.80
MnO	0.19
LOI	0.80
Total	100

Table 2. Composition of the granite-based geopolymer.

Mix design components (Wt%)				
Mix Design	Solid	Liquid	$Zn(NO_3)_2.6H_2O$ Wt%	Number of molecules of Zn^{2+}
Geo-0%Zn	66.23	53.77	–	–
Geo-1%Zn	66.23	53.77	1	1.21×10^{22}

Table 3. Granite-based mix designs examined for pumping time.

To be considered in the reactants' composition								Not to be considered due to low concentrations					
Composition	SiO_2	Al_2O_3	Fe_2O_3	CaO	MgO	Na_2O	K_2O	TiO_2	MnO	SrO	BaO	LOI	Total
W%	63	13	1.5	10	4.5	2.34	3.81	0.8	0.19	0.01	0.01	0.72	100

Table 4. Composition considered for controlled system under study derived from original precursor (Table 2).

Computational chemistry model description. Density functional theory (DFT) calculations were performed to support the experimental evidence of the retardation effect of Zn^{2+} in the geopolymerization reaction following the method presented by Yang et al.[30]. For such, dehydration reactions between the $Si(OH)_4$ and $[Al(OH)_4]^-$, $[Zn(OH)_3]^-$ and $[Zn(OH)_4]^{2-}$ species were used to model the formation of the Al–O–Si and Zn–O–Si bonds[31]. In our model, Si, Al, and Zn are coordinated by hydroxides, which is consistent with the high alkaline condition (pH around 13.0 to 13.5) used in the experimental setup[32]. In this range of pH, there is an

144

Component in compositions	Chemical replacement	Chemical formula	Number of molecules
Si	Silica flour	SiO_2	$4.423 \times 10^{+24}$
Al	Aluminum Nitrate Nanohydrate	$Al(NO_3)_3 \cdot 9H_2O$	$5.358 \times 10^{+23}$
Fe	Iron (II) Sulfate	$FeSO_4$	$3.94 \times 10^{+22}$
Ca	Calcium Hydroxide	$Ca(OH)_2$	$7.47 \times 10^{+23}$
Mg	Magnesium Oxide	MgO	$4.75 \times 10^{+23}$
Na	Sodium Hydroxide	$NaOH$	$1.59 \times 10^{+23}$
K	Potassium Hydroxide	KOH	$1.71 \times 10^{+23}$
Zn	Zinc Nitrate Hexhydrate	$Zn(NO_3)_2 \cdot 6H_2O$	$1.21 \times 10^{+22}$

Table 5. List of composition, chemical replacement, and number of molecules for each replaced element.

Components (Purity > 90%)	Mix design components (g)	
	CNT-0%Zn	CNT-1%Zn
SiO_2	44.13	44.13
$Al(NO_3)_3 \cdot 9H_2O$	18.96	18.96
$FeSO_4$	0.99	0.99
$Ca(OH)_2$	9.19	9.19
MgO	3.18	3.18
$NaOH$	1.06	1.06
KOH	1.59	1.59
$Zn(NO_3)_2 \cdot 6H_2O$	–	0.79
Total	79.1	79.89

Table 6. Solid phase composition of controlled samples (CNT).

Mix design components (Wt%)				
Mix design	Solid	Liquid	$Zn(NO_3)_2 \cdot 6H_2O$	Number of molecules of Zn^{2+}
CNT-0%Zn	66.6	33.3	–	–
CNT-1%Zn	66.6	33.3	1	1.21×10^{22}

Table 7. Mix design of control samples.
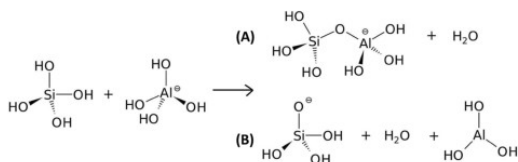
Figure 5. Dehydration reactions (**A**) with and (**B**) without condensation of the reactant species.

equilibrium between $[Zn(OH)_3]^-$ and $[Zn(OH)_4]^{2-}$ anionic species. Figure 5 presents two types of dehydration reactions considered in this study:

First, structure predictions of the reactants and products were performed with the conformer-rotamer ensemble sampling tool of the xtb software[33,34]. To globally explore conformers, the GFN2-xTB method was used in the framework of meta-dynamics[35,36]. Secondly, the minimum-energy conformers were chosen as guess structures for calculations of geometry optimizations with the ωB97X-D/6-311 + G(3df.2p)//6-31 + G(d.p) level of theory. The structures were optimized at the ωB97X-D/6-31 + G(d.p) level of theory, and single-point calculations were performed at the ωB97X-D/6-311 + G(3df.2p) on these structures. All calculations were performed with an

145

implicit solvent (water) using the polarizable continuum model. The ωB97X-D functional has presented a good performance in the description of structural kinetics and thermochemical properties[37,38]. The Gaussian 16 software package was used for all DFT calculations[39].

Data availability
The datasets generated during the current study are available from the corresponding author upon request.

References

1. Chamssine, F., Khalifeh, M., Eid, E., Minde, M. W. & Saasen, A. in *ASME 2021 40th International Conference on Ocean, Offshore and Arctic Engineering*.
2. Khalifeh, M., Saasen, A., Hodne, H. & Motra, H. B. Laboratory evaluation of rock-based geopolymers for zonal isolation and permanent P&A applications. *J. Pet. Sci. Eng.* **175**, 352–362 (2019). https://doi.org/10.1016/j.petrol.2018.12.065
3. Khalifeh, M., Motra, H. B., Saasen, A. & Hodne, H. in *International Conference on Offshore Mechanics and Arctic Engineering*. V008T011A037 (American Society of Mechanical Engineers).
4. Chamssine, F., Khalifeh, M. & Saasen, A. Effect of Zn2+ and K+ as retarding agents on rock-based geopolymers for downhole cementing operations. *J. Energy Resour. Technol.* **144** (2022). https://doi.org/10.1115/1.4053710
5. Garcia-Lodeiro, I., Palomo, A. & Fernández-Jiménez, A. in *Handbook of Alkali-Activated Cements, Mortars and Concretes* (eds F. Pacheco-Torgal *et al.*) 19–47 (Woodhead Publishing, 2015).
6. Khale, D. & Chaudhary, R. Mechanism of geopolymerization and factors influencing its development: A review. *J. Mater. Sci.* **42**, 729–746 (2007). https://doi.org/10.1007/s10853-006-0401-4
7. Wetzel, A., Umbach, C., Fehling, E. & Middendorf, B. Multifunctional prefabricated walls made of UHPC and foam concrete. *Insights Innov. Struct. Eng. Mech. Comput* **86**, 143–148 (2016).
8. Kosor, T., Nakić-Alfirević, B. & Gajović, A. Geopolymerization index of fly ash geopolymers. *Vib. Spectrosc.* **85**, 104–111 (2016).
9. Böke, N., Birch, G. D., Nyale, S. M. & Petrik, L. F. New synthesis method for the production of coal fly ash-based foamed geopolymers. *Constr. Build. Mater.* **75**, 189–199 (2015).
10. Wang, L. *et al.* The role of zinc in metakaolin-based geopolymers. *Cem. Concr. Res.* **136**, 106194 (2020).
11. Garg, N. & White, C. E. Mechanism of zinc oxide retardation in alkali-activated materials: an in situ X-ray pair distribution function investigation. *J. Mater. Chem. A* **5**, 11794–11804 (2017).
12. Alex, T. C. *et al.* Utilization of zinc slag through geopolymerization: Influence of milling atmosphere. *Int. J. Mineral Process.* **123**, 102–107 (2013). https://doi.org/10.1016/j.minpro.2013.06.001
13. Tommaseo, C. & Kersten, M. Aqueous solubility diagrams for cementitious waste stabilization systems. 3. Mechanism of zinc immobilizaton by calcium silicate hydrate. *Environ. Sci. Technol.* **36**, 2919–2925 (2002).
14. Cong, X., Zhou, W., Geng, X. & Elchalakani, M. Low field NMR relaxation as a probe to study the effect of activators and retarders on the alkali-activated GGBFS setting process. *Cem. Concr. Composites* **104**, 103399 (2019). https://doi.org/10.1016/j.cemconcomp.2019.103399
15. Zeng, Y. & Park, J. Characterization and coagulation performance of a novel inorganic polymer coagulant—Poly-zinc-silicate-sulfate. *Colloids Surf. A Physicochem. Eng. Asp.* **334**, 147–154 (2009). https://doi.org/10.1016/j.colsurfa.2008.10.009
16. Ortego, J. D., Barroeta, Y., Cartledge, F. K. & Akhter, H. Leaching effects on silicate polymerization. An FTIR and silicon-29 NMR study of lead and zinc in portland cement. *Environ. Sci. Technol.* **25**, 1171–1174 (1991). https://doi.org/10.1021/es00018a024
17. Chamssine, F., Gargari, P. & Khalifeh, M. in *Offshore Technology Conference*.
18. Rees, C. A., Provis, J. L., Lukey, G. C. & Van Deventer, J. S. In situ ATR-FTIR study of the early stages of fly ash geopolymer gel formation. *Langmuir* **23**, 9076–9082 (2007).
19. North, M. R. & Swaddle, T. W. Kinetics of silicate exchange in alkaline aluminosilicate solutions. *Inorg. Chem.* **39**, 2661–2665 (2000).
20. Morana, M., Mihailova, B., Angel, R. J. & Alvaro, M. Quartz metastability at high pressure: What new can we learn from polarized Raman spectroscopy?. *Phys. Chem. Miner.* **47**, 1–9 (2020).
21. Sun, J., Wu, Z., Cheng, H., Zhang, Z. & Frost, R. *Spectrochim. Acta Part A Mol. Biomol. Spectrosc.* **117**, 158 (2014)
22. Glasser, F. P., Marchand, J. & Samson, E. Durability of concrete—Degradation phenomena involving detrimental chemical reactions. *Cem. Concr. Res.* **38**, 226–246 (2008).
23. Palacios, M. & Puertas, F. Effect of carbonation on alkali-activated slag paste. *J. Am. Ceram. Soc.* **89**, 3211–3221 (2006).
24. Bernal, S. A., De Gutierrez, R. M., Provis, J. L. & Rose, V. Effect of silicate modulus and metakaolin incorporation on the carbonation of alkali silicate-activated slags. *Cem. Concr. Res.* **40**, 898–907 (2010).
25. Ritscherl, C., Mielcarekl, E., Wongpaz, J. & Lutz, F. J. W. New insights on geopolymerisation using molybdate, Raman, and infrared spectroscopy. *Strategic Mater. Comput. Des.* **31**(10), 17 (2010).
26. Nesbitt, H. W., O'Shaughnessy, C., Henderson, G. S., Bancroft, G. M. & Neuville, D. R. Factors affecting line shapes and intensities of Q3 and Q4 Raman bands of Cs silicate glasses. *Chem. Geol.* **505**, 1–11 (2019).
27. Oriakhi, C. O. & Oriakhi, C. O. in *Chemistry in Quantitative Language: Fundamentals of General Chemistry Calculations* 0 (Oxford University Press, 2009).
28. Nachbaur, L., Nkinamubanzi, P.-C., Nonat, A. & Mutin, J.-C. Electrokinetic properties which control the coagulation of silicate cement suspensions during early age hydration. *J. Colloid Interface Sci.* **202**, 261–268 (1998).
29. API, R. 10B-2. *Recommended Practice for Testing Well Cements* (2018).
30. Yang, R., Ren, X. & Sun, M. Optical spectra of bilayer borophene synthesized on Ag(111) film. *Spectrochim. Acta Part A Mol. Biomol. Spectrosc.* **282**, 121711 (2022). https://doi.org/10.1016/j.saa.2022.121711
31. Weng, L. & Sagoe-Crentsil, K. Dissolution processes, hydrolysis and condensation reactions during geopolymer synthesis: Part I—Low Si/Al ratio systems. *J. Mater. Sci.* **42**, 2997–3006 (2007).
32. Mesmer, R. E. & Baes, C. F. Jr. Hydrolysis of beryllium (II) in m sodium chloride. *Inorg. Chem.* **6**, 1951–1960 (1967).
33. Pracht, P., Bohle, F. & Grimme, S. Automated exploration of the low-energy chemical space with fast quantum chemical methods. *Phys. Chem. Chem. Phys.* **22**, 7169–7192 (2020).
34. Bannwarth, C. *et al.* Extended tight-binding quantum chemistry methods. *Wiley Interdiscip. Rev. Comput. Mol. Sci.* **11**, e1493 (2021).
35. Bannwarth, C., Ehlert, S., Grimme, S. Tight-Binding, B.P.S.-C. Quantum chemical method with multipole electrostatics and density-dependent dispersion contributions. *J. Chem. Theory Comput.* **15**, 1652–1671 (2019).
36. Grimme, S. Conformer-rotamer ensemble sampling tool (CREST). *J. Chem. Theor. Comput* **15**, 2847–2862 (2019).
37. Chai, J.-D. & Head-Gordon, M. Long-range corrected hybrid density functionals with damped atom–atom dispersion corrections. *Phys. Chem. Chem. Phys.* **10**, 6615–6620 (2008).

146

38. Verma, P. & Truhlar, D. G. Status and challenges of density functional theory. *Trends Chem.* **2**, 302–318 (2020).
39. Frisch, M. e. *et al.* (Gaussian, Inc. Wallingford, CT, 2016).

Acknowledgements

Author contributions

F.C.: conceptualization, methodology, investigation, data curation, writing—original draft preparation, writing-reviewing and editing. L.H.S.G.: methodology, investigation, data curation, writing-original draft preparation, writing—reviewing and editing, supervision. M.A.F.deS.: data modeling, data curation, writing-draft preparation, writing—reviewing and editing. M.K.: conceptualization, methodology, writing—reviewing and editing, resources, supervision, project administration, funding acquisition. J.C.deO.F.: methodology, writing—reviewing and editing, resources, supervision.

Competing interests

The authors declare no competing interests.

Additional information

Correspondence and requests for materials should be addressed to F.C.

Reprints and permissions information is available at www.nature.com/reprints.

Publisher's note Springer Nature remains neutral with regard to jurisdictional claims in published maps and institutional affiliations.

147

Appendix 8 – Paper V

RHEOLOGICAL AND MECHANICAL PROPERTIES OF ROCK-BASED GEOPOLYMERS DEVELOPED FOR WELL ABANDONMENT: EFFECT OF CHEMICAL ADMIXTURES AT ELEVATED TEMPERATURES

Fawzi Chamssine, Mahmoud Khalifeh, Arild Saasen

Appendix 9 – Paper VI

Temperature-Dependent Classification of Geopolymers Derived from
Granite Designed for Well Cementing Applications

Fawzi Chamssine, Madhan Agista, Mahmoud Khalifeh

Temperature-Dependent Classification of Geopolymers Derived from Granite Designed for Well Cementing Applications

Fawzi Chamssine*[1]; Madhan Nur Agista[1] and Mahmoud Khalifeh[1]

[1] Dept. of Energy and Petroleum Eng., Faculty of Science & Technology, University of Stavanger, Norway
*Corresponding author; email: fawzi.chamssine@uis.no

Abstract

Alternative materials such as geopolymer appear to have potential advantages compared to Portland cement. However, the application of geopolymers for all sections of the well is still a major challenge due to the difference in temperature ranges. To that end, the classification of the granite-based geopolymer mix designs requires a thorough investigation of various properties at a range of different operational temperatures. In this study, three mix designs are presented for different well sections from temperatures ranging from 5°C to 60°C. Three mix designs introduced were developed with each mix design possessing its own unique composition. Workability, rheology, compressive strength, and XRD analysis were conducted to conclude the performance of the mix designs under study. Results highlight the presence of Ca content (wt.%) in mix designs and its role in enhancing material performance at low operational temperatures. The study reveals a promising future application of the granite-based geopolymer for well construction and abandonment at varying depths with recommendations of further improving the performance by the addition of chemical admixtures. In addition, the relation between temperature and Ca content was highlighted, and more investigations into the kinetics governing these two parameters were recommended.

Keywords: Well Cementing; Abandonment; Cement; Geopolymer.

Introduction

Ordinary Portland cement (OPC) has been widely used as a zonal isolation material in the petroleum industry for establishing annular barriers and cement plugs. As a hydraulic binding material, OPC has undergone extensive research on its chemical admixtures and modifications to its chemistry, making it has a practical choice for well cementing operations. The industry is well aware of the existing limitations of Portland-based cement, including concerns related to its long-term durability, low flexibility, leaching when exposed to downhole chemicals, which can result in well integrity issues [1-3]. Moreover, with the global movement toward sustainability, OPC is not quite ideal to be continuously used due to its high environmental cost of CO_2 emission during its manufacture [4]. Alternative zonal isolation materials with similar or even better performance are indeed required to replace the dependency on Portland cement, especially for well construction and well abandonment.

Geopolymers, inorganic aluminosilicate polymers, are one of the potential green alternatives for OPC considering their production life cycle involving the utilization of solid-waste material [5, 6]. The implementation of geopolymers in the oil & gas sector as an isolation material have been under many challenges surrounding its applicability and efficiency in the field compared to the already established knowledge of OPC [7-9]. Solid precursors, of different origins, undergo a dissolution phase where components of highly complex minerals are disintegrated into smaller molecules, which form the basis of polymeric matrices composed of mainly Si-O-Al bonds [10]. Geopolymers require an activator (hardener), which acts as the dissolution medium of minerals where these hardeners can have a hydroxide nature such as potassium hydroxide (KOH) and sodium hydroxide (NaOH) or they can be of a silicate nature potassium/sodium silicate (K_2SiO_3/Na_2SiO_3) [11-14]. According to the work of different researchers Khalifeh *et al.* [15, 16] and Duxson *et al.* [17], geopolymers poses properties that make them superior to OPC such as low chemical shrinkage, low permeability, high durability in corrosive mediums, and the ability of not being affected significantly by oil-based mud contaminants. The challenges evolve around admixtures to be utilized, temperature range efficiency, and hurdles in acquiring adequate properties. Although with

156

these challenges, many efforts are being made by researchers to improve and formulate geopolymer mix designs into adequately applicable material in the field [18, 19]. To make the geopolymers viable and sustainable for the industry, researchers should narrow the number of mix designs and diversity of geopolymer types based on the precursors used. This can facilitate mass production and reproducibility of the technology.

It is well known that temperature affects the development of cementitious material significantly from workability to mechanical properties [20-22]. The development of geopolymer to have a working range of various temperatures can be of some challenge especially considering its ability to harden and form a solid material. In other words, one of the main remaining technical gaps for commercialization of geopolymers is the development of few consistent mix designs that can be used in different temperature ranges. However, the proper utilization of the Ca^{2+} content in solid precursors can be a turning point to ensure strength development at low temperatures [23].

In this study, three different mix designs, i.e., three classes of a granite-based geopolymer, are proposed considering the applicability of the geopolymer in well cementing and well abandonment operations using granite as a main solid precursor source. Calcium oxide (CaO) was introduced to mix designs to compensate for low reaction rates at low temperatures. Different classes have been assigned to different circulation temperatures ranging from 5°C to 60°C. The roles of operating temperature and granite-based composition are highlighted by studying geochemistry, workability and setting time, rheology, uniaxial compressive strength, and X-ray diffraction measurements.

Materials and Methods

Mix Designs. A granite-based geopolymer solid precursor mainly composed of granite was used as the main solid phase in this study. One of the most influential factors is the Si and Al content considering the influence of Ca content, which plays an important role specifically at lower temperatures, thus CaO (purity >90%) was introduced to the mix designs at low temperature up to 40°C [24]. Three mix designs were developed to tackle preliminary challenges of neat slurry where a range of temperature was considered for mix designs. Mix designs were labeled as M.D A, M.D B, & M.D C where the first and second have quite close composition, except Ca content which goes higher as the working temperature decreases, and the third is studied for elevated temperatures. Different components have been introduced to tune the chemical composition to suite specified ranges of temperature and pressure. The composition maintained a mixture of granite, blast furnace slag, and microsilica throughout the three mix designs. Each of these components was proportionally mixed to give specific compositions suitable for the allocated temperature ranges. The chemical composition of each mix design (M.D) is presented in Table 1.

Table 1 – Solid precursor composition of mix designs (wt.%)

Mix Design	SiO_2	Al_2O_3	Fe_2O_3	CaO	MgO	Na_2O	K_2O	TiO_2	MnO	SrO	BaO	S^{2-}	LOI	Total
M.D A	62.01	9.84	0.42	16.74	5.73	1.76	1.79	1.01	0.001	0.001	0	0.52	0.13	100
M.D B	62.51	9.92	0.43	16.06	5.78	1.78	1.81	1.02	0.01	0.01	0	0.58	0.13	100
M.D C	69.75	10.02	0.58	10.21	3.72	2.33	2.41	0.67	0.01	0.01	0.01	0.37	0.2	100

The mix designs presented have been inspired from previous work conducted on granite-based geopolymers. Mix designs with the purpose of operating at low temperature applications where inspired from the work of Agista *et al.* [25] where it was foreseen the efficiency of potassium hydroxide (KOH) solutions in geopolymer slurry, especially at low temperature. CaO, added to the dry blend, was used with the efforts to accomplish early mechanical properties and ensuring setting of the slurry at the recommended operational window [26, 27]. In addition, the use of CaO was combined with KOH solutions rather than potassium silicate (K_2OSiO_2) solutions to avoid the formation of coagulants that may occur while using silicate solutions [28]. On the other hand, M.D C has been inspired from

157

the work of Chamssine *et al.* [18] where no CaO have been added to the system since it is well known that at elevated temperatures neat slurries achieve setting and mechanical properties can be measured easily. In addition, temperature highly influences geopolymer chemistry which assists in the formation of a firm, dense, and bulk structure [29-31]. Utilization of K_2SiO_3 instead of Na_2SiO_3 is due to lower viscosity and prolonged pumpability of the potassium silicate system. Slurry preparation was conducted using API 10B-2 recommended practices [32]. Mix design components are presented in Table 2.

Table 2 - Mix design composition (wt.%).

Slurry Design (wt. %)

Mix Design	Density (SG)	Solid	CaO	KOH (4M)	K_2OSiO_2	Solid/Liquid Ratio
M.D A	1.88	69.5	3	30.5	-	2.28
M.D B	1.88	69.3	1	30.7	-	2.26
M.D C	1.98	66.7	-	-	33.3	2

Test Conditions. The temperature range used to test different mix designs was from 5 to 60ºC of BHCT. Temperatures were divided among the three mix designs as follows: M.D A was tested from 5 to 20ºC with a 5ºC increment between each test; M.D B was tested from 25 to 40ºC; M.D C was tested at 50 and 60ºC. Conditions of curing and testing are mentioned in Table 3. It must be noted that curing was done at the same mentioned temperatures since from field experience there is a risk of over cooling and uncertainty in reading downhole temperature, as the worst-case scenarios, which indicates BHCT and BHST are similar. This decision is justified when knowing the strength development of geopolymers is a strong function of temperature and wrong temperature selection can either result in flash setting or delayed setting. Such approach has been utilized in a study by Pernites *et al.* [33] on cement.

Table 3 - Operational conditions under study

Mix Design	Pressure (Bar)	Temperature (ºC)
M.D A	45	5
	55	10
	65	15
	80	20
M.D B	95	25
	115	30
	145	40
M.D C	175	50
	200	60

Workability. Atmospheric consistometer was used to evaluate workability of mix designs at different working temperatures. All operations were handled following API 10B-2 recommendations [32]. The selected ramp up rate for temperatures above 25°C selected to be 1°C per minute.

Conditioning. The atmospheric consistometer was used to condition samples for rheology and compressive strength samples preparations following API 10B-2 recommendations.

Rheology. To evaluate the rheological characteristics of the geopolymer mix design at a specified temperature, a scientific rheometer was used. This instrument was chosen due to its ability to perform tests at low temperatures, down to 5°C, which is not achievable with a standard API rotational viscometer. Rotational testing was conducted on each slurry, under a controlled shear rate, where the shear

stress was measured. Prior to testing, the samples were mixed and pre-conditioned using an atmospheric consistometer for 30 minutes at specified temperatures. The rheology test involved three different intervals, namely pre-shear, ramp-up, and ramp-down. The test began with pre-shearing at 100 1/s for 60 seconds, followed by ramp-up (0.01-511 1/s) and ramp-down (511-0.01 1/s) stages.

Compressive Strength. Destructive method was used to measure uniaxial compressive strength (UCS) of the samples, a loading rate of 7 kN/min was applied which is in accordance with API 10TR-7 [34]. To conduct the test, each slurry was prepared using the same procedures as mentioned earlier, and pre-conditioned at a specified temperature before being poured into cylindrical plastic molds (5 cm in diameter and 10 cm in height). The molds were then placed inside pressurized autoclave cells and cured under controlled pressure and temperature for 1 and 7 days.

X-Ray Diffraction. The Bruker-AXS Micro-diffractometer D8 Advance was utilized to study crystallography of the precursors and observe phase changes, using CuKα radiation (40.0 kV, 25.0 mA) with a 2θ range from 5° to 92°, with a 1°/min step and a 0.010° increment. The samples were cured for 7 days at the maximum temperature limit of their respective mix designs. M.D A, M.D B, and M.D C were cured at 20°C, 40°C, and 60°C, respectively. Prior to testing, the cured samples were manually ground and dried in a vacuum oven at room temperature for 24 hours.

Results and Discussion

X-Ray Diffraction. XRD patterns of the solid precursor and cured samples of M.D A, B, & C are presented below in Figure 1 and Figure 2, respectively. The main phases recorded in both, the solid precursor, and cured samples, are quartz (Qz), albite (Alb), microcline (Mic), and exclusively a phase belonging to illite (IL) in the solid precursor part. The main change observed was the consumption of the IL after reacting and curing the solid precursor. This consumption can be due to the IL's tendency to dissolve in high alkaline environments [35].The high concentration of Qz can be attributed to the presence of granite as the main precursor, a material rich of Si and Al species. It can be observed that the Qz concentration has decreased in M.D B indicating higher consumption of Si throughout the reaction in the allocated curing period. Seeing that the presence of Alb and Mic was detected, this can be an indicator of zeolite formation specifically since the material is in a K-activated system which favors the formation of zeolite phases [36]. This as well can be an explanation of why highly crystalline patterns were obtained where crystallinity was higher than 60% in all samples. High crystallinity can lead to an increase in strength development however under thermal curing this can inhibit the formation of crystalline zeolites which counteracts strength development by applying inner stress or local destruction to the geopolymer's matrix[37]. These results clearly indicate the effect of temperature on reaction rates and the need to consider the balance between temperature and composition, since neither elevated temperature nor higher Ca content can aid unless it is formulated in a balanced manner to serve the type of application and ensure favorable kinetics of reaction.
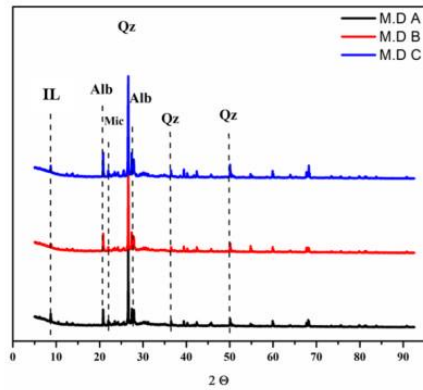
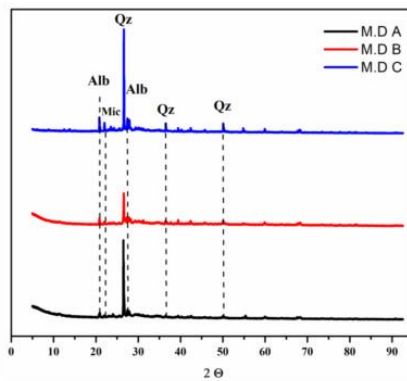Figure 1. XRD patterns for dry blend of M.D A, B, & C

Figure 2. XRD patterns for M.D A, B, & C cured for 7 days at 20, 40, & 60°C, respectively

Workability. The first field parameter to discuss is workability of the different mix designs under different temperatures. Workability measurements of different mix designs at different temperatures are presented in Figure 3. Each mix designs has been tested at the specific assigned range since it is foreseen from previous studies that the use of more Ca species at lower temperatures can be highly beneficial for the workability of the slurry and the opposite at higher temperatures [18, 23, 25]. It can be observed how temperature increase has an accelerating effect on the initial and final setting time of geopolymer mix designs, especially between M.D A-20 and M.D A-5. Temperature can facilitate the setting of geopolymer material which in turn can accelerate the development of hard structure [38, 39]. In addition, to properly understand how different material behave at the intermediate temperature zones, different mix designs

were tested at their temperature limitations. Focusing on M.D B, the temperature limitation can be observed at 45°C, an intermediate point between M.D B and M.D C. It must be noted that due to the rapid setting observed by M.D B-45, it was decided to switch to K_2OSiO_2 solution as it has proven its efficiency under elevated temperature conditions [18]. This shift to K_2OSiO_2 solution and a significant decrease in Ca content in M.D C created a synergy in the slurry allowing the prolongation and safe handling of slurry at temperatures exceeding the 45°C temperature limit to go up to 60°C.
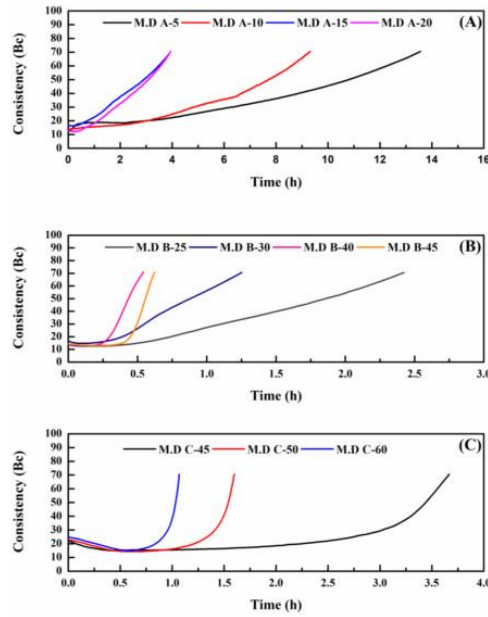

Figure 3. Workability measurement of mix designs at different temperatures. (A) M.D A, (B) M.D B, (C) M.D C – Each curve tested at the specific temperature indicated

Throughout this study, the criteria of assigning working temperatures for different mix designs depended on mainly Ca content in mix designs. Duxson *et al.* (Duxson et al. 2007) [40]highlighted the properties of low Ca geopolymer at low temperatures where hardening time is quite slow compared to samples cured at elevated temperature. Nath and Sarker [41]examined the efficiency of OPC for fly ash class F geopolymers cured at ambient conditions. They concluded that the presence of OPC not only accelerated the reaction of geopolymerization but also influenced the compressive strength of the material; they attributed this increase to OPC addition as a Ca source for the reaction which in turn yielded C-S-H phases that was able to accelerate the polycondensation phase of the reaction. -The proper utilization of the Ca^{2+} content in solid precursors can be a turning point to ensure strength development at low temperatures [23]. Thus, the tuning of Ca content can have a major effect on slurry properties at low temperatures as demonstrated in M.D A-5, which was handled at relatively low operational temperature but still managed to harden due to the higher Ca content in the dry blend.

Rheology. The rheological properties of each geopolymer mix design were assessed using rotational flow tests at their designated temperatures, as outlined in Table 3. As a time-dependent fluid, the viscosity of the slurry changes over time, necessitating consistent timing during the test to ensure reliable results. The samples were mixed and preconditioned for 30 minutes at the specified temperature before being placed in the rheometer cup, which was conditioned at the test temperature. The test began with an initial pre-shear to break down any formed gel and was followed by the ramp-up and ramp-down tests. In some cases, the inability to test certain samples was due to high viscosity resulting from hardening caused by the rapid geopolymerization reaction at high temperatures. The ramp-down test result is evaluated and presented in Figure 4. Ramp-down test is selected due to its representation of dynamic condition of the slurry. The effect of the temperature is noticeable in the different mix designs. Higher temperature will induce higher kinetic energy, increasing the molecule vibration of the carrier fluid hence reducing the slurry's viscosity [25]. This behavior can be seen in the mix design A which tested at 5°C to 20°C. On the other hand, the viscosity result for mix design B shows the opposite trend with the increasing temperature. Increasing temperature will result in increased viscosity of both mix designs. At this stage, the slurry is in the acceleration phase in which increasing temperature will fasten the geopolymerization reaction leading to the hardening. Moreover, the viscosity of M.D B-40 and M.D C-60 were not able to be measured due to fast hardening at that specific temperature. This finding is consistent with the consistency test results presented in Figure 3, indicating that both slurries were pumpable for less than an hour. The outcome of the study revealed that mix designs A and B are unsuitable for use at elevated temperatures as they are significantly affected by gelation and hardening due to the presence of Ca. Similarly, mix design C also experienced fast setting at temperatures above 60°C and could not perform well for low temperature as shown in Figure 3.
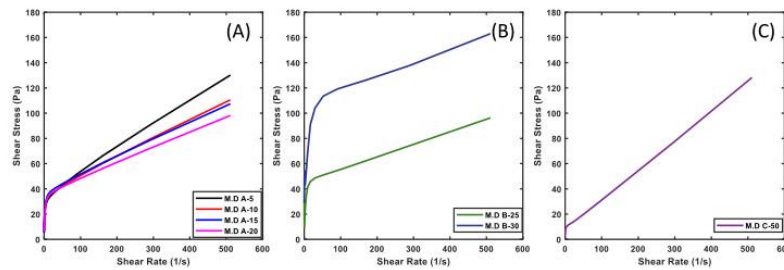

Figure 4. Rotational Flow (Ramp-Down) measurement of mix designs (A) M.D A, (B) M.D B, (C) M.D C

Compressive Strength. The performance of different mix designs at their designated temperature ranges is presented in Figure 5. The curing conditions under different operational temperatures have caused a significant change in the materials ability to withstand mechanical load. Temperature has a direct impact on the strength development of material, and it can be correlated to OPC at elevated temperatures [42] . However, the material's composition, specifically Ca content, contributes hugely to the reaction rate of the mix design and eventually its strength [27]. The increase in Ca content can promote the formation of minor C-S-H phases aiding the matrix's strength development phase [43]. It can be observed that M.D A at 5°C yielded the lowest compressive strength after 1-day of curing compared to samples cured at higher temperatures despite having a high Ca content. These results are expected due to the increase in temperature. However, interestingly observing M.D B-25 it starts to show that although with a lower Ca content in comparison to M.D A samples, compressive strength keeps on increasing with increasing temperature which highlights the significant effect temperature can make to the slurry reaction, hence the effect on compressive strength. In addition, M.D B-40 had the highest strength in comparison to all other samples which seems that the reaction at 40°C is more favorable kinetically where more intermolecular matrices are developing [44]. However, more investigation is required to observe kinetic behavior within every mix design individually at allocated

operational temperatures. Moreover, it was observed that mix designs M.D C-50 and M.D C-60 have measured quite close to each other. Although being cured at elevated temperatures, the temperature effect could not compensate for the missing Ca content in comparison to M.D B's composition. This leads up to a point of interest addressing the firm balance to be made between temperature effect and Ca content in every mix design, which asks for deeper understanding and development of a correlation between both parameters at a kinetic level.
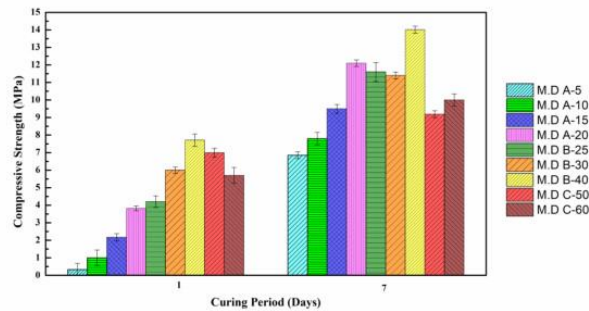

Figure 5. Compressive strength of mix designs cured at allocated temperatures.

Conclusion

Three geopolymer mixed designs were devised to handle different sections of well cementing, each having a unique composition. Different tests were performed at a range from 5 to 60°C considering applicability of each mix design at a specific temperature range. The results for each mix design have been treated individually where their behavior in different conditions, with different Ca content, was the focus point in this study. Based on XRD readings, the mix designs had consistent and similar mineral detection which indicates that Ca content, due to its minor presence in comparison to other elements such as Si and Al, was not highly visible. However, M.D B had an interesting Qz phase post curing which indicates favored reaction kinetics for the reaction at 40°C. Workability indicated the benefit of Ca content at lower temperatures and how temperature was one of the most sensitive parameters determining the performance of geopolymer material and affecting the selection of composition for each mix design. Furthermore, compressive strength increased with increasing curing temperature where MD. B achieved the had the highest performance at 40°C. This high performance can be attributed to favorable reaction conditions which was supported by XRD patterns of cured sample where high consumption of quartz can be observed in M.D B. The mean of developing geopolymer material for oil & gas application should consider a wide range of parameters that can be suitable for producing a successful material where composition and temperature range can highly impact the rate of reaction and thus the efficiency in developing strong matrices that can withstand external parameters. Further recommendations will be to aim for developing chemical admixtures, in different capacities, that would lift the material's properties and engineer compositions capable of successful implementation into field usage. Plus, the Ca content in geopolymer material must be tuned and considered for implementation in field applications due to its beneficial effect on the bulk matrix specifically in ensuring setting of slurry and achieving minimum acceptable compressive strength post setting.

163

References

[1]   R. Kiran *et al.*, "Identification and evaluation of well integrity and causes of failure of well integrity barriers (A review)," *Journal of Natural Gas Science and Engineering,* vol. 45, pp. 511-526, 2017.

[2]   C. Teodoriu and O. Bello, "A review of cement testing apparatus and methods under CO2 environment and their impact on well integrity prediction–Where do we stand?," *Journal of Petroleum Science and Engineering,* vol. 187, p. 106736, 2020.

[3]   T. Vrålstad, J. Todorovic, A. Saasen, and R. Godøy, "Long-Term Integrity of Well Cements at Downhole Conditions," in *SPE Bergen One Day Seminar*, 2016, vol. Day 1 Wed, April 20, 2016, D011S004R003, doi: 10.2118/180058-ms. [Online]. Available: https://doi.org/10.2118/180058-MS

[4]   L. Barcelo, J. Kline, G. Walenta, and E. Gartner, "Cement and carbon emissions," *Materials and structures,* vol. 47, no. 6, pp. 1055-1065, 2014.

[5]   M. Khalifeh, A. Saasen, H. Hodne, R. Godøy, and T. Vrålstad, "Geopolymers as an alternative for oil well cementing applications: A review of advantages and concerns," *Journal of Energy Resources Technology,* vol. 140, no. 9, 2018.

[6]   S. Salehi, N. Ali, M. Khattak, and H. Rizvi, "Geopolymer composites as efficient and economical plugging materials in peanuts price oil market," in *SPE Annual Technical Conference and Exhibition*, 2016: Society of Petroleum Engineers.

[7]   F. Chamssine, P. Gargari, and M. Khalifeh, "Impact of Admixtures on Pumpability and Short-Term Mechanical Properties of Rock-Based Geopolymer Designed for Zonal Isolation and Well Abandonment," in *Offshore Technology Conference*, 2022, vol. Day 3 Wed, May 04, 2022, D031S032R005, doi: 10.4043/31880-ms. [Online]. Available: https://doi.org/10.4043/31880-MS

[8]   S. Salehi, M. J. Khattak, N. Ali, C. Ezeakacha, and F. K. Saleh, "Study and Use of Geopolymer mixtures for Oil and Gas well cementing applications," *Journal of Energy Resources Technology,* vol. 140, no. 1, 2018.

[9]   X. Liu, S. D. Nair, K. L. Aughenbaugh, M. C. Juenger, and E. van Oort, "Improving the rheological properties of alkali-activated geopolymers using non-aqueous fluids for well cementing and lost circulation control purposes," *Journal of Petroleum Science and Engineering,* vol. 195, p. 107555, 2020.

[10]   D. Khale and R. Chaudhary, "Mechanism of geopolymerization and factors influencing its development: a review," *Journal of Materials Science,* vol. 42, no. 3, pp. 729-746, 2007/02/01 2007, doi: 10.1007/s10853-006-0401-4.

[11]   F. Pacheco-Torgal, J. Castro-Gomes, and S. Jalali, "Alkali-activated binders: A review: Part 1. Historical background, terminology, reaction mechanisms and hydration products," *Construction and Building Materials,* vol. 22, no. 7, pp. 1305-1314, 2008/07/01/ 2008, doi: https://doi.org/10.1016/j.conbuildmat.2007.10.015.

[12]   M. A. Aleem and P. Arumairaj, "Geopolymer concrete–a review," *International journal of engineering sciences & emerging technologies,* vol. 1, no. 2, pp. 118-122, 2012.

[13]   P. Krivenko, I. Garcia-Lodeiro, E. Kavalerova, O. Maltseva, and A. Fernández-Jiménez, "A review on alkaline activation: new analytical perspectives," *Mater. Construcc,* vol. 64, no. 315, p. e022, 2014.

[14]   J. L. Provis and S. A. Bernal, "Geopolymers and Related Alkali-Activated Materials," *Annual Review of Materials Research,* vol. 44, no. 1, pp. 299-327, 2014, doi: 10.1146/annurev-matsci-070813-113515.

[15] M. Khalifeh, J. Todorovic, T. Vrålstad, A. Saasen, and H. Hodne, "Long-term durability of rock-based geopolymers aged at downhole conditions for oil well cementing operations," *Journal of Sustainable Cement-Based Materials,* vol. 6, no. 4, pp. 217-230, 2017.

[16] A. Ogienagbon and M. Khalifeh, "Experimental Evaluation of the Effect of Temperature on the Mechanical Properties of Setting Materials for Well Integrity," *SPE Journal,* vol. 27, no. 05, pp. 2577-2589, 2022, doi: 10.2118/209794-pa.

[17] P. Duxson, A. Fernández-Jiménez, J. L. Provis, G. C. Lukey, A. Palomo, and J. S. J. van Deventer, "Geopolymer technology: the current state of the art," *Journal of Materials Science,* vol. 42, no. 9, pp. 2917-2933, 2007/05/01 2007, doi: 10.1007/s10853-006-0637-z.

[18] F. Chamssine, M. Khalifeh, E. Eid, M. W. Minde, and A. Saasen, "Effects of Temperature and Chemical Admixtures on the Properties of Rock-Based Geopolymers Designed for Zonal Isolation and Well Abandonment," in *ASME 2021 40th International Conference on Ocean, Offshore and Arctic Engineering,* 2021, vol. Volume 10: Petroleum Technology, V010T11A031, doi: 10.1115/omae2021-60808. [Online]. Available: https://doi.org/10.1115/OMAE2021-60808

[19] L. N. Assi, E. Deaver, and P. Ziehl, "Using sucrose for improvement of initial and final setting times of silica fume-based activating solution of fly ash geopolymer concrete," *Construction and Building Materials,* vol. 191, pp. 47-55, 2018/12/10/ 2018, doi: https://doi.org/10.1016/j.conbuildmat.2018.09.199.

[20] A. K. Schindler, "Effect of temperature on hydration of cementitious materials," *Materials Journal,* vol. 101, no. 1, pp. 72-81, 2004.

[21] R. He, N. Dai, and Z. Wang, "Thermal and mechanical properties of geopolymers exposed to high temperature: A literature review," *Advances in Civil Engineering,* vol. 2020, 2020.

[22] H. Castillo *et al.*, "Factors affecting the compressive strength of geopolymers: A review," *Minerals,* vol. 11, no. 12, p. 1317, 2021.

[23] G. M. Canfield, J. Eichler, K. Griffith, and J. D. Hearn, "The role of calcium in blended fly ash geopolymers," *Journal of materials science,* vol. 49, no. 17, pp. 5922-5933, 2014.

[24] M. Torres-Carrasco and F. Puertas, "Waste glass in the geopolymer preparation. Mechanical and microstructural characterisation," *Journal of cleaner production,* vol. 90, pp. 397-408, 2015.

[25] M. N. Agista, M. Khalifeh, and A. Saasen, "Evaluation of Zonal Isolation Material for Low Temperature Shallow Gas Zone Application," in *SPE Asia Pacific Oil & Gas Conference and Exhibition,* 2022, vol. Day 2 Tue, October 18, 2022, D021S009R005, doi: 10.2118/210751-ms. [Online]. Available: https://doi.org/10.2118/210751-MS

[26] S. Puligilla, "Understanding the role of calcium on the reaction mechanism of geopolymer cements through addition of nucleation seeds," University of Illinois at Urbana-Champaign, 2017.

[27] J. Temuujin, A. Van Riessen, and R. Williams, "Influence of calcium compounds on the mechanical properties of fly ash geopolymer pastes," *Journal of hazardous materials,* vol. 167, no. 1-3, pp. 82-88, 2009.

[28] L. Nachbaur, P.-C. Nkinamubanzi, A. Nonat, and J.-C. Mutin, "Electrokinetic properties which control the coagulation of silicate cement suspensions during early age hydration," *Journal of Colloid and Interface Science,* vol. 202, no. 2, pp. 261-268, 1998.

[29] A. A. Adam and X. Horianto, "The effect of temperature and duration of curing on the strength of fly ash based geopolymer mortar," *Procedia engineering,* vol. 95, pp. 410-414, 2014.

[30] A. M. M. A. Bakria, H. Kamarudin, M. BinHussain, I. K. Nizar, Y. Zarina, and A. R. Rafiza, "The Effect of Curing Temperature on Physical and Chemical Properties of Geopolymers," *Physics Procedia,* vol. 22, pp. 286-291, 2011/01/01/ 2011, doi: https://doi.org/10.1016/j.phpro.2011.11.045.

[31] B. S. Gebregziabiher, R. J. Thomas, and S. Peethamparan, "Temperature and activator effect on early-age reaction kinetics of alkali-activated slag binders," *Construction and Building Materials,* vol. 113, pp. 783-793, 2016/06/15/ 2016, doi: https://doi.org/10.1016/j.conbuildmat.2016.03.098.

[32] R. API, "10B-2," *Recommended Practice for Testing Well Cements,* 2018.

[33] R. Pernites, J. Clark, F. Padilla, and A. Jordan, "New Advanced High-Performance Ultrafine Micromaterials for Providing Superior Properties to Cement Slurry and Set Cement in Horizontal Wells," in *SPE Annual Technical Conference and Exhibition,* 2018, vol. Day 2 Tue, September 25, 2018, D021S017R005, doi: 10.2118/191451-ms. [Online]. Available: https://doi.org/10.2118/191451-MS

[34]   R. API, "API TR 10TR7," *Mechanical Behavior of Cement,* 2017.

[35]   S. Carroll, M. Smith, and K. Lammers, "Chlorite, Biotite, Illite, Muscovite, and Feldspar Dissolution Kinetics at Variable pH and Temperatures up to 280 C," Lawrence Livermore National Lab.(LLNL), Livermore, CA (United States), 2016.

[36]   M. Khalifeh, H. Hodne, A. Saasen, O. Integrity, and E. I. Eduok, "Usability of Geopolymers for Oil Well Cementing Applications: Reaction Mechanisms, Pumpability, and Properties," presented at the SPE Asia Pacific Oil & Gas Conference and Exhibition, Perth, Australia, 2016/10/25/, 2016. [Online]. Available: https://doi.org/10.2118/182354-MS.

[37]   M. Criado, A. Fernández-Jiménez, A. De La Torre, M. Aranda, and A. Palomo, "An XRD study of the effect of the SiO2/Na2O ratio on the alkali activation of fly ash," *Cement and concrete research,* vol. 37, no. 5, pp. 671-679, 2007.

[38]   D. L. Kong and J. G. Sanjayan, "Effect of elevated temperatures on geopolymer paste, mortar and concrete," *Cement and concrete research,* vol. 40, no. 2, pp. 334-339, 2010.

[39]   P. Rovnaník, "Effect of curing temperature on the development of hard structure of metakaolin-based geopolymer," *Construction and building materials,* vol. 24, no. 7, pp. 1176-1183, 2010.

[40]   P. Duxson, S. W. Mallicoat, G. C. Lukey, W. M. Kriven, and J. S. van Deventer, "The effect of alkali and Si/Al ratio on the development of mechanical properties of metakaolin-based geopolymers," *Colloids and Surfaces A: Physicochemical and Engineering Aspects,* vol. 292, no. 1, pp. 8-20, 2007.

[41]   P. Nath and P. K. Sarker, "Use of OPC to improve setting and early strength properties of low calcium fly ash geopolymer concrete cured at room temperature," *Cement and Concrete Composites,* vol. 55, pp. 205-214, 2015/01/01/ 2015, doi: https://doi.org/10.1016/j.cemconcomp.2014.08.008.

[42]   M. Collepardi, *The new concrete*. Grafiche Tintoretto, 2006.

[43]   S. Pangdaeng, T. Phoo-ngernkham, V. Sata, and P. Chindaprasirt, "Influence of curing conditions on properties of high calcium fly ash geopolymer containing Portland cement as additive," *Materials & Design,* vol. 53, pp. 269-274, 2014/01/01/ 2014, doi: https://doi.org/10.1016/j.matdes.2013.07.018.

[44]   J. Provis and C. Rees, "Geopolymer synthesis kinetics," in *Geopolymers*: Elsevier, 2009, pp. 118-136.

166